

Design and fabrication of a simple, cost-effective, passive,
continuous-flow microfluidic device for one-step synthesis of
bioactive molecule loaded liposomes

Ryan V. Tien Sing Young

Biomat'X Research Laboratories

Department of Biomedical Engineering

McGill University

April 6th, 2015

A thesis submitted to McGill University in partial fulfillment of the
requirements of the degree of Master of Engineering

© Ryan V. Tien Sing Young, 2015

Table of Contents

Table of Contents	2
List of Figures.....	5
List of Tables.....	7
List of Abbreviations.....	8
List of Equations.....	9
Abstract	10
Abrégé.....	11
Acknowledgements	12
Chapter 1 – Introduction.....	13
Chapter 2 – Background & Literature Review.....	14
2.1 – What are Liposomes?	14
2.2 – Liposome Synthesis Techniques	17
2.2.1 – Bangham Method	17
2.2.2 – Detergent-Depletion Method	18
2.2.3 – Direct Injection	19
2.2.4 – Reverse-Phase Evaporation.....	19
2.2.5 – Electroformation.....	20
2.2.6 – Heating	20
2.2.7 – Supercritical Fluid Techniques	21
2.2.8 – High-Pressure Homogenization.....	24
2.2.9 – Dual Asymmetric Centrifugation	24
2.2.10 – Freeze Drying	25
2.2.11 – Freeze Thawing	25
2.2.12 – Crossflow Injection.....	26
2.2.13 – Microfluidic Methods.....	27
2.2.14 – Membrane Contactors	28
2.3 – Bioactive Molecule Loading of Liposomes.....	28
2.3.1 – Passive Encapsulation Methods.....	28
2.3.2 – Active Encapsulation Methods	29
2.4 – Microfluidic Methods for Liposome Synthesis	30
2.4.1 – Microfluidic Electroformation	31
2.4.2 – Extrusion	32
2.4.3 – Flow Focusing.....	33
2.4.4 – Pulsed Jetting	34

2.4.5 – Double Emulsion Templates	35
2.4.6 – Ice Droplet Hydration	37
2.4.7 – Transient Membrane Ejection	38
2.4.8 – Droplet Emulsion Transfer	39
2.4.9 – Discussion	40
Chapter 3 – Objectives	41
Chapter 4 – Materials & Methods	42
4.1 – Channel Design & Fluid Dynamics Modelling	42
4.2 – Materials	45
4.3 – Device Fabrication & Assembly	46
4.4 – Device Flow Visualization	48
4.5 – Microfluidic Liposome Synthesis (Unloaded & Loaded)	49
4.6 – Conventional Liposome Synthesis via Ethanol Injection	51
4.7 – Size Characterization	51
4.8 – Fluorescence Visualization & Measurement	53
4.9 – Statistical Analysis	54
Chapter 5 – Channel Design, Simulations & Flow Visualization	55
5.1 – Device Requirements & Constraints	55
5.2 – Channel Designs & Iterations	58
5.3 – CAD Modelling	62
5.4 – Fluid Junction CFD Simulation	64
5.5 – Qualitative Flow Visualization	67
Chapter 6 – Device Characterization	70
6.1 – DSPC Concentration Optimization	70
6.1.1 – Varying Concentrations at FRR 20	70
6.1.2 – Varying Concentrations at FRR 150	71
6.2 – Flow Rate Ratio Correlation	72
6.3 – Discussion	73
Chapter 7 – Hydrophobic Drug Model Loading	75
7.1 – Particle Diameter Comparison	76
7.2 – Qualitative Assessment of Encapsulation Using Microscopy Techniques	77
7.3 – Fluorescence Emission Spectroscopy	81
7.4 – Discussion	83
Chapter 8 – Conclusions & Future Work	85
8.1 – Summary	85
8.2 – Future Work	87

References	90
Appendix	96
A1 – Microfabrication Steps	96
A2 – Flow Visualization Image Capture Setup.....	97
A3 – CFD Simulations Results	98

List of Figures

Fig. 2.1.1: Liposome formation and classification. A) Liposome Formation – a) Individual phospholipid molecules, b) Lipid bilayer formation, c) Bilayer closure into vesicles, d) Close-up of lipid bilayer. B) Liposome conformations. <i>Adapted from</i> ⁹ , <i>with permission from Annual Reviews</i>	14
Fig. 2.4.1.1: Overview of microfluidic electroformation platform. Channel widths and depths of 300 μm and 500 μm, respectively. <i>Adapted from</i> ⁷³ , © IOP Publishing. <i>Reproduced by permission of IOP Publishing. All rights reserved</i>	32
Fig. 2.4.2.1: Microfluidic extrusion platform with patterned array (middle layer). <i>Adapted from</i> ⁷⁵ , <i>with permission from the Royal Society of Chemistry</i>	33
Fig. 2.4.3.1: Microfluidic flow focusing. Schematic representation of IPA diffusion from flow focusing. <i>Adapted from</i> ⁶⁰ . <i>Not subject to U.S. Copyright</i>	34
Fig. 2.4.4.1: Encapsulation via pulsed jetting. (a) Formation of liposomes with encapsulated material. (b) Demonstration of formation of satellite vesicles. <i>Adapted from</i> ⁷⁷ , <i>with permission from the American Chemical Society</i>	35
Fig. 2.4.5.1: A) Coaxial flow double emulsion templates depicting various flows within device. <i>Adapted from</i> ⁷⁸ , <i>with permission from the American Association for the Advancement of Science</i> . B) Multi-platform process for double emulsion template. <i>Adapted with permission from Tan et al.</i> ⁸⁰ <i>Copyright 2006 American Chemical Society</i>	36
Fig. 2.4.6.1: Microfluidic ice droplet hydration method demonstrated by Sugiura <i>et al.</i> <i>Adapted from</i> ⁸¹ , <i>with permission from the American Chemical Society</i>	37
Fig. 2.4.7.1: Membrane ejection methods. A) (a-c) Flow mechanism for liposome formation, (d) Microbubble generation via IR laser on aluminium grid. <i>Adapted from</i> ⁸² , <i>with permission from John Wiley and Sons</i> . B) Vesicle formation via perpendicular pneumatic side valves. <i>Adapted from</i> ⁸³ , ©2011 IEEE	38
Fig. 2.4.8.1: Droplet emulsion transfer platforms. A) Initial device by Matosevic <i>et al.</i> demonstrating process. <i>Adapted from</i> ⁸⁴ , <i>with permission from the American Chemical Society (ACS Author's Choice)</i> . B) Droplet emulsion with pinched flow by Lu <i>et al.</i> <i>Adapted from</i> ⁸⁹ , <i>with permission from Springer</i>	39
Fig. 4.1.1: Isometric view of channel design with mesh.....	43
Fig. 4.1.2: 2D view of channel design with mesh.....	44
Fig. 4.3.1: Assembled microfluidic device with inlet and outlet tubing. Inlets shall henceforth be referred to by their numerical designation.	48
Fig. 4.7.1: DLS sample data.....	52
Fig. 5.1.1: 'Microfluidic remote loading' by Hood <i>et al.</i> ⁹⁵ : (a-c) Exploded view of device. (d) Assembled device. (e) Fluid pathways within platform. (f) Side view, showing underside inlets for dialysis. <i>Adapted from</i> ⁹⁵ , <i>with permission from the Royal Society of Chemistry</i>	57
Fig. 5.2.1: v1.0 – Simple HFF with Y-junction.....	58

Fig. 5.2.2: v1.5 – Y-junction with curvature for 3D flow focusing	59
Fig. 5.2.3: v2.2.3 – Simple HFF with merged focused flow filets	60
Fig. 5.2.4: v2.3.2 – Dual-sheathe & 30° junction inlets	60
Fig. 5.2.5: v4.0 – Dual sheathe with curved outer channels <i>Not to scale - Dimensions in millimeters (mm)</i>	61
Fig. 5.2.6: v4.1 – Dual sheathe with straight outer channels <i>Not to scale - Dimensions in millimeters (mm)</i>	61
Fig. 5.3.1: v4.0 – Isometric view of 3D model	62
Fig. 5.3.2: v4.1 – Isometric view of 3D model	63
Fig. 5.3.3: Render of assembled v4.0 prototype	63
Fig. 5.3.4: Representative geometry for CFD - Junction of v4.0 & v4.1	64
Fig. 5.4.1: v4.0 Junction CFD simulation for FRR 5	65
Fig. 5.4.2: v4.0 Junction CFD simulation for FRR 50	65
Fig. 5.4.3: v4.0 Junction CFD simulation for FRR 100	66
Fig. 5.4.4: v4.0 Junction CFD simulation for FRR 150	66
Fig. 5.5.1: Flow focusing junction – Diffusion visualization, inlets 2 & 3 only.	67
Fig. 5.5.2: Flow focusing junction – Inlets 1, 2 & 3.....	68
Fig. 5.5.3: Inertial Effects on Sheathe Flow	69
Fig. 6.1.1.1: DSPC:EtOH Concentration vs Particle Diameter at FRR 20.	71
Fig. 6.1.2.1: DSPC:EtOH Concentration vs Particle Diameter at FRR 150.	72
Fig. 6.2.1: Flow Rate Ratio vs Particle Diameter at 3 mg/mL DSPC:EtOH.	72
Fig. 7.1.1: Particle Diameters for Microfluidic Synthesis Methods	76
Fig. 7.1.2: Particle Diameters for Conventional Synthesis Methods.....	76
Fig. 7.2.1: Dehydroergosterol (DHE) Imaged with Various Filters. (A) Optical microscopy, (B) DAPI, (C) TRITC, (D) Cy5.	77
Fig. 7.2.2: Microscopy of DHE On-Chip/Passively Loaded Liposomes (batch B).....	79
Fig. 7.2.3: Microscopy of DHE Actively Loaded Conventional Liposomes (Batch E).....	80
Fig. 7.3.1: Emission Spectra Measurement of Microfluidic Synthesized Batches (Excitation wavelength: 324 nm)	81
Fig. 7.3.2: Emission Spectra of Conventionally Synthesized Batches (Excitation wavelength: 324 nm) ...	82
Fig. A1: Soft lithography protocol.....	96
Fig. A2: Camera setup for flow visualization using food dyes within microfluidic device.	97
Fig. A3-1: v4.0 Junction CFD Simulation for FRR 2	98
Fig. A3-2: v4.0 Junction CFD Simulation for FRR 5	99
Fig. A3-3: v4.0 Junction CFD Simulation for FRR 10	100
Fig. A3-4: v4.0 Junction CFD Simulation for FRR 20	101

Fig. A3-5: v4.0 Junction CFD Simulation for FRR 30	102
Fig. A3-6: v4.0 Junction CFD Simulation for FRR 40	103
Fig. A3-7: v4.0 Junction CFD Simulation for FRR 50	104
Fig. A3-8: v4.0 Junction CFD Simulation for FRR 100	105
Fig. A3-9: v4.0 Junction CFD Simulation for FRR 15	106

List of Tables

Table 4.1.1: Flow Velocities for CFD Simulations	44
Table 4.5.1: Batch description for samples prepared via microfluidic synthesis.	50
Table 4.6.1: Batch description for samples prepared via conventional synthesis.	51
Table 4.8.1: Organization of 96-well plate for spectrophotometry measurements	53
Table 7.1: Batch Descriptions	75

List of Abbreviations

ANOVA	Analysis of Variance
CAD	Computer Aided Design
CCD	Charge-Couple Device
CFD	Computational Fluid Dynamics
CoQ10	Coenzyme Q10
CO ₂	Carbon Dioxide
DAC	Dual Axisymmetric Centrifugation
DC	Direct Current
DHE	Ergost-5,7,9(11),22-tetraen-3 β -ol or Dehydroergosterol
DHE:MeOH	Mixture of DHE and MeOH
DLS	Dynamic Light Scattering
DSPC	1,2-distearoyl-sn-glycero-3-phosphocholine
DSPC:EtOH	Mixture of DSPC and EtOH
EDTA	Ethylenediaminetetraacetic Acid
EtOH	Ethanol or Ethyl Alcohol (Anhydrous)
FRR	Flow Rate Ratio
GUV	Giant Unilamellar Vesicles
HFF	Hydrodynamic Flow-Focusing
HPLC	High Pressure Liquid Chromatography
IPA	Isopropyl Alcohol
ISCRPE	Improved Super Critical Reverse Phase Evaporation
ITO	Indium Tin Oxide
LMV	Large Multilamellar Vesicles
MeOH	Methanol or Methyl Alcohol
MEMS	Microelectromechanical Systems

MilliQ	Ultra-pure water from Millipore filtration system
MLV	Multilamellar Vesicles
PDMS	Polydimethylsiloxane
Re	Reynolds Number
RFU	Relative Fluorescence Units
SUV	Small Unilamellar Vesicles
SCRPE	Super Critical Reverse Phase Evaporation
TFF	Tangential Flow Filtration
w/o/w	Water-in-Oil-in-Water
w/w ratio	Weight to Weight ratio
3D	Three Dimension(al)

List of Equations

Eq. (2-1)	Reynolds Number	29
Eq. (4-1)	Navier-Stokes Equation (Vector Notation)	41
Eq. (4-2)	Continuity Equation	41
Eq. (4-3)	Flow Rate Ratio	43

Abstract

Liposomes are currently well-established as biocompatible vehicles for the delivery of a range of bioactive molecules, such as the anthracycline doxorubicin, for cancer therapy, or enzymes for industrial processes, such as cheese ripening agents in the dairy industry. However, these nanoparticles manufactured via conventional techniques tend to rely on time-consuming processes, costly and cumbersome equipment, synthesis under unstable reaction parameters and several pre- and post-processing steps. Herein, we introduce a simple alternative: a double flow-focusing microfluidic geometry capable of the rapid one-step synthesis and controlled loading of liposomes. Not only does it allow for more precise reaction control, but it also reduces the synthesis time from days to hours compared to traditional solvent evaporation methods. With 1,2-distearoyl-sn-glycero-3-phosphocholine lipid as the liposome building block, we demonstrated an inverse relation between flow rate ratio and particle diameter, and observed no characteristic trend with regards to the latter and increasing lipid concentration. Furthermore, ergost-5,7,9(11),22-tetraen-3 β -ol, a fluorescent hydrophobic drug model, was encapsulated on-chip, visualized using fluorescence microscopy and qualitatively assessed via spectrophotometry. Our results validate this easy-to-use platform as a viable alternative to the current laborious liposome production protocols, as well as the possibility of on-chip bioactive agent loading within these vesicles.

Abrégé

Les liposomes sont actuellement bien établis comme étant des modes de transport pour véhiculer plusieurs types de molécules bioactives, telles que l'anthracycline doxorubicine pour les thérapies anticancéreuses. Ils sont également utilisés dans l'industrie alimentaire, en particulier dans l'industrie des produits laitiers pour encapsuler des enzymes. Cependant, les procédés de fabrication conventionnels ont tendance à être longs, onéreux et encombrants. En outre, ils requièrent une multitude d'étapes additionnelles. Nous proposons ici une alternative simple: un dispositif microfluides à focalisation de flux double permettant la synthèse et le chargement rapide et contrôlé des liposomes. Contrairement aux méthodes traditionnelles d'évaporation de solvant, ce procédé nous procure un contrôle précis de la synthèse tout en permettant de diminuer significativement la durée de la fabrication des liposomes. Ainsi, en utilisant le 1,2-distearoyl-sn-glycero-3-phosphocholine, nous démontrons une relation inverse entre le ratio du débit et le diamètre des liposomes. Cependant nous n'observons aucun lien entre le diamètre de ces dernières et l'augmentation de la concentration des lipides. De plus, l'encapsulation sur puce d'un modèle fluorescent de médicament hydrophobe, notamment l'ergost-5,7,9(11),22-tetraen-3 β -ol, a été évaluée par microscopie fluorescente et spectrophotométrie. Nos résultats confirment que la plateforme est simple d'utilisation et peut être considérée comme étant une alternative très prometteuse aux protocoles de synthèse de liposomes actuels, ainsi que son éventuelle utilisation en tant que moyen d'encapsulation de diverses molécules bioactives, soit hydrophile ou hydrophobe, et ceci sur un seul dispositif fluidique.

Acknowledgements

First and foremost, I would like to express immense gratitude to my supervisor, Prof. Maryam Tabrizian, for having given me this opportunity to further my knowledge in this innovative and rewarding field. I would like to also thank her for having taken a chance on me and having faith in my ability to excel. Her advice, suggestions, feedback and motivation were all crucial to the completion of this project.

Secondly, I would like to thank Dr. Jamal Daoud, Dr. Mina Mekhail & Dr. Kristen Bowey for their guidance, advice and recommendations throughout my project. On that same note, equal thanks goes out to all of the Biomat'X Research Laboratories members, Samira Taherkhani, Lamees Nayef, Sandrine Filion-Côté, Kaushar Jahan, Rosey Rasoda, Laila Benameur, Dr. Amir Foudeh, Khalil Heileman, Rafael Castiello-Flores & Timothy Johns, for providing such an awesome, wonderful and fulfilling (knowledge and hunger-wise) work environment, one to which I did not mind going to day after day. I would also like to thank Ms. Pina Sorrini & Ms. Nancy Abate for their wonderful help and advice regarding administrative matters.

In the McGill Nanotools-Microfab, I would like to acknowledge John Li & Seddik Benhammedi for having taken the time to train me on all the necessary equipment, as well as for the assistance with the HF bench!

I am extremely thankful for the love and support of my parents, my grandmother and my brothers throughout all of these years. Thank you for always checking up on me, making sure everything was alright and keeping me sane in the tougher times.

Last but not least, all of my friends who have been there to support me along the way, especially Jun Xiao, Alexander Capozzi, Kyriakos Moditis & Ihsan Mas. A very special thank you goes out to Krista Leetmaa & Leif Tiltins for being instrumental in getting me through these last couple of months, and to Alice, for all those random out-of-town impromptu trips.

Chapter 1 – Introduction

Liposomes, since their discovery by Bangham *et al.* in 1965,¹ have been used in many areas, ranging from drug delivery platforms^{2,3}, to cosmetics⁴ to food nanotechnology⁵. As a drug delivery vehicle, these multi-faceted lipid nanocapsules offer many advantages including longer circulation times within the body, protection and controlled release of the encapsulated compounds and the ability to overcome biological barriers necessary for targeted delivery.⁶

However, despite their numerous advantages, the processes necessary for the synthesis of these vesicles tend to rely on bulky, cumbersome equipment, are very time consuming, require large reagent volumes and necessitate multiple apparatuses for encapsulation. Herein, in order to address the aforementioned issues, we developed a straightforward, low-cost microfluidic device with novel geometries for a one-step liposome synthesis and bioactive agent encapsulation platform.

The following sections will introduce liposomes, the conventional synthesis methods, encapsulation techniques and recent developments with regards to microfluidic fabrication. The objectives and materials and methods are then established. Furthermore, the design process and validation is described. Moreover, liposome synthesis and molecule encapsulation is performed and characterized. Finally, we conclude with a summary and future considerations.

Chapter 2 – Background & Literature Review

2.1 – What are Liposomes?

Liposomes are dual-layered phospholipid capsule-like particles, commonly referred to as vesicles, that were discovered by Alec D. Bangham and colleagues in 1965.¹ Owing to their similarity, they were initially used as a model membrane for cell membrane studies.⁷ Phospholipids are naturally occurring compounds which consist of a polar and non-polar segment (Fig. 2.1.1A(d)).⁸ The non-polar tail-end is made up of a hydrophobic diglyceride chain, meaning two chains consisting of carbon, hydrogen and oxygen atoms. On the other hand, the polar head, composed of a phosphate group, is hydrophilic. The combination of these two parts thus results in a molecule that is amphiphilic.⁹

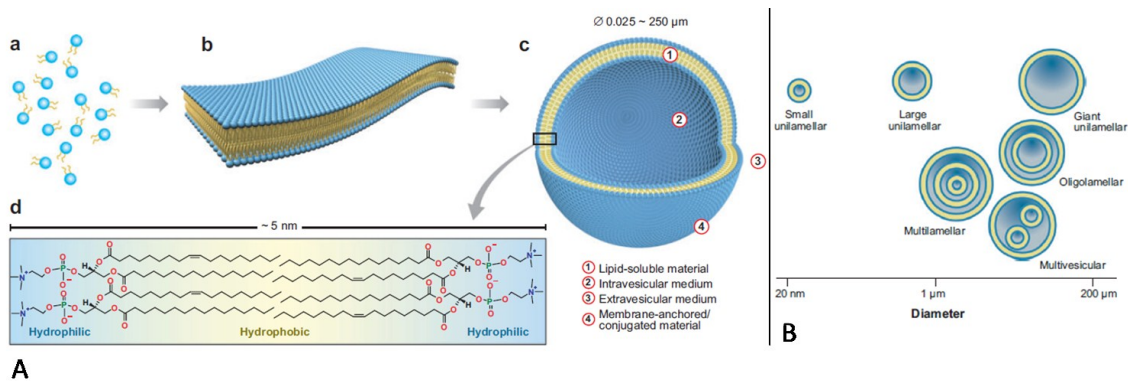


Fig. 2.1.1: Liposome formation and classification. A) Liposome Formation – a) Individual phospholipid molecules, b) Lipid bilayer formation, c) Bilayer closure into vesicles, d) Close-up of lipid bilayer.

B) Liposome conformations. *Adapted from ⁹, with permission from Annual Reviews.*

Due to the amphiphilic nature of these molecules, their biocompatibility and their versatility, liposomes have not only found a place in medicine and pharmacology, but in the realms of cosmetics and food science as well. The following examples demonstrate some of the possibilities of this multi-faceted compound. An important contribution to the use of liposomes in therapeutic treatments was the investigation performed by Barenholz *et al.* demonstrating increased circulation time and improved accumulation of doxorubicin, an anthracycline used for cancer therapy, encapsulated within a polyethylene-glycol coated liposome formulation.¹⁰ A more recent development is combination of nanoliposomes with self-propelled magnetotactic bacteria by Taherkhani *et al.* for improved control over targeted delivery of therapeutic or imaging compounds.¹¹

Cosmetceuticals refers to the nomenclature given to the combination of cosmetics and pharmaceuticals. Rahimpour *et al.* provide a comprehensive overview of recent developments in the field.⁴ A potentially more known example would be coenzyme Q10 (CoQ10) encapsulated within liposomes, as demonstrated by Lee *et al.*, used to improve the efficacy of topically applied CoQ10 to reduce wrinkles caused by photoaging.¹² With regards to the food nanotechnology sector, we refer the reader to the review by Mozafari *et al.* for a concise summary.⁵ Within that domain, Larivière *et al.* previously demonstrated that the enzyme trypsin could be encapsulated into liposomes via a Microfluidizer™ and used to accelerate the cheese ripening process.¹³ Other encapsulable compounds also include antimicrobial agents, vitamins or flavouring.¹⁴

The actual mechanism of vesicle formation is fairly complex,¹⁵ and goes beyond the scope of this review. However, put simply, and somewhat dependent on the fabrication method, the individual phospholipid particles align tail to tail, i.e. hydrophobic-end-to-hydrophobic-end, and form phospholipid bilayer sheets (see Fig. 2.1.1 A(b)). This bilayer conformation is highly unstable, and when they reach a certain length, the sheets fold upon themselves and form the liquid-filled vessels, or liposomes (see Fig. 2.1.1 A(c)).

Liposomes are not always unilamellar, meaning to consist of a single layer, but come in a variety of configurations (see Fig. 2.1.1B). They are additionally classified by size, ranging from small, in the nanoscale, to giant, in the upper-microscale. With regards to their conformation, firstly there are unilamellar liposomes, as seen in Figs. 2.1.1 A(c) & B (top row), which consist simply of one phospholipid bilayer. Secondly, there are the oligolamellar particles, which are vesicles consisting of a few concentric layers. Thirdly, there are the multilamellar vessels (MLV), which are composed of numerous concentric lamellae. Finally, multivesicular liposomes are made up of several non-concentric vesicles.⁹

Size classification of liposomes ranges from the nanoscale to the upper microscale (see Fig. 2.1.1 B). Nanoscale vesicles, below 400 nm in diameter, are typically referred to as being small. The second classification is the large particles,

encompassing molecules ranging from 400 nm to several microns. Finally, there are the giant liposomes, which are greater than 200 μm in diameter.⁹ These classification terms are oftentimes combined to create more general categorisation groups, such as small unilamellar vesicles (SUV), large multilamellar vesicles (LMV)¹⁶ and giant unilamellar vesicles (GUV), to name a few.

2.2 – Liposome Synthesis Techniques

Modern preparation procedures, utilizing present-day microfabrication methods or supercritical fluid setups, were not available when liposomes were discovered; the particles had to be synthesized using crude, cumbersome and bulky manufacturing methods. These processes have become the norm in industry and in academia. The methods used by the majority of the scientific, food and even cosmetics community have remained fairly unchanged in the past decades. The procedures usually revolve loosely about the following three steps: i) the dissolution of the phospholipid in an organic solvent, ii) the dispersion of said mixture in an aqueous phase, and iii) the post-processing of the liposomes to achieve desired sizes and configurations.¹⁷ The following sub-sections describe the conventional methods, as well as some of the more recent developments.

2.2.1 – Bangham Method

The Bangham method¹, named after the researcher that discovered this vesicle, involves dissolving the chosen lipids in an organic phase, the evaporation of the solvent

under vacuum, and the eventual formation of a lipid film. Finally, dispersion and rehydration is carried out simultaneously with agitation, or vortexing, to remove the molecules from the vessel surface, which leads to the formation of spherical capsules. This synthesis method usually produces MLVs on the order of several microns, which can in turn be filtered to produce smaller more uniform particles.⁹ This method is however, not feasible for large-scale production, or methods requiring large amounts of uniform product. Another drawback is caused by the initial solvent removal step, which is very time-consuming.¹⁷

2.2.2 – Detergent-Depletion Method

The detergent-depletion method is a process that does not follow the characteristic bilayer sheet formation of liposome synthesis. It is a mild technique which consists of the initial formation of detergent-lipid inverse micelles, which are spherical single-layer phospholipid aggregations with the polar, hydrophilic heads, located at the center. The detergent acts to block the hydrophobic tail from any interaction with the aqueous phase, allowing the phospholipids to form inverse micelles. The detergent is then removed by dilution, and the now-uncovered hydrophobic ends are left to bind to “free” phospholipids suspended in the solution.¹⁸ The final outcome of this process is dependent on both the detergent removal rate, as well as the initial phospholipid:detergent ratio.¹⁹ However, in addition to being time consuming, this method occasionally results in leeching out of encapsulated molecules.

2.2.3 – Direct Injection

This process involves the injection of lipids dissolved in an organic medium into the aqueous buffer, which ultimately leads to the formation of lipid vesicles. The organic phase in this case is usually either ethanol or ether.¹⁹ The first instance of this process was described by Batzri and Korn in 1973, whereby the ethanol injection utilizes a very fine needle to inject the lipid solution evenly into the aqueous media.²⁰ Another injection method uses ether as the organic phase while preserving the same setup.^{21,22} The main difference, and advantage, of this latter method is that unlike ethanol injection, the ether is completely removed from the final product. On the other hand, in the ethanol injection method, the organic phase sometimes remains within the final product, which could be detrimental to the encapsulated molecules. This synthesis method typically leads to larger vesicles. Nevertheless, post-processing filtration, as with the Bangham method, can bring them down to the desired size.²³

2.2.4 – Reverse-Phase Evaporation

The reverse-phase evaporation method, first demonstrated by Szoka in 1978 consists of the lipid initially dissolved in an organic solvent, albeit with a small volume of the aqueous buffer.²⁴ The mixture is then sonicated, or agitated, which results in the formation of inverted micelles, which has been previously described. Using a rotary evaporator, commonly referred to as a rotavap, the solvent is then removed, and all that remains is a thin film of phospholipids. Finally, the mixture is then rehydrated, which

results in the formation of liposomal vesicles.^{17,19} Although dependent on the molecule loading method, which will be described in the following section, this process could potentially affect fragile molecules if they were included in the initial aqueous phase due to contact with organic solvents.

2.2.5 – Electroformation

This process, demonstrated in 1985 by Angelova and Dimitrov, relies on the use of external electric fields for the formation of liposomes from dried thin films. The dissolved lipids are dropped onto parallel electrodes and the solvent is evaporated under a stream of nitrogen. This process could be repeated to achieve multiple layers. The external electric field, at a DC voltage below 3 V to prevent the formation of gas bubbles, is applied and the aqueous media is added. These conditions cause budding of the layers off from the electrode surface, and the eventual formation of vesicles. For thicknesses below 10 bilayers, they synthesized giant vesicles of approximately 30 μm in diameter with a relatively narrow size distribution.²⁵

2.2.6 – Heating

The heating method, adapted to liposome synthesis in the early 2000s by Mozafari *et al.*, is a technique which aims to minimize the use of volatile solvents simply by the use of heat and some post-processing.²⁶ The phospholipids are separately hydrated for over an hour and are then combined with glycerol at temperatures up to 120°C in a silicone oil bath. The glycerol is used as an alternative to harsher solvents

used in the other conventional synthesis techniques.²⁷ This hydrophilic, non-toxic agent, also does not necessitate full removal from the preparation in part from its ability to act as a dispersant to aid with preventing the formation of aggregates, ultimately improving the stability of the liposome preparation.²⁸ The temperature at which the solutions are combined depends on the presence of sterols in the liposome formulation. If the mixture consists entirely of phospholipids, the sample can be prepared at lower temperatures (60 - 70°C), due to the majority of phospholipids having their transition temperatures below 60°C.²⁹

2.2.7 – Supercritical Fluid Techniques

Supercritical fluids refer to substances which are above their critical point. The latter refers to the temperature and pressure at which the liquid and gaseous phases become indistinguishable.³⁰ This enables the substance to uphold both solvation properties of the liquid phase and the mass transport characteristics of the gaseous phase, and thus acts as a highly effective, tunable solvent.³¹ These properties have enabled supercritical fluids to substitute harsh organic solvents in processes such as separation, purification or size reduction.³²⁻³⁴ With regards to liposome synthesis, carbon dioxide (CO₂) is typically used since it has reasonable critical parameters (304.19 K and 73.82 bar)³⁵, is non-flammable, non-toxic, non-corrosive, inexpensive and environmentally acceptable.¹⁷ Unlike other harsh solvents, the CO₂ can afterwards be removed and recovered simply by exposure to atmospheric conditions. This

processing method also enables for synthesis under sterile operating conditions, and can ease issues related to current liposome sterilization.^{31,36} However, in addition to necessitating complex equipment and very elevated pressures and temperatures, these techniques also require highly trained technicians to perform the synthesis.¹⁹

2.2.7.1 – Supercritical Fluid Decompression and Injection

First described by Castor and Chu in a patent issued in 1998, the decompression and injection methods were developed as a means for large scale synthesis of pharmaceutical grade liposomes which are sterile, of a controllable size, and relatively free of harmful organic solvents.³⁷ In the decompression method, the phospholipid, hydrophobic drug, aqueous phase and critical fluid is mixed, and is in turn decompressed to remove the solvent from the blend. The rate at which the solvent is removed by depressurization would ultimately determine the final size of the formed liposomes. With regards to the injection method, an initial mixture of lipid, hydrophobic drug and compressed fluid is prepared, and subsequently injected into an aqueous phase. The pressurized gas is then returned to its atmospheric state, where it can preferably be recycled for further use. These processes have been shown to produce liposomes of a chosen size with narrow polydispersity.³⁸

2.2.7.2 – Supercritical Fluid Method

Similar to the aforementioned method, the supercritical liposome method consists of a mixture of a phospholipid and cholesterol dissolved under pressure in

supercritical CO₂, which is then injected into an aqueous phase containing a hydrophilic compound.³⁹ The main difference with this method developed by Frederiksen *et al.* is the encapsulation of a water-soluble molecule. They have demonstrated the ability to produce SUVs with an average size of 200 nm. Although this method is an improvement on the ethanol injection method developed by Batzri and Korn,²⁰ the overall encapsulation efficiency was lower than what has been achieved with other conventional synthesis methods.³⁹

2.2.7.3 – Supercritical Reverse Phase Evaporation (SCRPE)

By combining the reverse phase evaporation method developed by Szoka²⁴ and the advantages of using supercritical fluids, Otake *et al.* developed the technique known as supercritical reverse phase evaporation.³¹ Also referred to as SCRPE, this method combines the lipid, organic co-solvent and the pressurized gas into a variable volume view cell with mixing capabilities at a temperature above the phase transition temperature of the lipid, all while keeping the pressure constant. After attaining equilibrium, an aqueous phase is gradually introduced via a high-performance liquid chromatography (HPLC) pump, the pressure is lowered by the release of the supercritical fluid, and liposomes are formed. In comparison to the Bangham method, Otake *et al.* achieved a 5-fold increase in encapsulation using a hydrophilic compound, and a 63% increase using a hydrophobic molecule. Further development on this method

by the same group led to the improved supercritical reverse phase evaporation method (ISCRPE), which endeavoured to eliminate the use of organic solvents.⁴⁰

2.2.8 – High-Pressure Homogenization

High-pressure homogenizers, also referred to as microfluidizers⁴¹, are devices which utilize high pressures and fixed-geometry micro-channels to produce solutions with a uniform particle distribution.^{42,43} The sample enters at a set inlet pressure and is then divided into streams in the reaction chamber. The streams reconverge with high shear and impact forces, resulting in a solution with very fine particles. A cooling coil is an optional addition to the process. The characteristics of the solution prepared by high-pressure homogenization ultimately depends on the pressure, as well as the number of passes through the cycle.⁴¹ The utilization of microfluidizers tends to produce very small unilamellar liposomes, which is better suited for intravenous applications.¹⁹

2.2.9 – Dual Asymmetric Centrifugation

Dual asymmetric centrifugation, or DAC, is a type of centrifugation in which the samples are not only spun about a central rotation axis, but with an additional counter-rotating motion about the central axis of the vessel encompassing the sample.⁴⁴ The former results in motion of the sample towards the outside of the centrifuge, and the latter continuously forces the material towards the center of the centrifuge, thus causing high shear forces, resulting in an efficient means for homogenization. Massing *et al.* first demonstrated in 2008 the ability to synthesize 60 nm liposomes with a size distribution

of ± 5 nm.⁴⁴ More recently, Adrian *et al.* adapted DAC for the production of liposomes for targeted delivery of siRNA to neuroblastoma cells.⁴⁵

2.2.10 – Freeze Drying

The freeze drying method, proposed by Li *et al.*, is a process whereby the lipids and sucrose are dissolved in a co-solvent solution, tert-butyl alcohol/water, to produce a uniform, transparent monophasic solution.⁴⁶ The mixture is then sterilized via filtration through 0.22 μm pores, and subsequently lyophilized using a lab-grade freeze dryer. Once the lyophilization process was over, the samples are filled with nitrogen gas, sealed, and stored at 4°C.⁴⁷ An aqueous solution, water in this case, is then added to the product, and a homogeneous mixture of nanoliposomes is formed. Wang *et al.* have equally demonstrated the ability of this synthesis method to encapsulate either hydrophobic or hydrophilic compounds.⁴⁸ However, they equally determined that when bioactive molecules are simply loaded passively, the encapsulation efficiency is fairly low.

2.2.11 – Freeze Thawing

The freeze-thaw technique is a process that involves the preparation a desired liposome solution, freezing said mixture at -196°C in liquid nitrogen, and then thawing at a temperature above the transition temperature of the phospholipid.⁴⁹ The freeze-thaw cycle may be repeated to further achieve specific results, such as reducing the number of bilayers⁵⁰, lowering the polydispersity of the system⁵¹, or increasing the amount of

molecules being encapsulated⁵². A recent study by Costa *et al.*, in addition to including an annealing step, demonstrated the importance of cryo-concentration, or fusion/destabilization of the liposomes, on the actual mechanism behind the encapsulation via freeze-thaw cycling.⁵³ By better understanding the fundamentals behind entrapment, they were able to eliminate the need for additional freeze-thaw cycles, or post-processing techniques.

2.2.12 – Crossflow Injection

Developed by Wagner *et al.*, the crossflow injection method is an enhancement of the classic ethanol injection process developed in the 70s.⁵⁴ As opposed to being simply injected into a bulk volume of buffer, the ethanol/lipid blend, via a nitrogen pressure device, is slowly introduced into a strongly shearing buffer solution within an “injection module”.⁵⁵ The aforementioned device consists of two stainless steel tubes welded together to form a perpendicular junction. The orifice connecting the channels is created by electrical discharge machining, resulting in drill holes of 150 and 250 μm .⁵⁵ With such a setup, changes in the lipid concentration, injection hole sizing, nitrogen introduction pressure and aqueous buffer flow rate all influence the final liposome qualities.^{55,56} More recently, Zhong *et al.* adapted and simplified the crossflow injection method, by replacing the labour-intensive stainless steel injection module with a plastic Y-connector, and demonstrated the feasibility of such a technique for large scale

applications, in this case, drug loaded nanoliposomes synthesized for hepatocellular carcinoma therapy.⁵⁷

2.2.13 – Microfluidic Methods

Microfluidics has been a tool utilized by many research groups as of late as an important tool for numerous applications ranging from pathogen detection⁵⁸ to drug screening⁵⁹. These devices allow for more efficient and controlled reactions due to larger surface area to volume ratios and improved manipulation of reagent volumes. Recently, microfluidics have been adapted for use in the synthesis of liposomes, with the first mention in 2004, by Jahn *et al.*⁶⁰ Their method, also an adaptation of the ethanol injection technique, consisted of hydrodynamically focusing, in two-dimensions, a phospholipid/isopropyl alcohol mixture between two aqueous buffer streams, within a microfluidic junction with a channel depth of 40 μm and maximum width of 200 μm . By adjusting the rate of flow of each stream, a very narrow, sub-micrometer sheath could be formed in which diffusive mixing occurs. The latter then resulted in the self-assembly of liposomes at the fluid interface. Hood *et al.* have recently demonstrated the ability to manufacture a three-dimensional device able to produce fairly monodisperse solutions of small (<200nm) liposomes.⁶¹ Section 2.4 will delve further into the recent developments regarding microfluidic liposome synthesis.

2.2.14 – Membrane Contactors

Membrane contactors have previously been used for the preparation of emulsions, precipitates and polymeric and lipidic nanoparticles, but have only recently been applied to the realm of liposome synthesis.⁶² The membrane in this case refers to the tubular membranes, porous glass in this instance, used as an intermediate step between the organic and aqueous phases of the process. Typically, an aqueous phase is pumped through the inner core, and the organic phase flows tangentially via a pressurized vessel.^{62,63} Depending on the solvent and buffer choice, the particles may either be formed via precipitation, or emulsion. When used for liposome synthesis, Laouini *et al.* demonstrated the ability to produce small multilamellar vesicles with an entrapment efficiency of 93%.⁶⁴

2.3 – Bioactive Molecule Loading of Liposomes.

2.3.1 – Passive Encapsulation Methods

Passive encapsulation of bioactive molecules refers to the method whereby the agent is loaded into the liposome without any external force. The majority of these processes occur during the vesicle formation stages of some of the aforementioned synthesis methods. The most common method for passive encapsulation is the thin film, or Bangham, method. As previously described, a thin lipid bilayer is formed, however, rehydration is then performed with a solution containing the desired biomolecule. Upon rehydration, invagination and swelling of the membrane occurs, resulting in the

encapsulation within the vesicle of a certain volume of the aqueous mixture.^{15,65}

Although this is a fairly simple method for encapsulation, the actual volume entrapped is fairly minimal, and may be well below the therapeutic dosage required.

2.3.2 – Active Encapsulation Methods

In order to address the aforementioned issue of low encapsulation amounts, techniques were devised in order to load the vesicles after their synthesis. These methods usually rely on the formation of a chemical gradient between the aqueous core and the external environment. Deamer and Nichols were the first to demonstrate such a method, initially in order to determine the feasibility of creating such gradients in model membranes and the potential ability for uptake and concentration of catecholamines (e.g. dopamine, norepinephrine, and epinephrine).^{66,67} A pH gradient between the internal and external domains was generated by synthesizing the liposomes in a low pH citrate buffer, and subsequently adding a basic solution to achieve a gradient of approximately 3 units (5.0 within and 8.0 in the external media). The bioactive agents diffuse into the intravesicular space and undergo a chemical transformation, which then results in the entrapment of the compound within the liposome. Other methods used to incorporate compounds into liposomal cores include the ammonium sulfate gradient developed by Haran *et al.*⁶⁸, the transmembrane acidic ammonium phosphate gradient demonstrated by Fritze *et al.*⁶⁹, or the ethylenediaminetetraacetic acid (EDTA) ion gradient method by Gubernator *et al.*⁷⁰ The aforementioned methods, due to the

encapsulation mechanism, typically yield high encapsulation efficiencies approaching 100%.

2.4 – Microfluidic Methods for Liposome Synthesis

As previously described, microfluidics is a useful tool for the synthesis of nano- and microparticles. In addition to the aforementioned techniques devised by Jahn *et al.*⁶⁰ and Hood *et al.*⁶¹, there are many other methods ranging from facile methods relying on simple T-junctions and syringe needles, to other more complex techniques like the ice hydration process.

In these systems, the fluid flow is characterized by the Reynolds number (Re), a ratio between the inertial forces and viscous forces, which is defined as:

$$\text{Re} = \frac{\rho v L}{\mu} \quad (2-1),$$

where ρ and μ denote the fluid density and viscosity respectively, and v and L represent characteristic velocities and lengths.⁷¹ In microfluidic systems, the latter values are usually taken to be the working fluid velocity and channel width. A large Re denotes that inertial forces take precedence over viscous forces, and vice versa. Fluid flow can be categorized into several regimes, notably laminar, transient and turbulent. Typically, for Re below 2300, the flow is considered to be laminar, which is the case in microfluidic systems, as the characteristics lengths are usually on the order of millimeters or less.

Microfluidic processes can further be categorized into being active or passive, which refer to the method whereby the process occurs. Active methods typically

encompass techniques which require external energy input to the system, such as the electroformation and transient membrane ejection methods described below. On the other hand, passive techniques simply rely on the fluid flow within the device to perform their functions, such as the flow focusing or double emulsion templates explained below.⁷²

The following sections will briefly cover the state-of-the-art in liposome synthesis using microfluidic methods.

2.4.1 – Microfluidic Electroformation

Taking upon the work demonstrated by Angelova and Dimitrov, previously described in section 2.2.5, Kuribayashi *et al.* adapted this process to a microfluidic platform in order to reduce the amount of buffer required to rehydrate the lipid layers.⁷³ Their device consisted of a simple channeled silicone sheet enclosed between ITO glass sheets. The electrode preparation steps were as previously described. In addition to the formation of mainly giant unilamellar vesicles, they also demonstrated the ability of on-chip encapsulation by using fluorescent nano-/micro beads suspended in the hydration buffer.

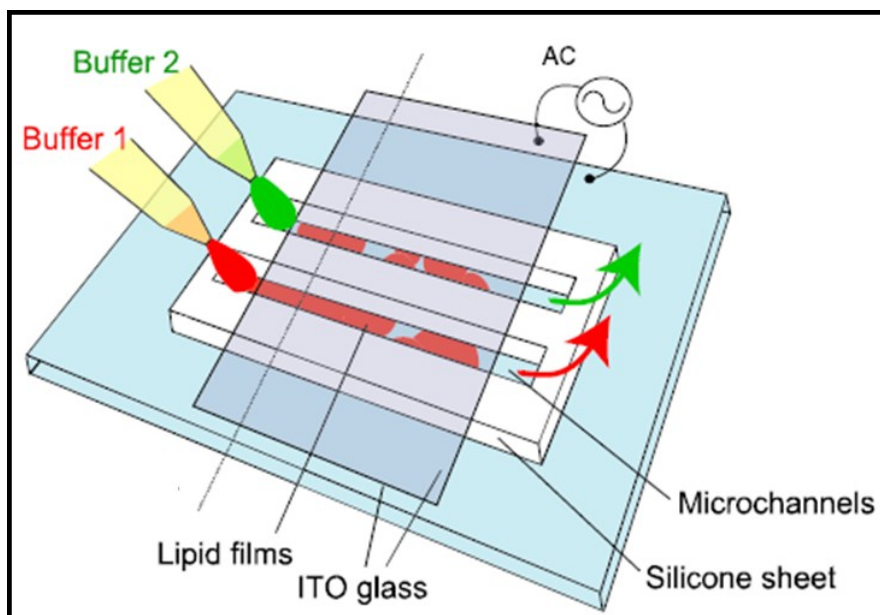


Fig. 2.4.1.1: Overview of microfluidic electroformation platform. Channel widths and depths of 300 μm and 500 μm , respectively. Adapted from ⁷³, © IOP Publishing. Reproduced by permission of IOP Publishing.

All rights reserved

2.4.2 – Extrusion

Initially demonstrated by Olson *et al.* as a means to decrease the polydispersity of lipid vesicle solutions, this method is traditionally used as a post-processing step to achieve specific liposome sizes.⁷⁴ Once the liposome solution is prepared, it is extruded through a polycarbonate membrane. This results in a monodisperse solution consisting mainly of unilamellar vesicles. The sample can also be extruded multiple times to achieve a more uniform solution.

Dittrich *et al.* devised a method whereby a silicon chip patterned with an array of holes is temporarily used as a dried lipid bilayer frame that is sandwiched between channeled polydimethylsiloxane (PDMS).⁷⁵ The device is assembled by simple

adhesion. A buffer is introduced from the top, which results in the formation of lipid structures either vesicles, cylinders or even tubules, and is harvested from the bottom channels. Utilizing this process, they achieved synthesis of giant unilamellar vesicles with fairly large polydispersity.

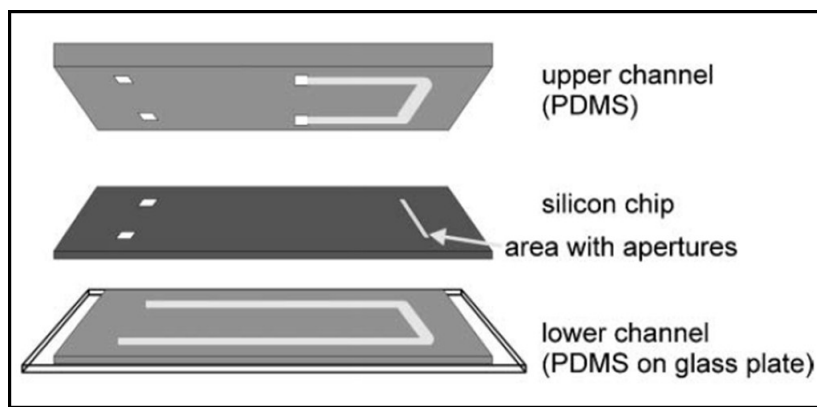


Fig. 2.4.2.1: Microfluidic extrusion platform with patterned array (middle layer).

Adapted from ⁷⁵, with permission from the Royal Society of Chemistry.

2.4.3 – Flow Focusing

Fig. 2.4.3.1 demonstrates the theorized synthesis of liposomes within a flow focusing method, as devised by Jahn *et al.*⁶⁰ However, the microfabrication facilities required to manufacture the devices described in section 2.2.13 may not always be readily available, and thus, render the accessibility of such platforms difficult to certain groups wishing to pursue such research. In order to address this, Pradhan *et al.* demonstrated a simple method for liposome synthesis using nothing more than a syringe pump, syringes, needles, an elbow connector and plastic tubing.⁷⁶ Utilizing this

straightforward method, they attained the synthesis of sub-300 nm particles. They did not, however, comment on the lamellarity of the particles, nor the polydispersity.

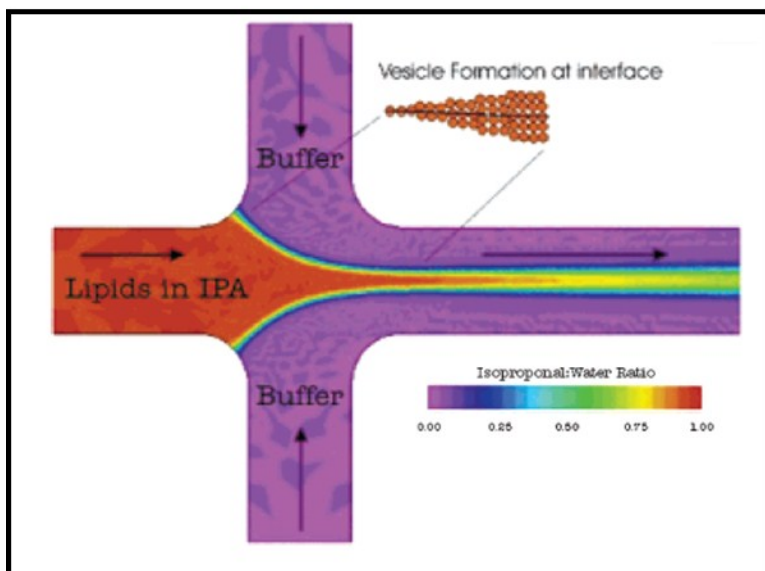


Fig. 2.4.3.1: Microfluidic flow focusing. Schematic representation of IPA diffusion from flow focusing.

Adapted from ⁶⁰. Not subject to U.S. Copyright.

2.4.4 – Pulsed Jetting

This process has no liposomal synthesis macroscale analog; however, it is reminiscent of the action of blowing a soap bubble from a thin film. This method, developed for liposomes by Funakoshi *et al.* consists of forming a lipid bilayer membrane from separate monolayers and using a fine needle or nozzle in close proximity to dispense a fine amount of aqueous buffer at a high flow rate towards the film.⁷⁷ Due to the high speed, the ejected volume is encompassed within the layer as it passes through, and eventually results in a lipid vesicle. This method has the advantage of fully encapsulating the liquid being dispensed, however, this could potentially also

include the solvent used as the buffer. One drawback, for pharmaceutical applications, of this technique is the large ($\varnothing = 300 - 600 \mu\text{m}$) unilamellar vesicles formed. Additionally, this process occasionally results in the formation of “satellite” vesicles from the trailing bilayer.

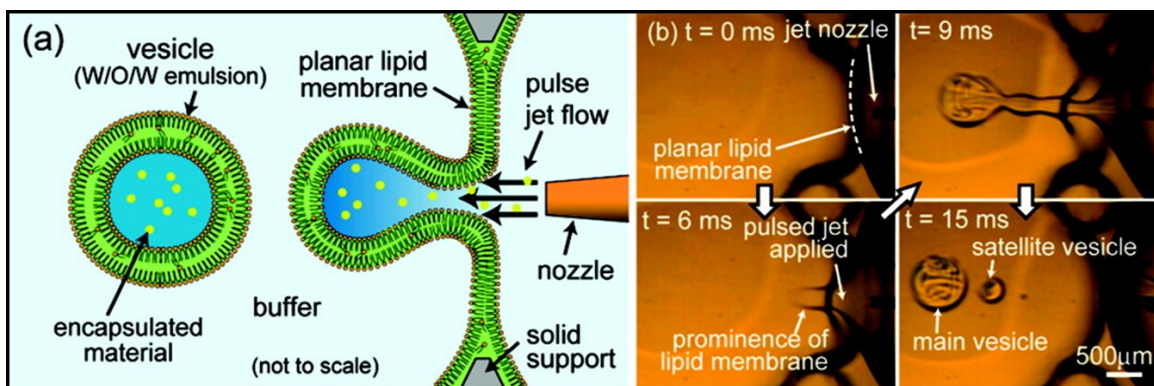


Fig. 2.4.4.1: Encapsulation via pulsed jetting. (a) Formation of liposomes with encapsulated material.

(b) Demonstration of formation of satellite vesicles.

Adapted from ⁷⁷, with permission from the American Chemical Society

2.4.5 – Double Emulsion Templates

This process, adapted from the glass microcapillary work demonstrated by Utada *et al.*⁷⁸, consists of using a continuous-flow water-in-oil-in-water (W/O/W) system to generate liposomes. This method, previously used to create diblock copolymer polymersomes, was modified by Shum *et al.* to allow for the gentle removal of the solvent from the resulting W/O/W emulsions.⁷⁹ When used with phospholipid emulsions, the solvent evaporation step resulted in bilayer disruption. By reducing the evaporation rate, they diminished the occurrence of bilayer breakage. Another modification to the process was the solvent removal via dialysis with an anodized alumina filter.

Tan *et al.* demonstrated a similar process utilizing a channel-patterned PDMS device.⁸⁰ The platform consists of using a T-junction to create a phospholipid micelle with an aqueous core. The sample is then harvested and pipetted into an ethanol/water solution. The original solvent dissolves into the ethanol, and the remaining dissolved phospholipid molecules are forced to form a bilayer with the micelles, and ultimately, lipid vesicles.

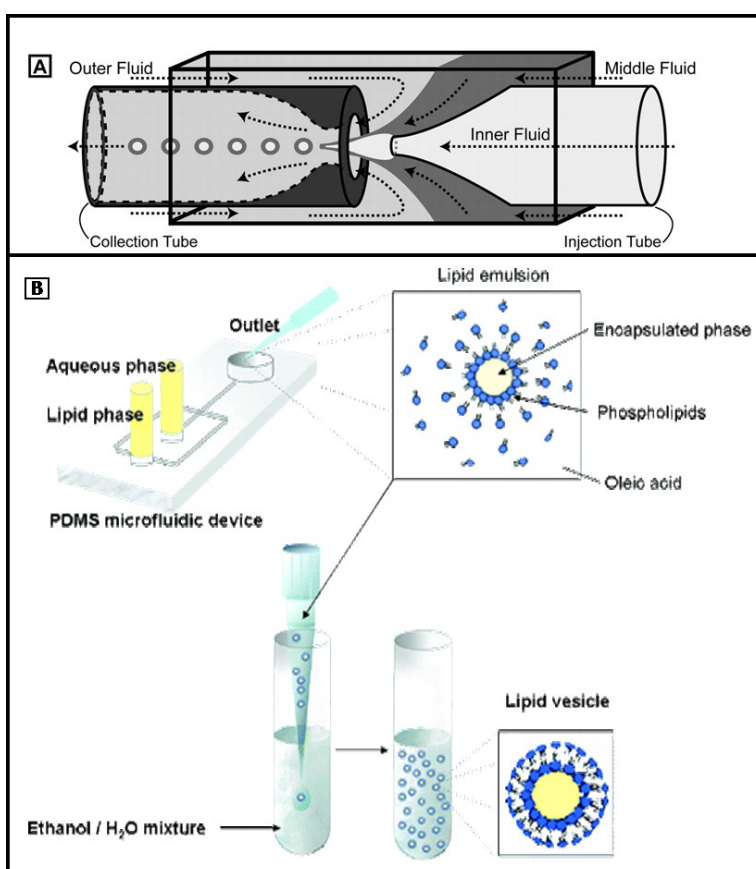


Fig. 2.4.5.1: A) Coaxial flow double emulsion templates depicting various flows within device. Adapted from⁷⁸, with permission from the American Association for the Advancement of Science. B) Multi-platform process for double emulsion template. Adapted with permission from Tan *et al.*⁸⁰ Copyright 2006

American Chemical Society.

2.4.6 – Ice Droplet Hydration

This method, developed by Sugiura *et al.*, uses a microfluidic device to fabricate a stable water-in-oil emulsion with surfactants span-80 and stearylamine.⁸¹ The emulsion is then cooled, and the aqueous core is frozen. The surfactants are then removed and replaced with the phospholipids, and the droplets are removed from the supernatant. The oil phase is in turn evaporated, and with the water still frozen, an aqueous medium is added. This process ultimately results in the formation of giant unilamellar vesicles.

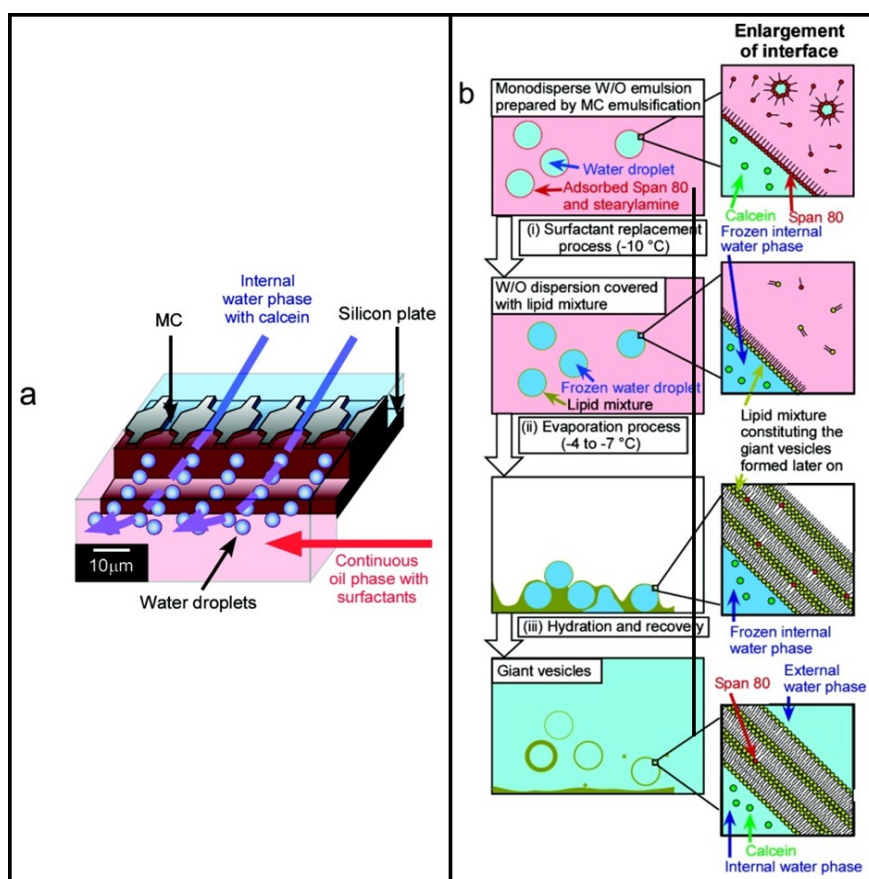


Fig. 2.4.6.1: Microfluidic ice droplet hydration method demonstrated by Sugiura *et al.*

Adapted from ⁸¹, with permission from the American Chemical Society.

2.4.7 – Transient Membrane Ejection

This captivating method demonstrated by Ota *et al.* combines a simple geometric channel with perpendicular side junctions connected to an optically controlled microbubble generator.⁸² A lipid bilayer film is loaded onto the junction and an infrared laser is used to generate a microbubble in the side channels. This in turn results in a gentle outward flow of the bilayer into the main channel, which eventually breaks off and forms lipid vesicles, similar to the pulse jetting process described in section 2.5.3. Eventually, the bilayer is depleted and must be replenished. A similar method devised by Kurakazu *et al.* utilized pneumatic valves attached to the side channels, as opposed to the microbubble generator.⁸³

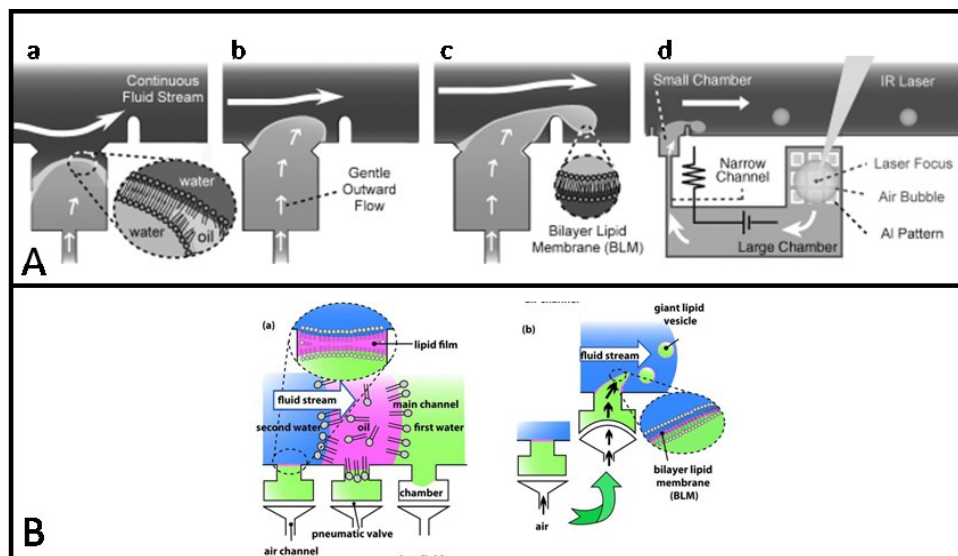


Fig. 2.4.7.1: Membrane ejection methods. A) (a-c) Flow mechanism for liposome formation, (d) Microbubble generation via IR laser on aluminium grid. Adapted from ⁸², with permission from John Wiley and Sons. B) Vesicle formation via perpendicular pneumatic side valves. Adapted from ⁸³, ©2011 IEEE

2.4.8 – Droplet Emulsion Transfer

The microfluidic droplet emulsion transfer was demonstrated by Matosevic *et al.* in 2011.⁸⁴ This process involves the formation of water-in-oil droplets which are eventually forced by a solid obstacle into an adjacent aqueous stream. This shift results in the accumulation of a second monolayer of phospholipids at the droplet interface. Again, this device resulted in the formation of giant unilamellar vesicles, with smaller liposomes being more difficult to attain due to the difficulty in achieving such sizes.⁸⁵ Additionally, one potential drawback with this device is the presence of residual oil within the bilayer after liposome formation.⁸⁶ Recently, by implementing pinched flow fractionation^{87,88}, Lu *et al.* were able to achieve giant unilamellar vesicles without the presence of any excess stabilizing material within the bilayer.⁸⁹

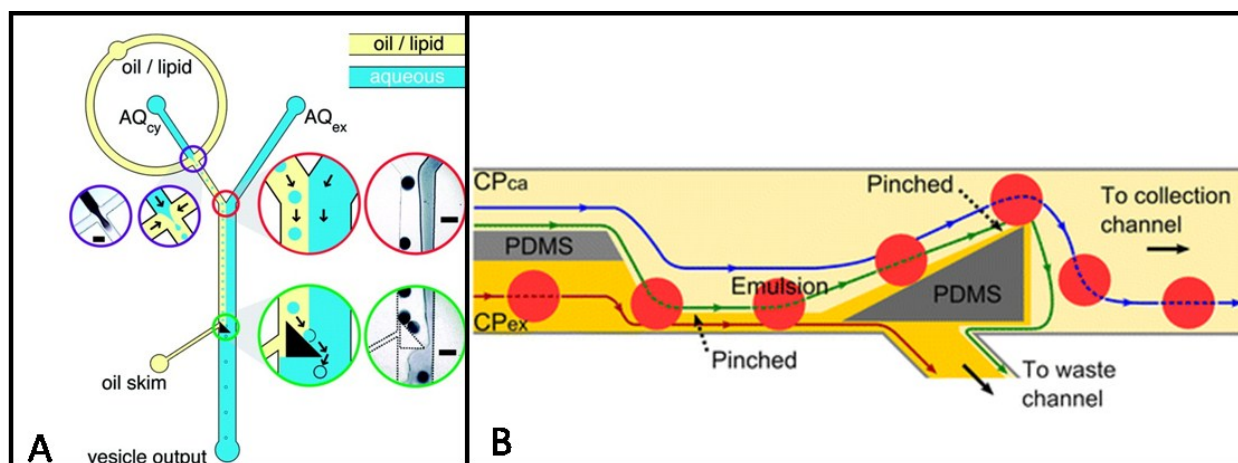


Fig. 2.4.8.1: Droplet emulsion transfer platforms. A) Initial device by Matosevic *et al.* demonstrating process. Adapted from ⁸⁴, with permission from the American Chemical Society (ACS Author's Choice).

B) Droplet emulsion with pinched flow by Lu *et al.* Adapted from ⁸⁹, with permission from Springer.

2.4.9 – Discussion

Although there are many novel developments with regards to microfluidics and liposome synthesis, as demonstrated by the previous sections, the majority of these manufacturing platforms result in particles which are unsuitable for use as drug delivery vehicles. With the exception of extrusion and flow focusing, the processes resulted in mainly giant vesicles and/or fairly polydisperse populations of liposomes at the output. Additionally, these platforms rely mainly on active processes within the microfluidic devices, such as is the case with jetting or electroformation. We therefore feel that there is a need for simple microfluidic platforms for liposomal synthesis, whether it would be for multiplexed synthesis or even predictable small scale fabrication.

Chapter 3 – Objectives

The purpose of this study was three-fold; the primary task being the design and conception of a simple, low-cost, rapid, passive microfluidic device for the synthesis of liposomal nanoparticles and on-chip molecule encapsulation; secondly, the characterization of particles obtained under varying microfluidic synthesis parameters should be performed, notably varying phospholipid concentrations and flow rate ratios; and finally, the encapsulation of a drug analog should be evaluated to validate this platform. This device should also endeavour to reduce the synthesis times associated with current cumbersome production methods and eliminate the requirement for post-processing (such as filter extrusion). Ideally, the device would produce SUVs, ranging between 50 – 300 nm, which are ideally suited for use as drug delivery systems.⁹⁰ Once a suitable concept is devised, correlations with respect to synthesized particle diameters between phospholipid:solvent concentration and fluid flow rates will be determined. Finally, the encapsulation of a fluorescent hydrophobic drug model should be performed to demonstrate the feasibility of this proof-of-concept platform as a one-step solution for bioactive molecule-encapsulated liposomes.

Chapter 4 – Materials & Methods

4.1 – Channel Design & Fluid Dynamics Modelling

As with most design studies, the initial conception phase consisted of hand-drawn sketches or back of the envelope illustrations. The design was primarily based on previous work done by Jahn *et al.* with liposomes, utilizing flow focusing as an effective means of mixture by diffusion.⁶⁰ Once a suitable prototype was achieved, the channels were modelled using computer aided design (CAD) software (SolidWorks 2013 - Dassault S.A., Vélizy, France) for further use in computational fluid dynamics (CFD) studies via COMSOL Multiphysics 3.5 (COMSOL Inc., Burlington, MA, USA) and microfabrication.

With regards to the simulations, for the sake of simplicity and computational efficiency, in the 3D Space dimension, a ‘Steady-State Analysis’ in the ‘Incompressible Navier-Stokes’ category within the ‘MEMS Module/Microfluidics’ toolbox was selected for flow modelling. This module is governed by the following equations:

$$\rho \frac{\partial \mathbf{u}}{\partial t} - \nabla \cdot \left[-p \mathbf{I} + \eta (\nabla \mathbf{u} + (\nabla \mathbf{u})^T) \right] + \rho \mathbf{u} \cdot \nabla \mathbf{u} = \mathbf{F} \quad (4-1)$$

$$\nabla \cdot \mathbf{u} = 0 \quad (4-2),$$

where equation (4-1) is the Navier-Stokes equation in vector notation, and (4-2) represents the continuity equation.⁹¹ As before, ρ denotes the fluid density (kg/m^3), \mathbf{u} is

the velocity vector (m/s), p is the pressure (Pa), I is the identity vector, η is the dynamic viscosity (Pa•s), and F is a body force term (N/m³).

The simulation assumes water as the working fluid, with the subdomain settings as follows: density (ρ) of 1.0×10^3 kg/m³, dynamic viscosity (η) of 1.0×10^{-3} Pa-s and relative permittivity (ϵ) of 80. The no-slip boundary condition for the walls was applied, and the inlets and outlets were defined as the openings at the extremities of the solid model, contrary to the configuration of the actual device, whereby the inlets and outlets are through the upper surface of the channels. The normal inflow sample and buffer inlet velocities were set to the values demonstrated in Table 4.1.1 below. The outlet boundary was set to a pressure, p , of 0 Pa. The mesh was chosen to be adequate when the area of interest, the junction, had a visually satisfying number of elements and nodes, typically consisting of at least 100 000 elements.

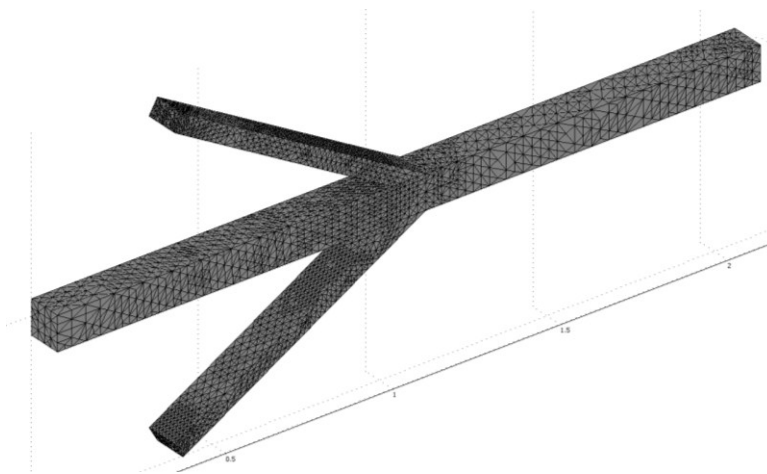


Fig. 4.1.1: Isometric view of channel design with mesh.

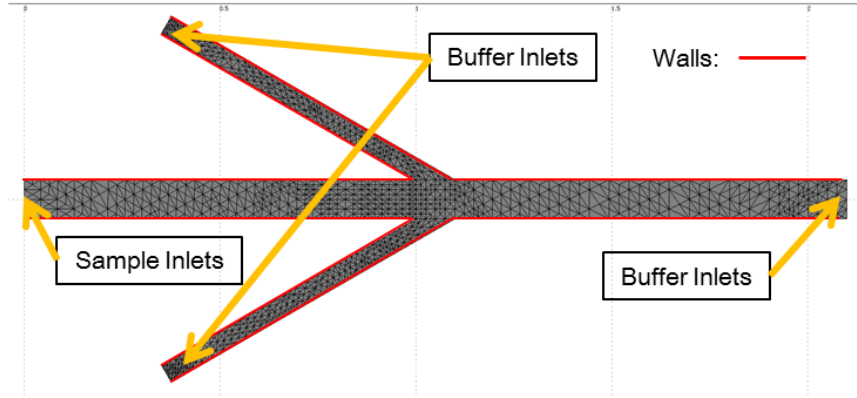


Fig. 4.1.2: 2D view of channel design with mesh

The main variable in these simulations are the inlet fluid velocities. Flow focusing devices are typically characterized by their Flow Rate Ratio (FRR), which is defined as follows:

$$FRR = \frac{TotalVolumetricFlowRate}{SampleFlowRate} \quad (4-3)$$

The flow rates were as follows:

Sample Flow Velocity (m/s)	Buffer Flow Velocity (m/s)	Flow Rate Ratio
0.001	0.001	2
0.001	0.004	5
0.001	0.009	10
0.001	0.019	20
0.001	0.029	30
0.001	0.049	50
0.001	0.099	100
0.001	0.149	150

Table 4.1.1: Flow Velocities for CFD Simulations

Chapter 5 will delve further into the various design iterations, as well as demonstrate the results obtained via CFD simulations.

4.2 – Materials

Negative photoresist, SU-8 2050, was purchased from Microchem Corp (Boston, MA, USA). Sylgard 184 elastomer kits, consisting of a prepolymer and a curing agent of PDMS, were purchased from Dow Corning Corp. (Saint-Laurent, QC, Canada). Tygon 0.020" ID microbore tubing was purchased from Cole-Parmer Canada Inc. (Montreal, QC, Canada). A quick setting epoxy adhesive was purchased from LePage-Henkel (Mississauga, ON, Canada). 2-propanol (IPA), acetone, methanol (MeOH), all analytical grade, and glass microscope slides were purchased from Fisher Scientific (Waltham, MA, USA). Anhydrous ethyl alcohol (EtOH) was purchased from GreenField Specialty Alcohols Inc. (Brampton, ON, Canada). Ergost-5,7,9(11),22-tetraen-3 β -ol (dehydroergosterol or DHE) and trichloro(1H,1H,2H,2H-perfluorooctyl)silane were purchased from Sigma Aldrich (Oakville, ON, Canada). 1,2-distearoyl-sn-glycero-3-phosphocholine (DSPC) was purchased from Avanti Polar Lipids Inc. (Alabaster, AL, USA). Glass vials were purchased from VWR International (Radnor, PA, USA). Ultra-pure water (MilliQ) from a Millipore filtration system (resistivity above 18.2 M Ω -cm) was used for all experiments.

4.3 – Device Fabrication & Assembly

The microfluidic channels were manufactured via negative photolithography onto a silicon wafer, followed by soft lithography in PDMS. The initial step consists of utilizing the previously constructed CAD geometry to create a chrome photomask comprised of a top view of the channels. For this negative lithographic process, a dark field photomask was created. The pattern or channels to be created are transparent, and everything else was covered in chrome. The photomask was obtained from Fineline Imaging, Inc. (Colorado Springs, CO, USA – *No longer provide this service*).

In the McGill Nanofab-Microtools facility (Montreal, QC, Canada), the photomask was used to create a positive mould onto a silicon wafer. Firstly, the process consists of spinning a negative photoresist, SU-8 2050, at 1700 rpm for 30s to achieve a thickness of 100 μm . Conventional ultraviolet photolithography was performed using the aforementioned photomask, whereby the exposed negative photoresist was cross-linked and thus becomes insoluble to the developer. Please refer Fig. A1 in the Appendix for more detailed protocol parameters.

Once the mould was obtained, it was treated with trichloro(1H, 1H, 2H, 2H-perfluorooctyl)silane via chemical vapour deposition to aid with the demoulding process. Several drops were placed in a glass vial, which was then placed alongside the wafer inside a vacuum desiccator. The vacuum was applied, resulting in the vaporization of the silane, and the desiccator shut-off valve was closed. The vapour was allowed to

deposit for 1 hour, after which the vacuum was released and the wafer was removed from the container.

The soft lithography process involves the pouring of an elastomer, PDMS, onto the previously silanized mould. The elastomer kit is composed of a pre-polymer and a curing agent, which was mixed in a 10:1 w/w ratio, as per the manufacturer's protocol. The prepared mixture was poured onto the wafer, which was then degassed in the vacuum desiccator to remove any bubbles within the elastomer and cured at 70°C for 3 hours. Once cured, the channels are carefully cut and removed from the cured polymer with a surgical scalpel or razor blade. The bottom face, containing the channels, was temporarily covered with transparent packing tape so as to avoid any contamination or dust deposits. A 1.2 mm biopsy punch was then used to puncture the inlet and outlet ports.

The base of the device was a standard glass microscopy slide (25 mm x 75 mm), and was cleaned by subsequently rinsing and wiping with acetone, IPA, soapy water and MilliQ water. The patterned PDMS and glass slide are then treated with oxygen plasma (PE-50 – PlasmaEtch, Carson City, NV, USA), which renders the surfaces hydrophilic, and pressed together to create a fairly strong bond. Finally, the Tygon microbore tubing was inserted into the inlets and outlet and sealed using quick-setting epoxy adhesive. Fig. 4.3.1 demonstrates an assembled device.

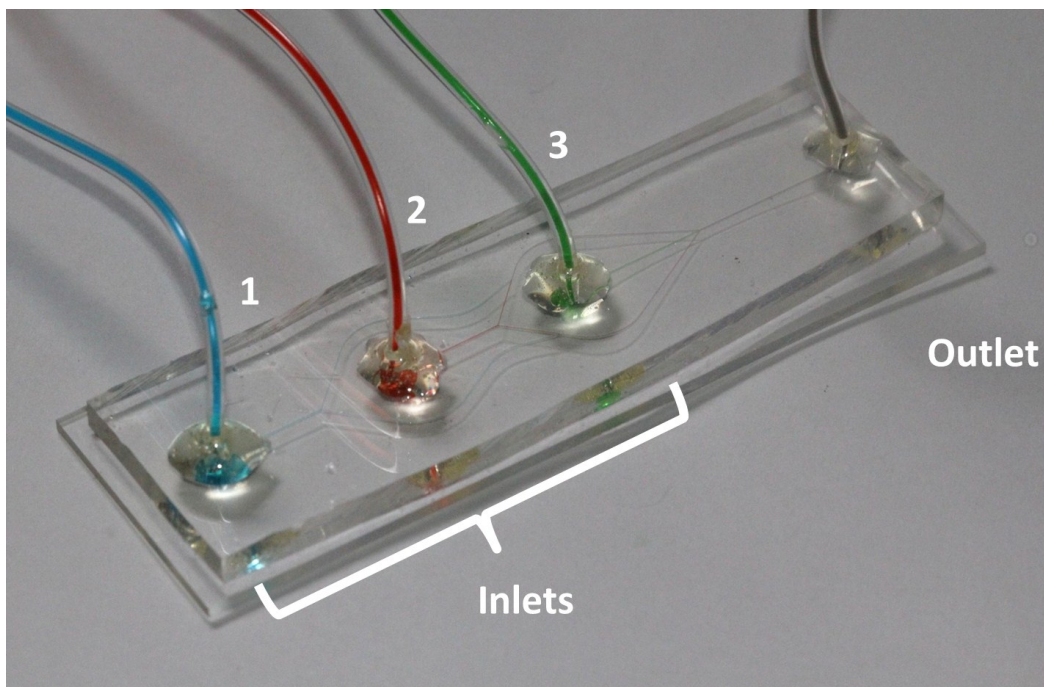


Fig. 4.3.1: Assembled microfluidic device with inlet and outlet tubing. Inlets shall henceforth be referred to by their numerical designation.

4.4 – Device Flow Visualization

For this part of the study, the fluid flow rates were controlled with a Nexus 3000 syringe pump (Chemyx Inc. – Stafford, TX, USA) in conjunction with syringes of various volumes (BD Medical – Mississauga, ON, Canada). The image acquisition setup consisted of an EOS 60D DSLR camera and a MP-E 65mm f/2.8 1-5x Macro Photo lens (both, Canon Canada Inc. – Mississauga, ON, Canada), placed atop a tripod for stability (see Fig. A2 in Appendix for setup). MilliQ water, coloured with readily available food dyes, was used as the working fluid. The pump was set to flow at $10 \mu\text{L}/\text{min}$ for a 1 mL BD plastic syringe. Using the same pump with different diameter syringes (10 mL for inlets 1 & 2, 1 mL for inlet 3; blue, red & green respectively), we obtained a FRR of 19.4.

4.5 – Microfluidic Liposome Synthesis (Unloaded & Loaded)

The phospholipid used for this investigation was DSPC. The solvent was EtOH. DSPC and EtOH were mixed in glass vials so as to avoid any contamination, and stored at 4°C. The buffer was MilliQ water. For the encapsulation study, DHE was used as a fluorescent hydrophobic drug model. This compound has previously been used as a cholesterol analog for sterol trafficking studies⁹² and has been proven to mimic cholesterol in bilayer structure and dynamics⁹³. The solvent used to prepare the stock solution was MeOH. The excitation wavelength of DHE is of 324 nm, and its emission wavelength is of 375 nm. A volume of 2.5 mL of MeOH was injected into the 5 mg vial of DHE to attain a stock concentration of 2 mg/mL (DHE:MeOH) and was in turn stored at -20°C.

Multiple flow rates were required for the synthesis experiments, thus a second syringe pump, a KDS220 multi-channel syringe pump (KD Scientific Inc. – Holliston, MA) was used in conjunction to the Nexus 3000 pump. This equally allowed for the use of a larger (20 mL) syringe for the buffer, which resulted in less setup time between experiments. For the unloaded trials, inlet 1 was blocked, MilliQ water flowed through inlet 2 and the DSPC:EtOH mixture flowed through inlet 3. Firstly, the FRR was set to 20, and the concentrations of the DSPC:EtOH mixture tested were of 1, 3, 6, 10 & 15 mg/mL. Secondly, after crudely testing the inlet burst flow rate, which was approximately 1500 µL/min or 1.5 mL/min, the FRR was set to 150, and liposome

synthesis was re-tested for 1, 3, 6, 10 & 15 mg/mL DSPC:EtOH mixtures. Finally, the concentration was fixed to 3 mg/mL and liposomes were further synthesized at FRRs of 5, 10, 20, 30, 40, 50 & 100 to obtain a correlation between FRR and particle diameter.

For the encapsulation study, a 0.5 mg/mL DHE:MeOH solution was prepared alongside the 3mg/mL DSPC:EtOH solution. The control, batch A, was prepared by flowing MilliQ water, 3 mg/mL DSPC:EtOH and MeOH through inlets 1, 2 and 3 respectively. Batch B consisted of an identical setup, except for 0.5 mg/mL DHE:MeOH flowing through inlet 3. The flow rates are as in Table 4.5.1

Active encapsulation into the liposomes (batch E), that is through simple diffusion after liposome synthesis, was achieved by adding DHE:MeOH to the already synthesized liposomes. DHE:MeOH was added in a ratio of 1:40 with respect to the volume of liposomes produced by the device, and the particles were allowed to diffuse over 24 hours.

All products were stored at 4°C. The prepared batches were as follows:

Batch	Description
A (Control)	MilliQ Water @ 480 μ L/min 3 mg/mL DSPC:EtOH @ 10 μ L/min MeOH @ 10 μ L/min
B (On-Chip/Passive Loading)	MilliQ Water @ 480 μ L/min 3 mg/mL DSPC:EtOH @ 10 μ L/min 0.5 mg/mL DHE:MeOH @ 10 μ L/min
E (Active Loading)	MilliQ Water @ 480 μ L/min 3 mg/mL DSPC:EtOH @ 10 μ L/min MeOH @ 10 μ L/min Actively loaded with 0.5 mg/mL DHE:MeOH for 24 hours

Table 4.5.1: Batch description for samples prepared via microfluidic synthesis.

4.6 – Conventional Liposome Synthesis via Ethanol Injection

For conventional ethanol injection, the liposomes were synthesized by injection of the 3 mg/mL DSPC:EtOH solution into a glass vial containing MilliQ water. A volume of 1 mL of the DSPC:EtOH mixture was injected through Tygon tubing at 10 μ L/min into 20 mL of MilliQ water.

For the actively loaded lot, batch C, the synthesized liposomes were loaded with DHE at the same ratio of 1:40, DHE solution to products. The batches produced were as follows:

Batch	Description
C (Active Loading)	MilliQ Water as Aqueous Phase 3 mg/mL DSPC:EtOH injected @ 10 μ L/min Actively loaded with 0.5 mg/mL DHE:MeOH for 24 hours
D (Control)	MilliQ Water as Aqueous Phase 3 mg/mL DSPC:EtOH injected @ 10 μ L/min Conventional Synthesis Control

Table 4.6.1: Batch description for samples prepared via conventional synthesis.

4.7 – Size Characterization

The particle diameters were determined by use of dynamic light scattering (DLS) via a ZetaPALS Zeta Potential Analyzer (Brookhaven Instruments Corp. – Holtsville, NY, USA). DLS relies on the Brownian motion of particles suspended in a solution to obtain a diffusion coefficient, from which the particle size is determined.⁹⁴ Typically, a red laser (675 nm) is emitted at a 90° angle. The recording chamber temperature was set to 6°C, and each run consisted of ten 10 second readings.

A representative sample of data obtained via DLS is shown in Fig. 4.7.1 below.

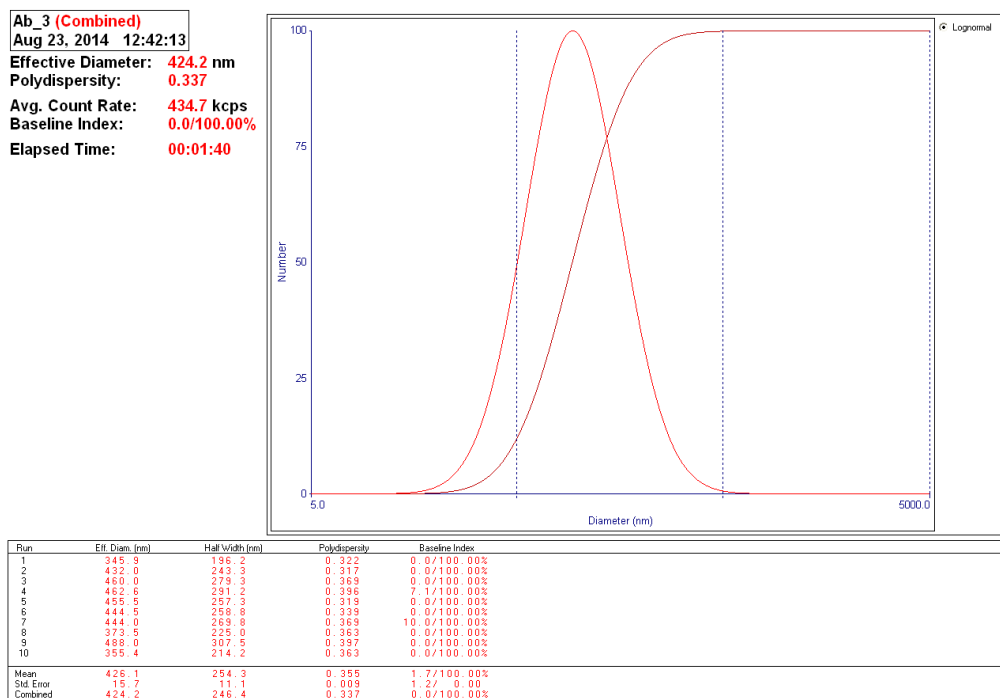


Fig. 4.7.1: DLS sample data

These charts demonstrate the measurements obtained for the particle diameter, as well as the polydispersity, which is an estimate of the width of the distribution of the particles suspended in the solution. In general, a lower polydispersity value is preferred (≈ 0.300).

Optical microscopy was performed using an Eclipse TE 2000-U inverted microscope (Nikon Canada Inc. – Mississauga, ON, Canada). A volume of 5 μ L was pipetted onto the glass slides then covered with cover slips. The images were captured using a CCD camera (Retiga-2000R, Qimaging – Surrey, BC, Canada) and NIS Elements-D (Nikon Canada Inc. – Mississauga, ON, Canada) as quickly as possible so as to avoid any evaporation or the eventual collapse of the lipid nanoparticles.

4.8 – Fluorescence Visualization & Measurement

For qualitative assessment of the loaded nanoparticles, using the same optical setup as above, a fluorescence light source was utilized in conjunction with a DAPI filter, which results in excitation with an ultraviolet source, and detection through a blue/cyan filter. The excitation and emission values for DHE, as stated above, are of 324 and 375 nm respectively.

A SpectraMax i3 Multi-Mode Microplate Reader (Molecular Devices – Sunnyvale, CA, USA) was used to quantify the fluorescence intensity of the various liposomal solutions. The fluorescence excitation was set to 324 nm, and the emission readings were performed as a sweep between 350 and 450 nm, with a step size of 5 nm. The relative fluorescence unit (RFU) intensity was normalized with respect to the empty vesicles which did not contain any encapsulated DHE. The 96 well-plate (Corning Incorporated – Corning, NY, USA) was loaded with 100 μ L of the samples per well as follows:

	1	2	3	4	5	6	7	8	9	10	11	12
A	Aa				Ab				Ac			
B	Ba				Bb				Bc			
C	Ca				Cb				Cc			
D	Da				Db				Dc			
E	Ea				Eb				Ec			
F	MilliQ:EtOH:MeOH						MilliQ					
G	DHE @ 0.5 mg/mL						Blank					
H	DHE Stock @ 2 mg/mL						Blank					

Table 4.8.1: Organization of 96-well plate for spectrophotometry measurements

4.9 – Statistical Analysis

Data were expressed as mean \pm standard deviation of at least 3 replicates per group. Statistical analyses were performed for multiple comparisons via one-way ANOVA and Student's *t*-test was used for direct result comparison. Differences were considered significant for $p < 0.05$.

Chapter 5 – Channel Design, Simulations & Flow Visualization

5.1 – Device Requirements & Constraints

The priorities of this platform were above all else achieving simplicity; simplicity in design, simplicity in manufacturing and simplicity in use. Many of the conventional methods used for liposome synthesis, as described in Chapter 2, rely on large, bulky or tedious apparatuses for manufacturing, such as the rotary evaporator used in reverse-phase evaporation, microfluidizers required for high-pressure homogenization or even simple polycarbonate filter holders for extrusion. By adopting microfluidics for this platform, in combination with the group's expertise with the multi-faceted tool, our aim was to achieve a synthesis platform that would not only be relatively cheap, efficient, highly tunable and predictable, but one that also possibly allowed for multiple loading schemes.

In terms of device footprint, our constraints were that the device must fit within the dimensions of readily available glass microscopy slides, 25 x 75 mm. To achieve channel simplicity for this initial prototype, the device was to rely mainly on planar channel geometries and avoid any complex three-dimensional routing. To satisfy this condition, hydrodynamic flow-focusing (HFF) was chosen as the basis of this device. The device will also rely on continuous flow, as opposed to pulsatile flow. Contrary to popular belief, the particulate synthesis process will not be producing the nanoparticles by droplet formation, but rather by diffusion, as described in section 2.2.13.

A notable recent development was the work by Hood *et al.* regarding the demonstration of a single-step liposomal technique using 'microfluidic remote loading'.⁹⁵ In addition to the HFF work developed by Jahn *et al.*,⁶⁰ they created a multi-tiered platform which included a counterflow microdialysis section to allow for the generation of transmembrane ion gradients, and subsequently, the loading of amphipathic weak bases into the vesicles, all within the device (see Fig. 5.1.1). Their platform incorporated the benefits of HFF for liposome synthesis, i.e. small monodisperse unilamellar vesicles, with the benefits of an active pH gradient loading method, as described by Haran *et al.*⁶⁸ However, this platform was fairly complex and consisted of multi-leveled channels, an intermediate filter layer, and even underside inlets. Therefore, we endeavoured to achieve a simpler platform for a similar process.

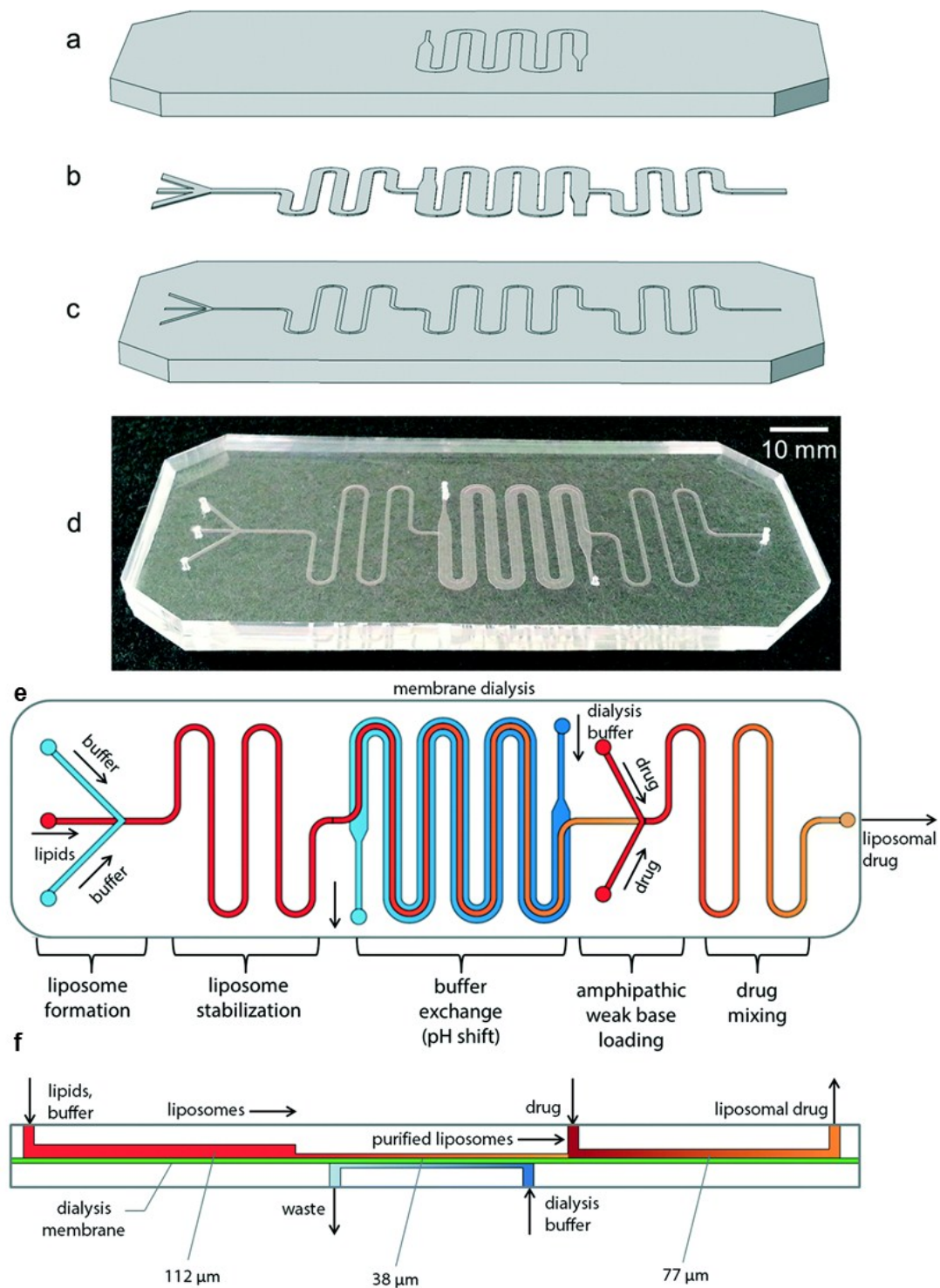


Fig. 5.1.1: 'Microfluidic remote loading' by Hood *et al.*⁹⁵: (a-c) Exploded view of device. (d) Assembled device. (e) Fluid pathways within platform. (f) Side view, showing underside inlets for dialysis.

Adapted from ⁹⁵, with permission from the Royal Society of Chemistry.

5.2 – Channel Designs & Iterations

The following ‘sketches’ represent digital reconstructions of hand-drawn sketches for clarity.

The basis of HFF is the simple Y- or T-Junction, the former of which was the starting point of this design process. An initial concept, v1.0 was devised as follows:

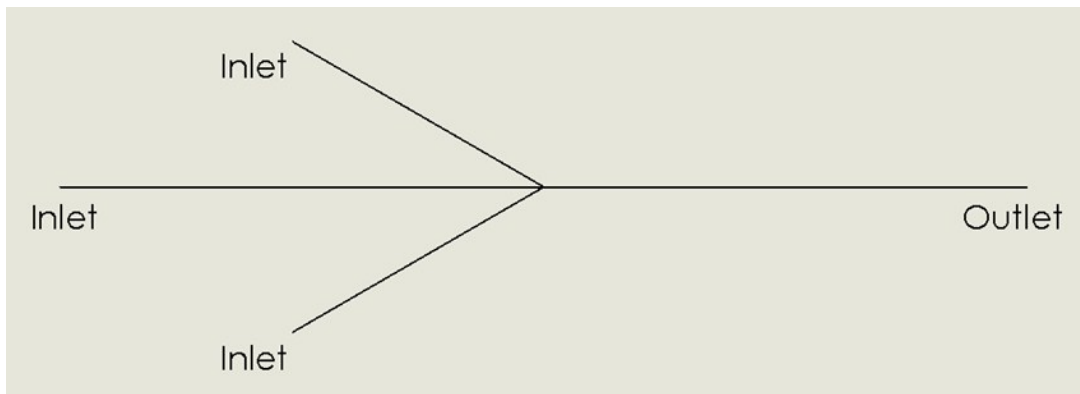


Fig. 5.2.1: v1.0 – Simple HFF with Y-junction

From this concept, in order to incorporate an element of three-dimensional (3D) focusing without the necessity for 3D geometries, inertial microfluidics, as reviewed by di Carlo⁹⁶, were included. By implementing curvature in the channel following the junction, which would result in the formation of Dean flow combined with the planar focusing within this section, it was hoped to achieve focusing out of plane as well. This phenomenon is caused by the formation of secondary flows, in the form of vortices, within the channel, perpendicular to the flow. The fluid closer to the inside of the curve flows at a faster rate as opposed to that of the fluid towards the outside of the curve, thus forming two super-imposed vortices. The implementation of 3D HFF could

theoretically allow for the formation of smaller particles due to the increase in the amount of focusing and larger surface area to volume ratio for diffusion. This led to the concept behind v1.5:

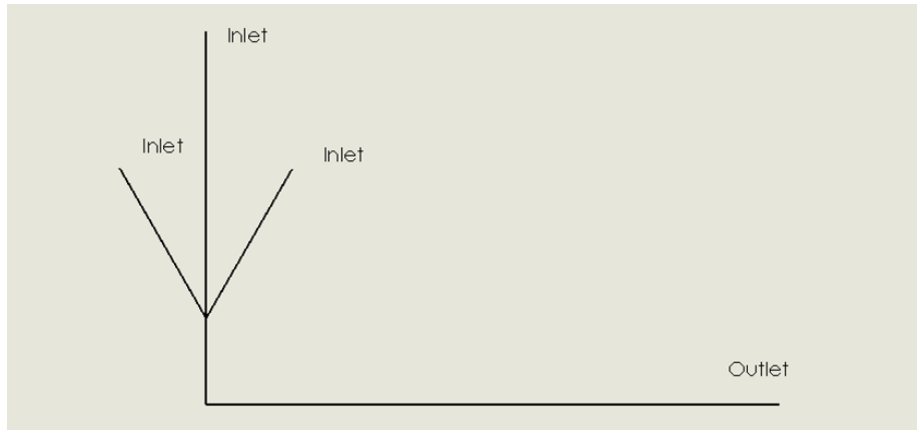


Fig. 5.2.2: v1.5 – Y-junction with curvature for 3D flow focusing

However, upon further consideration, and due to the device footprint requirements, it was decided that the implementation of a curved section in the outlet would be kept for a latter iteration of the physical device, so as to minimize the amount of parameters at play and adhere to the primary goal of channel geometry simplicity. On that same note, as opposed to having two separate channels for the buffer inlets, one possible improvement was to merge them into a single inlet. This would not only require one less syringe during injection, but should also result in more evenly distributed flow from the focusing channels. And thus, v2.2.3 (Fig. 5.2.3) was devised. This geometry also satisfies the dimensional constraints that the device must adhere to, with the joint inlets enabling the use of a much narrower platform.

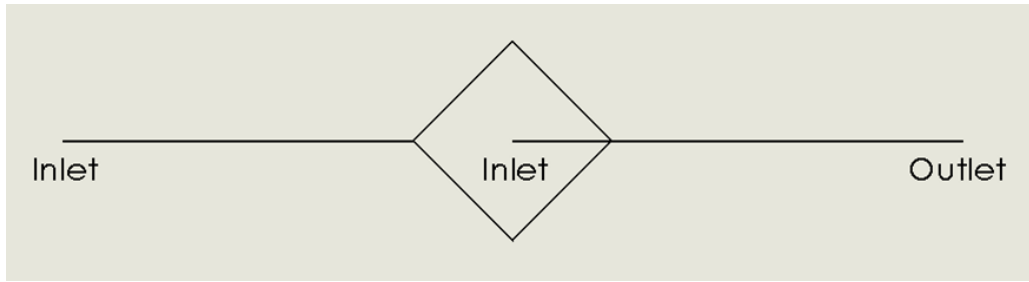


Fig. 5.2.3: v2.2.3 – Simple HFF with merged focused flow filets

The previous models consisted of only a single sheathe flow, however, for a device capable of incorporating encapsulation or loading, a dual-sheathe setup would be required. Furthermore, a study by Liu *et al.* correlated the influence on buffer inlet angle with respect to droplet size formed for droplet microfluidics and flow focusing, with an angle of 30° offering the smallest particles.⁹⁷ Although this was for a droplet method, as opposed to continuous flow, we felt that it could still be applied for our device. Therefore, the next iteration, v2.3.2 (Fig. 5.2.4), combined a dual sheathe setup and the junction inlet angle criteria.

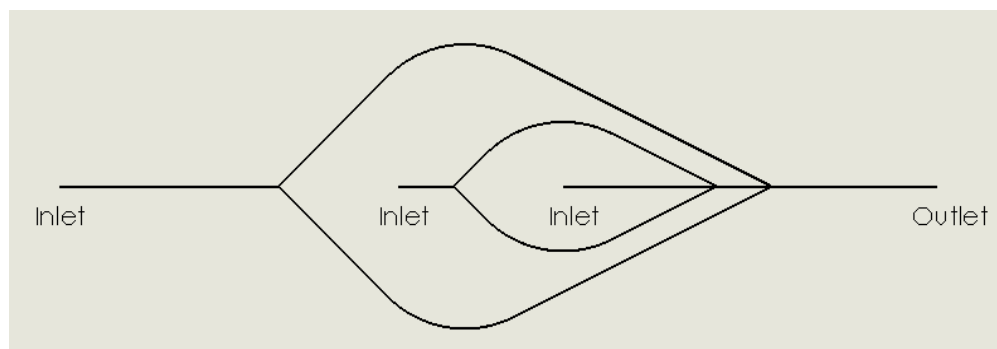


Fig. 5.2.4: v2.3.2 – Dual-sheathe & 30° junction inlets

The main issue which arose from v2.3.2 was the width and length of the glass substrate that would be required for such a configuration. After taking measurements

from previously manufactured microfluidic devices, it was determined that there should be at least 5 mm of clearance around the inlets in addition to the 1.2 mm diameter of the biopsy punch. With this in mind, and some preliminary measurements, the outermost sheathe channels could potentially lead to some manufacturing issues. Therefore, the furthest sheathe channels were moved backwards along the longitudinal axis, and connected just aft of the second inlet bifurcation. The following aesthetically pleasing models, v4.0 and v4.1, Figs. 5.2.5 & 5.2.6 respectively, were conceived.

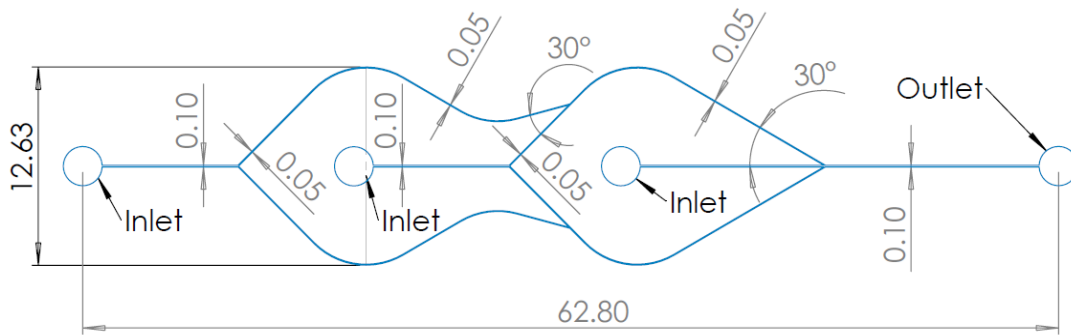


Fig. 5.2.5: v4.0 – Dual sheathe with curved outer channels

Not to scale - Dimensions in millimeters (mm)

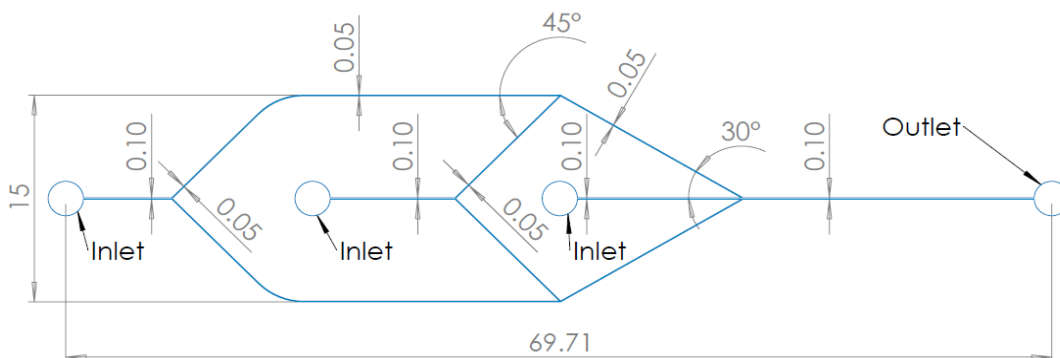


Fig. 5.2.6: v4.1 – Dual sheathe with straight outer channels

Not to scale - Dimensions in millimeters (mm)

Model v4.0 maintains the optimal focusing angle criterion, whereas model v4.1 was designed in the event of any undesirable effects on the due to the curvature of the channels in-line with the second bifurcation. The reasoning behind the incorporation of this double-curvature feature was to have the outermost sheathe join the innermost sheathe at an optimal flow-focusing angle of 30° , for reasons previously described. Designs v4.0 and v4.1 were chosen to create the first physical prototypes for the device, as per the protocol described in section 4.3.

5.3 – CAD Modelling

Once a final design was achieved, the sketches were converted into 3D models. The primary use of these models was for the CFD simulations, creation of the photomask, and ultimately, the physical mould for device fabrication. Herein, we include isometric views for v4.0 and v4.1 (Figs. 5.3.1 & 5.3.2), as well as a render of v4.0 as a complete device (Fig. 5.3.3).

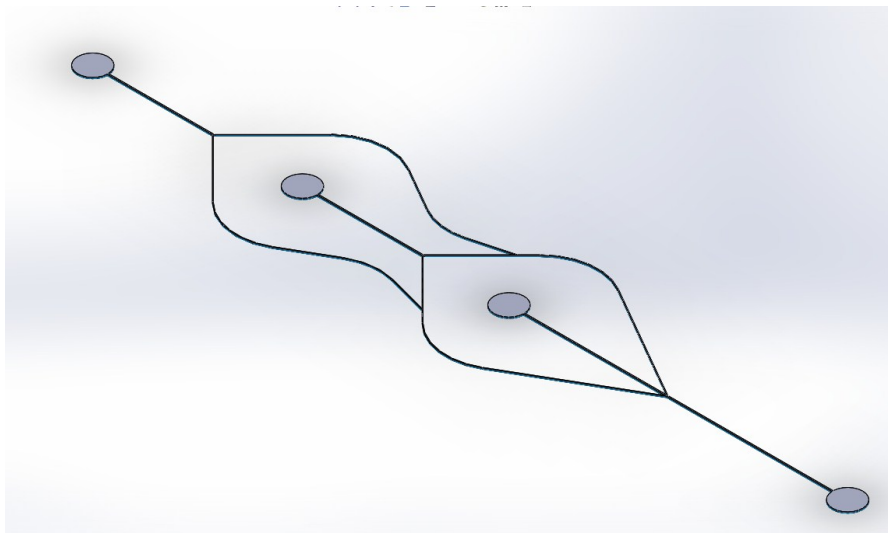


Fig. 5.3.1: v4.0 – Isometric view of 3D model

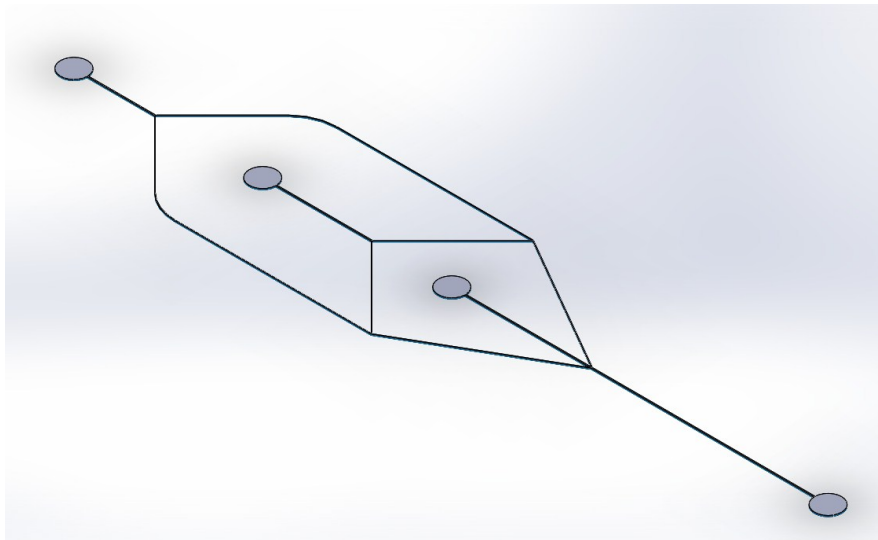


Fig. 5.3.2: v4.1 – Isometric view of 3D model

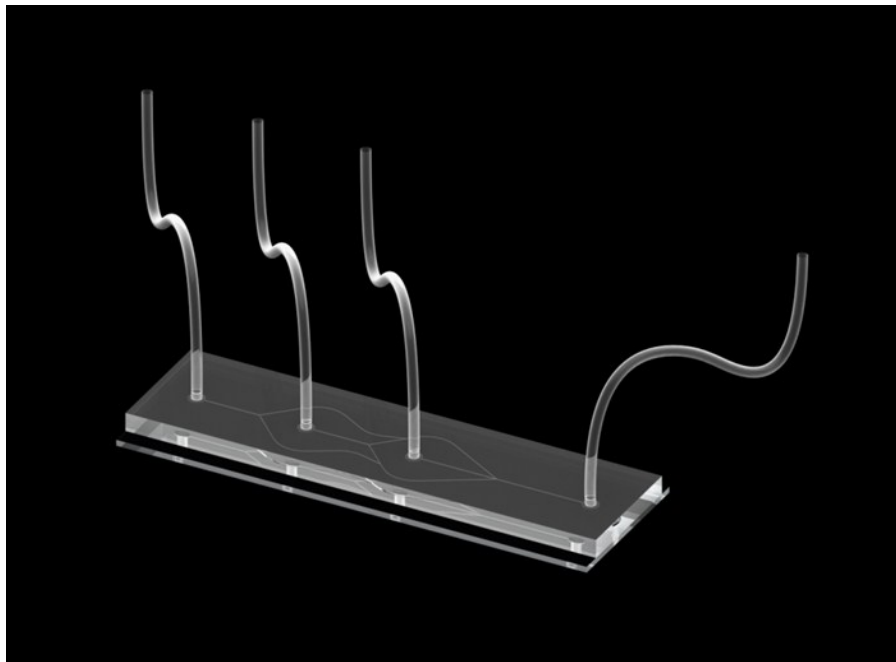


Fig. 5.3.3: Render of assembled v4.0 prototype

With regards to the model required for the CFD simulation, for simplicity and under the assumption that the flow would be steady and developed by the time the

junction is reached, only a representative section of the channel was chosen, that of the final flow focusing junction. The geometry was as seen in Fig. 5.3.4 below, with the dimensions as in Fig. 5.2.5 or 5.2.6.

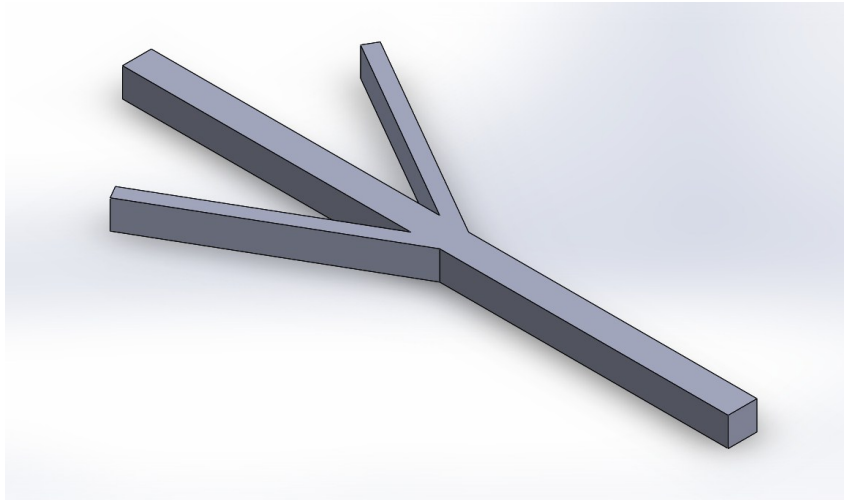


Fig. 5.3.4: Representative geometry for CFD - Junction of v4.0 & v4.1

5.4 – Fluid Junction CFD Simulation

As per the parameters defined in section 4.1 regarding the fluid dynamics modelling, the following results were obtained (FRR 5, 50, 100 & 150 respectively). Only a representative set of results are shown below, with enlarged versions and the remaining data found in section A3 of the Appendix. The results demonstrate both the streamlines, as well as the velocity field at various locations within the channels. The legends on the left were all set to display a constant range from 0.0 – 0.315 m/s.

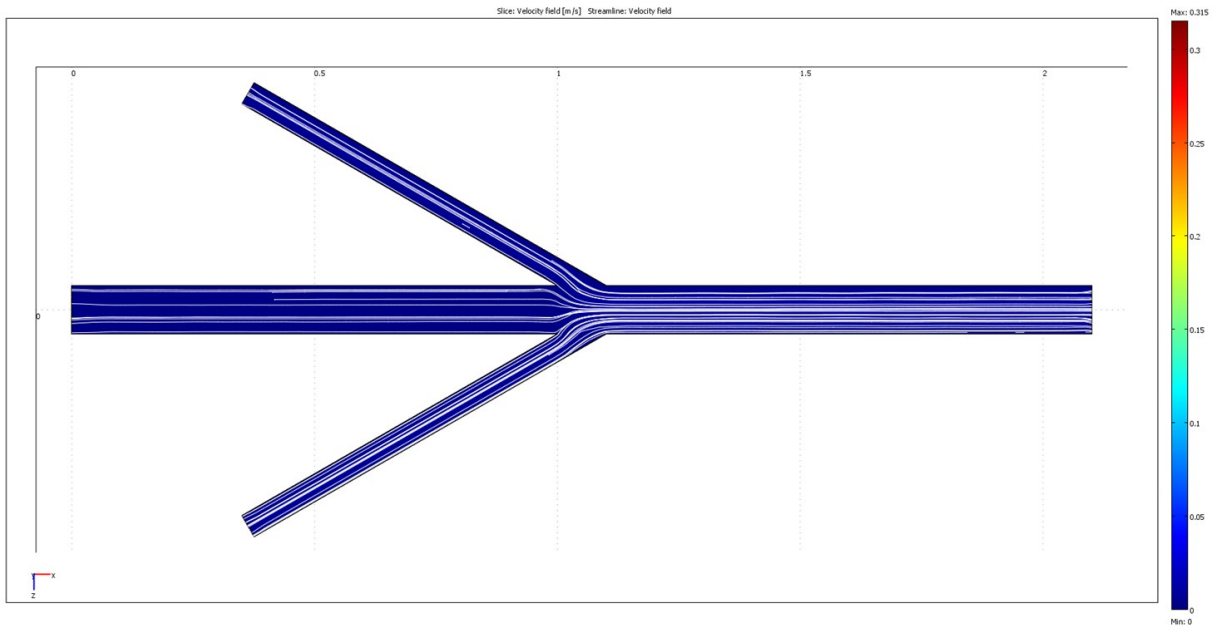


Fig. 5.4.1: v4.0 Junction CFD simulation for FRR 5

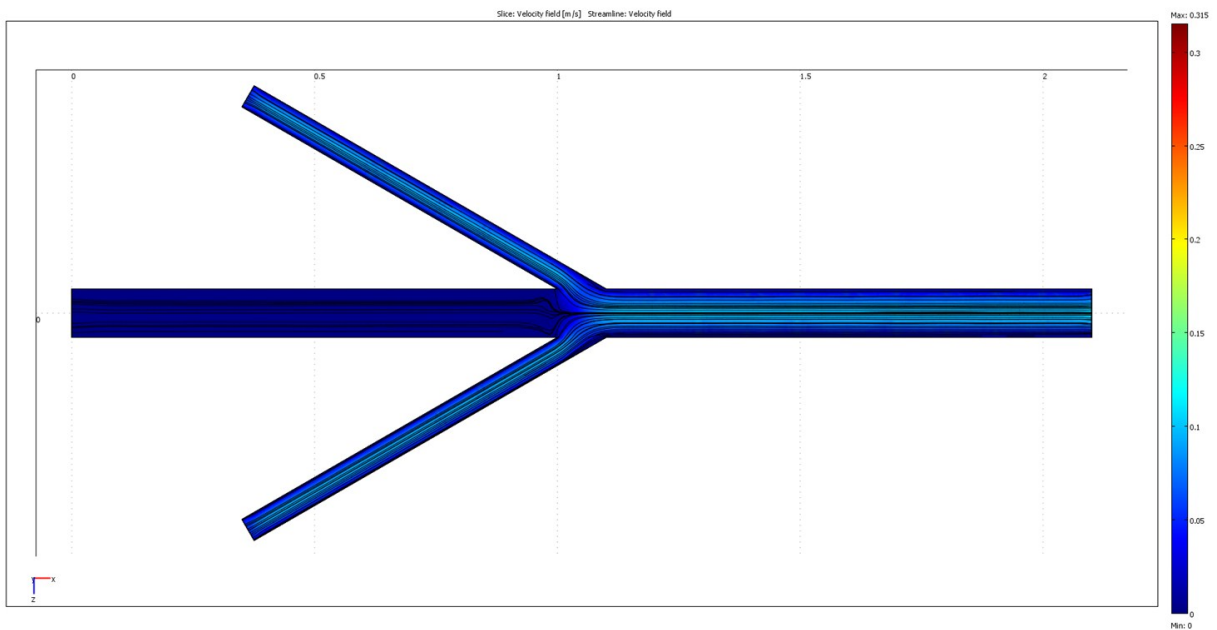


Fig. 5.4.2: v4.0 Junction CFD simulation for FRR 50

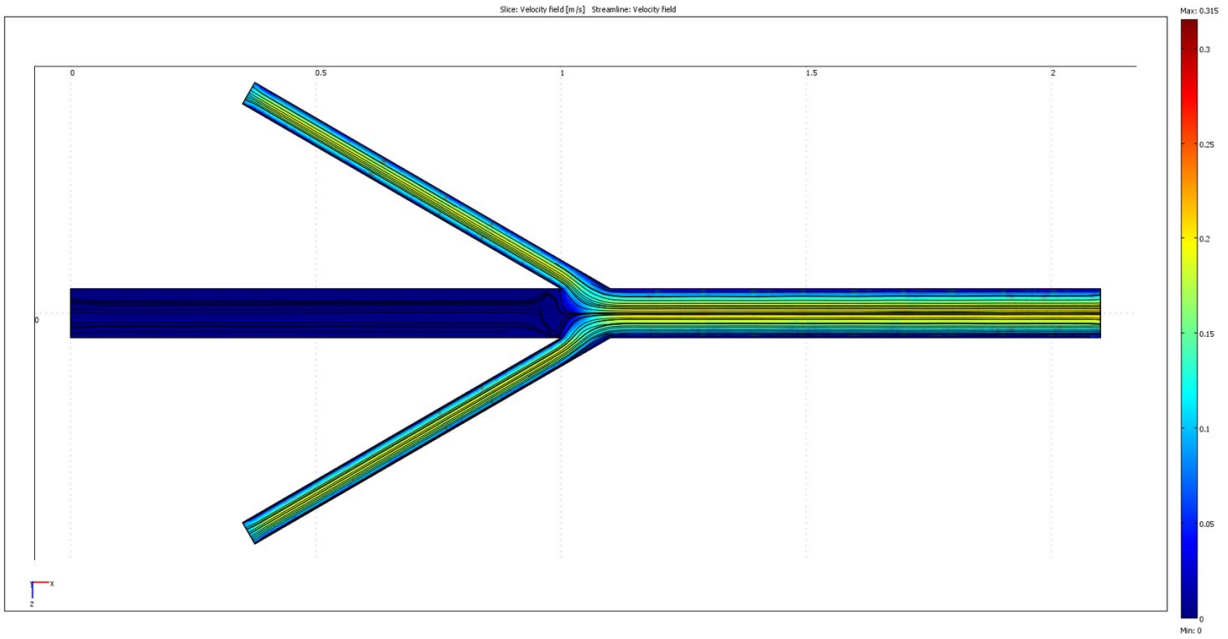


Fig. 5.4.3: v4.0 Junction CFD simulation for FRR 100

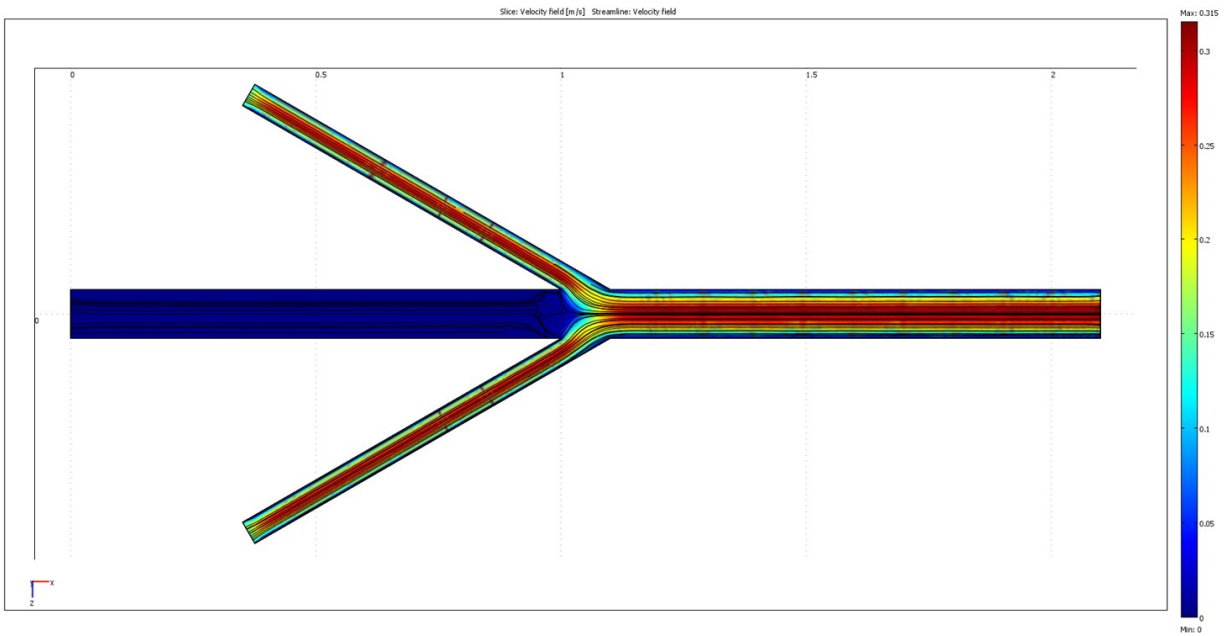


Fig. 5.4.4: v4.0 Junction CFD simulation for FRR 150

It can be observed that the central sheath streamlines increasingly converged towards the centerline with increasing FRR. This is to be expected, as the working fluid used in this simulation is water, and the parameters were set to incompressible flow. With a higher buffer flow rate, one would therefore expect a greater amount of flow focusing.

5.5 – Qualitative Flow Visualization

The device was manufactured and the flow was visualized as per the processes described in sections 4.3 and 4.4.

The figures below demonstrate the flow characteristics at the junction of device v4.0. Of note, in Fig. 5.5.1, it can be observed that diffusion occurs following the intersection of the fluids. The red dye from the central stream was observed to be diffusing into the outer sheathe by a darkening of the flow.

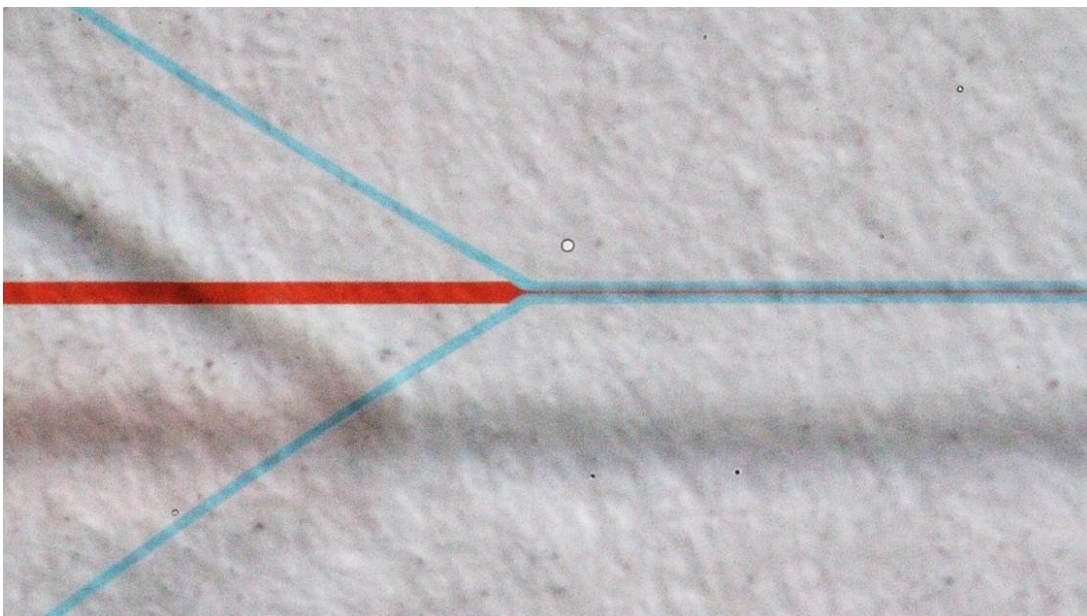


Fig. 5.5.1: Flow focusing junction – Diffusion visualization, inlets 2 & 3 only.

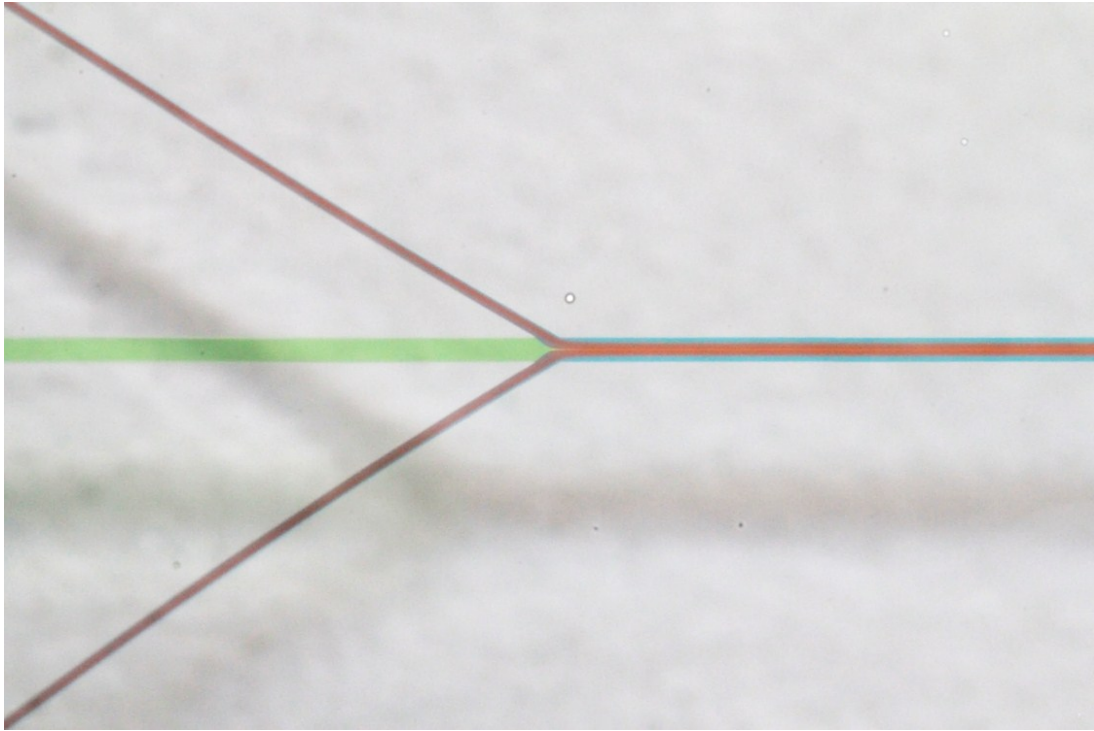


Fig. 5.5.2: Flow focusing junction – Inlets 1, 2 & 3.

Fig. 5.5.1 was obtained during the testing phase of the image acquisition setup, accounting for the difference in fluid stream colours. Once the apparatus arrangement was deemed satisfactory, the fluids were flowed as per section 4.4.

In both figures, flow focusing was clearly visible, with the central streams being compressed to approximately a tenth of their original widths. A secondary observation can be seen in Fig 5.5.2, in which the fluid within the buffer channels were not horizontally parallel, i.e. blue on the outside and red on the inside, but rather reversed and of unequal widths, even though the flow rates were the same. This was possibly due to inertial effects of the curvature of the outer channels adjacent to inlet 3, as described by di Carlo.⁹⁶

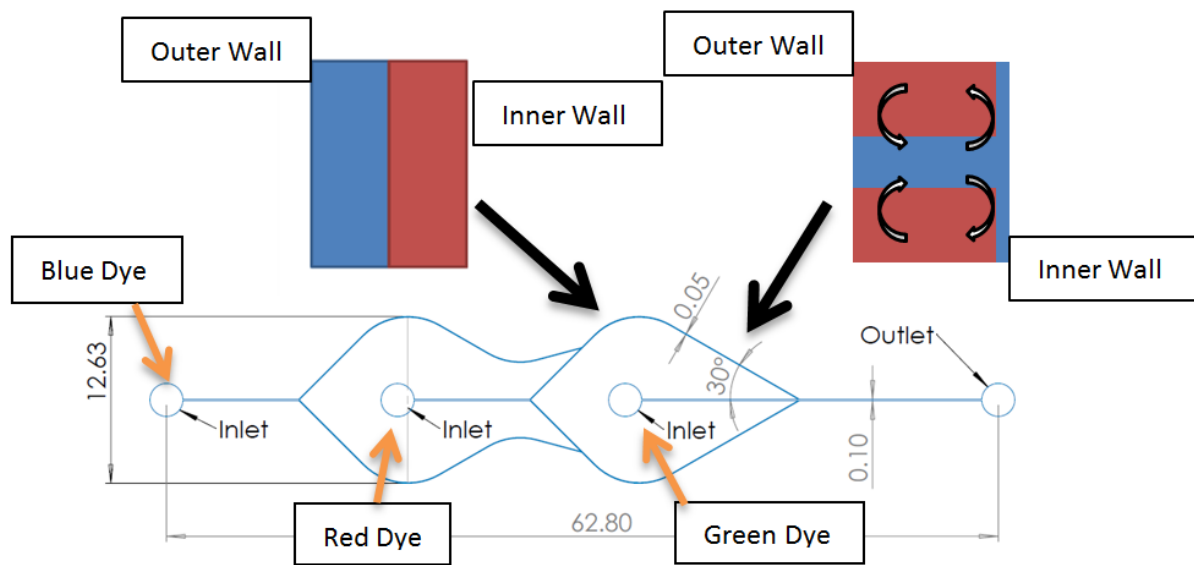


Fig. 5.5.3: Inertial Effects on Sheath Flow

The presence of this phenomenon could potentially affect the final properties of the loaded nanoparticles. However, it was observed that the fluids eventually rearrange themselves in the proper orientation after the junction. Additionally, the fluid flow rates of the two innermost channels would most likely be at least one order of magnitude smaller than that of the buffer flow, as opposed to the experimental setup seen here.

In this chapter, we outlined the iterative design process whereby an initial physical prototype was developed, demonstrated the steps taken in order to create a 3D model of said concepts, and finally, visualized the fluid flow within the channels via both CFD simulations and physical testing. The following chapter will deal with a preliminary study characterizing the platform by varying phospholipid concentration and FRRs.

Chapter 6 – Device Characterization

The effects of varying the concentration and flow parameters for the synthesis of DSPC liposomes within the platform were assessed with regards to size and polydispersity. The results were compared by analysis of the hydrodynamic diameters of the nano- or microparticles.

6.1 – DSPC Concentration Optimization

For both setups, liposomes were synthesized for concentrations of 1, 3, 6, 10 and 15 mg/mL of DSPC:EtOH at FRRs of 20 and 150.

6.1.1 – Varying Concentrations at FRR 20

The synthesis of liposomes at a low FRR of 20 resulted in the formation of microparticles, as seen from Fig 6.1.1.1 below. Samples from concentrations of 1 and 3 mg/mL, which were not significantly different from one another, resulted in significantly smaller particles compared to concentrations of 6, 10 and 15 mg/mL. For concentrations of 6 and 10 mg/mL, there was an approximate doubling in size of liposomes produced, compared to the lower concentration lots. Compared to the 15 mg/mL sample, concentrations of 1 and 3 mg/mL resulted in microparticles which were approximately 40% smaller.

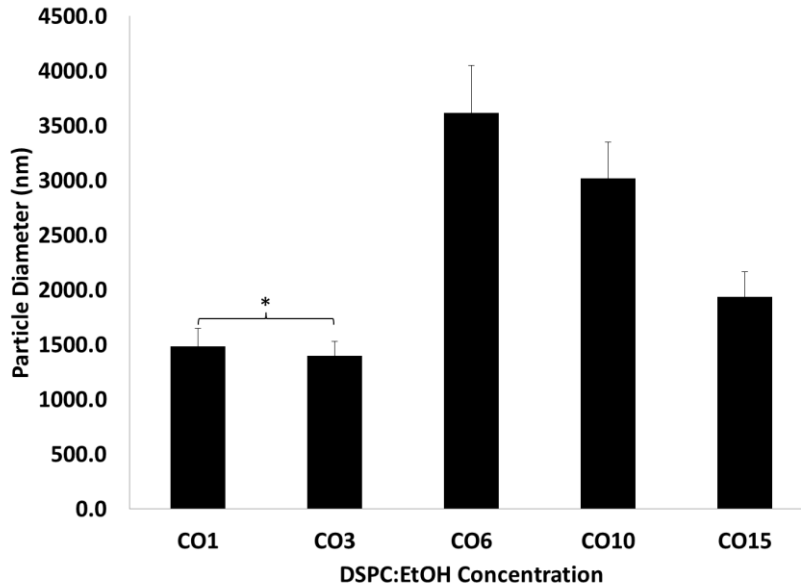


Fig. 6.1.1.1: DSPC:EtOH Concentration vs Particle Diameter at FRR 20.

6.1.2 – Varying Concentrations at FRR 150

Lipid vesicles were then produced at a FRR of 150 (see Fig. 6.1.2.1 below). This FRR resulted in the formation of sub-micron scale vesicles. In this instance, the particles of significantly smaller diameter (360.2 ± 32.0 nm) occurred when a DSPC:EtOH concentration of 3 mg/mL was used. For the three larger concentrations, the device gave rise to in particles at least twice the size of the former.

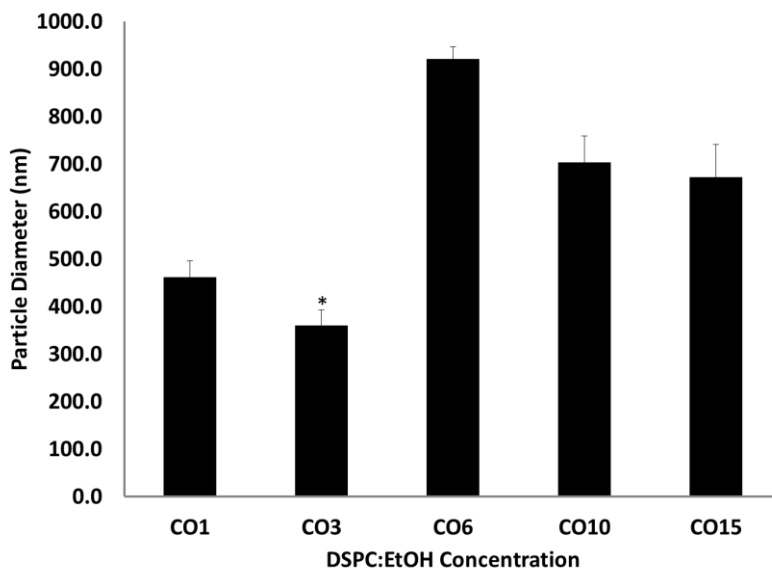


Fig. 6.1.2.1: DSPC:EtOH Concentration vs Particle Diameter at FRR 150.

6.2 – Flow Rate Ratio Correlation

For the final characterization step, the concentration of DSPC:EtOH was fixed to 3 mg/mL and FRRs of 5, 10, 20, 30, 40, 50 and 100 were investigated. Fig. 6.2.1 demonstrates the results.

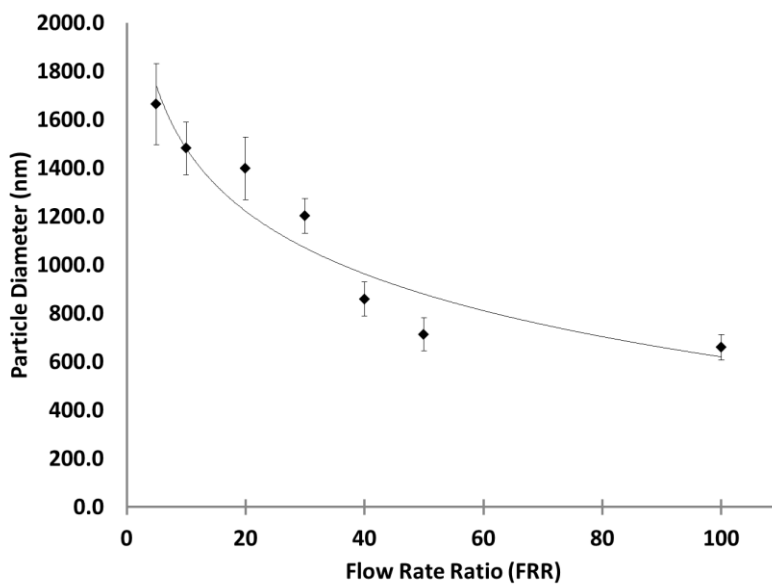


Fig. 6.2.1: Flow Rate Ratio vs Particle Diameter at 3 mg/mL DSPC:EtOH.

Using a logarithmic fit, it can be observed that there is a decreasing trend with increasing FRR. All non-neighbouring results were statistically different, except for particles synthesized at FRR5 and FRR20.

6.3 – Discussion

Comparing both sets of varying concentration data, an interesting trend was observed, whereby the particle diameter initially decreases, to suddenly rise, and ultimately fall again, in a somewhat fascinating jigsaw pattern. In both cases, there was a rather sharp increase in particle diameter between DSPC:EtOH concentrations of 3 and 6 mg/mL, and a subsequent decrease thereafter.

Regarding the trend observed with increasing phospholipid concentrations, unfortunately, to date, the dynamics and mechanisms of liposomes formed via ethanol injection are still not well understood. Other investigations using phosphatidylcholine-based lipids as a bilayer constituent demonstrated an increase in liposome size with increasing concentrations^{29,98,99}, or a bell-shaped trend, as demonstrated by Balbino *et al.*¹⁰⁰ In this study, the use of DSPC led to the appearance of a jagged-edge trend, which could possibly be due to the formation of lipid vesicles well below the transition temperature (T_c) of DSPC, which is of 55°C.²⁹

For increasing FRR, the resulting trend of decreasing particle diameters was as expected, as previously demonstrated with other liposomal formulations.^{29,99,101} The formation of very thin sample streams at higher FRRs (see Fig. 5.5.2) and increased

outwards diffusion (see Fig. 5.5.1), also previously demonstrated by Jahn *et al.*¹⁰², can account for the formation of smaller vesicles. Not only would this result in greater shear forces at the interface, but also greater diffusion out of the sample stream, and in due course, the formation of smaller liposomal particles.

Chapter 7 – Hydrophobic Drug Model Loading

The following section investigates loading of a hydrophobic drug model into the liposomes using the microfluidic flow focusing method, as well as the conventional ethanol injection. The FRR for the microfluidic synthesis method was 50. This FRR was chosen to achieve nanoparticles and be able to observe said particles via optical microscopy. Previous attempts at using a higher FRR, e.g. 150, resulted in a final solution which was extremely dilute and difficult to image. Additionally, the concentration of DSPC:EtOH was fixed to 3 mg/mL.

As a reminder, the batches were prepared as follows:

Batch	Synthesis Method	Description
A	Microfluidic (Control)	MilliQ Water @ 480 μ L/min 3 mg/mL DSPC:EtOH @ 10 μ L/min MeOH @ 10 μ L/min
B	Microfluidic (On-Chip/Passive Loading)	MilliQ Water @ 480 μ L/min 3 mg/mL DSPC:EtOH @ 10 μ L/min 0.5 mg/mL DHE:MeOH @ 10 μ L/min
C	Conventional (Active Loading)	MilliQ Water as Aqueous Phase 3 mg/mL DSPC:EtOH injected @ 10 μ L/min Actively loaded with 0.5 mg/mL DHE:MeOH for 24 hours
D	Conventional (Control)	MilliQ Water as Aqueous Phase 3 mg/mL DSPC:EtOH injected @ 10 μ L/min Conventional Synthesis Control
E	Microfluidic (Actively Loading)	MilliQ Water @ 480 μ L/min 3 mg/mL DSPC:EtOH @ 10 μ L/min MeOH @ 10 μ L/min Actively loaded with 0.5 mg/mL DHE:MeOH for 24 hours

Table 7.1: Batch Descriptions

7.1 – Particle Diameter Comparison

Figs. 7.1.1 and 7.1.2 demonstrate the diameter of the particles in the encapsulation study synthesized via microfluidic and conventional methods respectively.

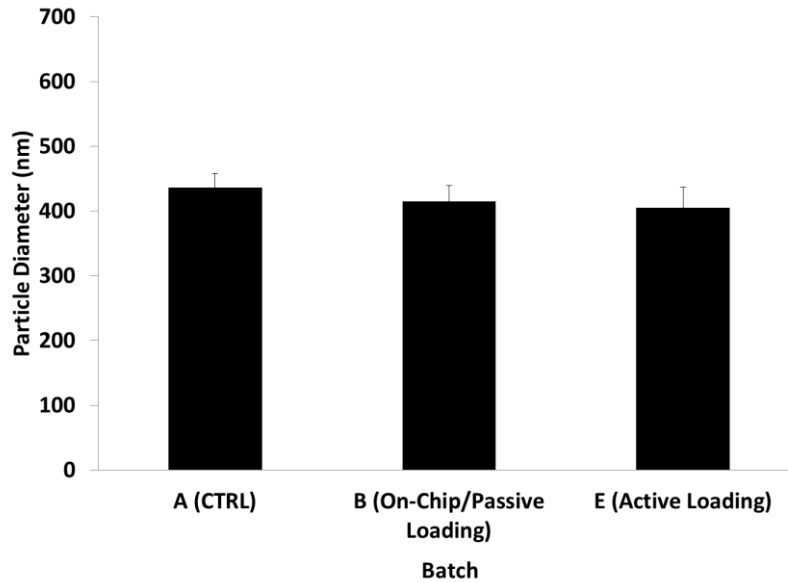


Fig. 7.1.1: Particle Diameters for Microfluidic Synthesis Methods

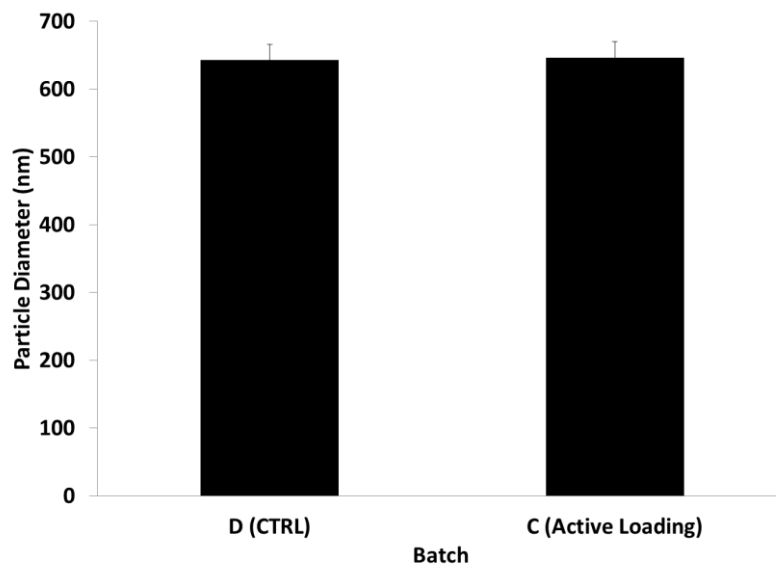


Fig. 7.1.2: Particle Diameters for Conventional Synthesis Methods

The particles produced via microfluidic synthesis have a mean diameter of 418.63 ± 20.97 nm, whether unloaded (batch A), passively loaded (batch B) or actively loaded (batch E). These were significantly smaller than those produced via conventional methods (batches C & D), the latter being 644.64 ± 21.56 nm or 45% larger.

In both synthesis methods, there was no statistically significant difference between the unloaded and loaded liposomes.

7.2 – Qualitative Assessment of Encapsulation Using Microscopy Techniques

Prior to any further investigation, the chosen hydrophobic drug analog, DHE, was observed using light and fluorescence microscopy. As demonstrated in Fig. 7.2.1 below, DHE was observed under fluorescence with DAPI, Cy5 and TRITC filters. Having an emission wavelength of 375 nm, in the ultraviolet range, the DHE molecules were visible using the DAPI filter.

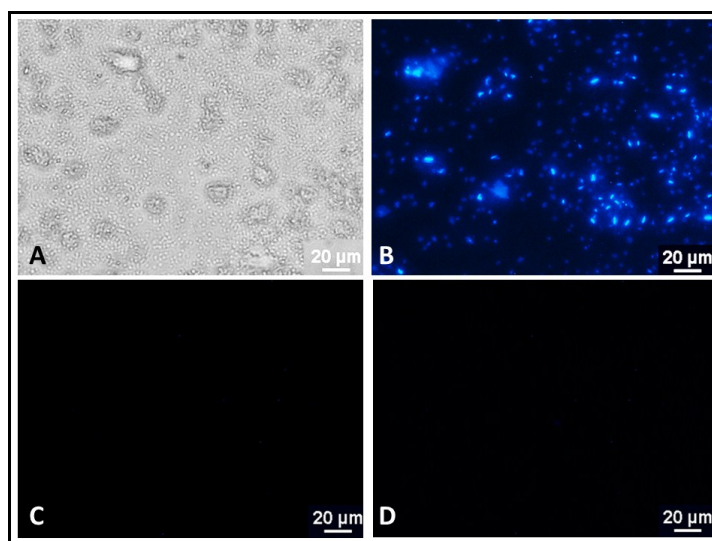


Fig. 7.2.1: Dehydroergosterol (DHE) Imaged with Various Filters.

(A) Optical microscopy, (B) DAPI, (C) TRITC, (D) Cy5.

Subsequently, liposomes containing DHE were observed via microscopy, Figs. 7.2.2 & 7.2.3 below. The representative sets of figures consist of side by side images of the same location, visualized under fluorescence with the DAPI filter (left) and light microscopy (right), of on-chip, passively loaded liposomes (batch B) and actively loaded liposomes (batch E). The reader's eye is drawn to areas-of-interest by the yellow squares.

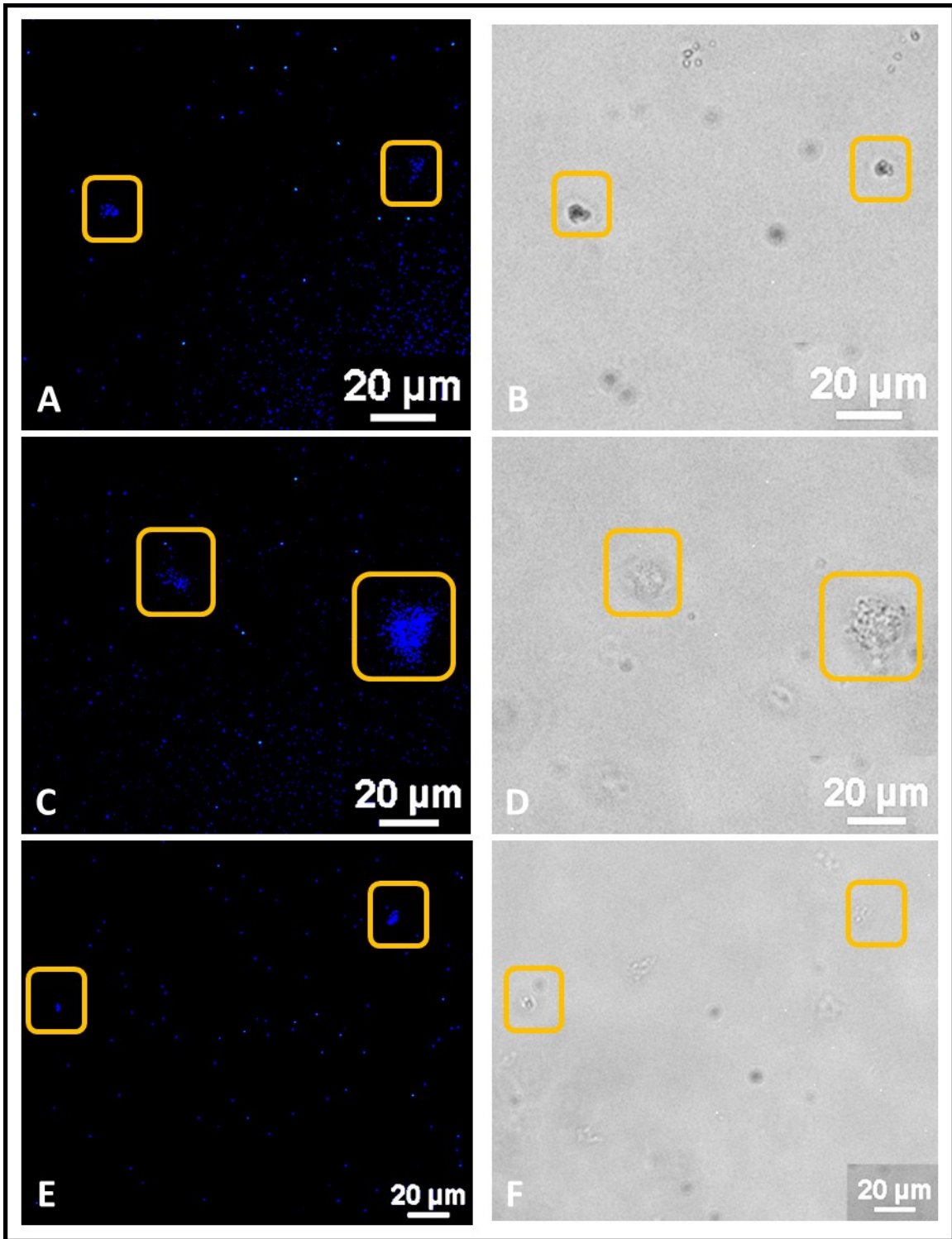


Fig. 7.2.2: Microscopy of DHE On-Chip/Passively Loaded Liposomes (batch B)

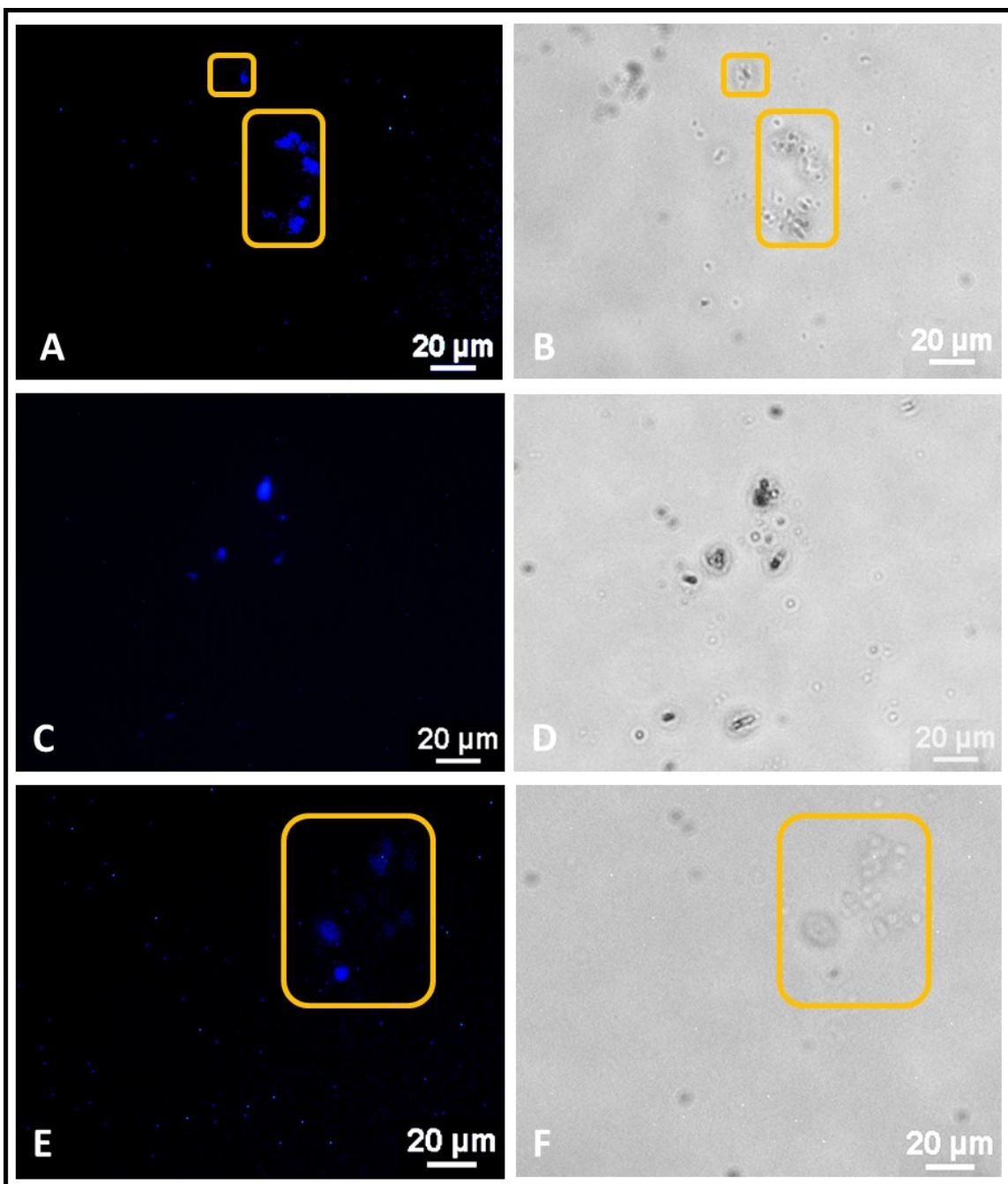


Fig. 7.2.3: Microscopy of DHE Actively Loaded Conventional Liposomes (Batch E)

From the figures above, it can be observed that the fluorescence and vesicles overlap. Secondly, in Figs. 7.2.2D, 7.2.3B & 7.2.3F, the particles appear to aggregate, and form large vesicle clumps. Finally, the liposomal solutions produced were fairly

dilute. However, this step was for qualitative purposes only, and was performed to determine the presence, or absence, of the fluorescent molecule within the liposomes.

7.3 – Fluorescence Emission Spectroscopy

The following figures (Figs. 7.3.1 & 7.3.2) depict the results from the spectrophotometry measurements, as described in section 4.8.

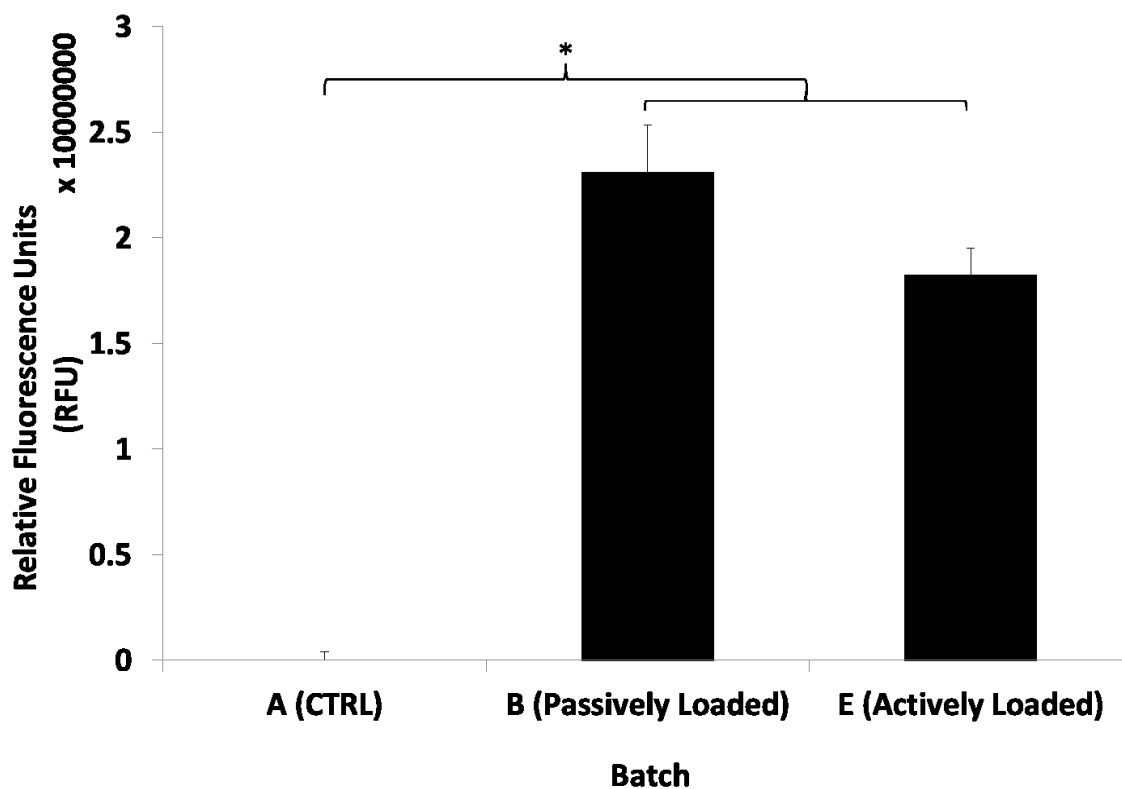


Fig. 7.3.1: Emission Spectra Measurement of Microfluidic Synthesized Batches

(Excitation wavelength: 324 nm)

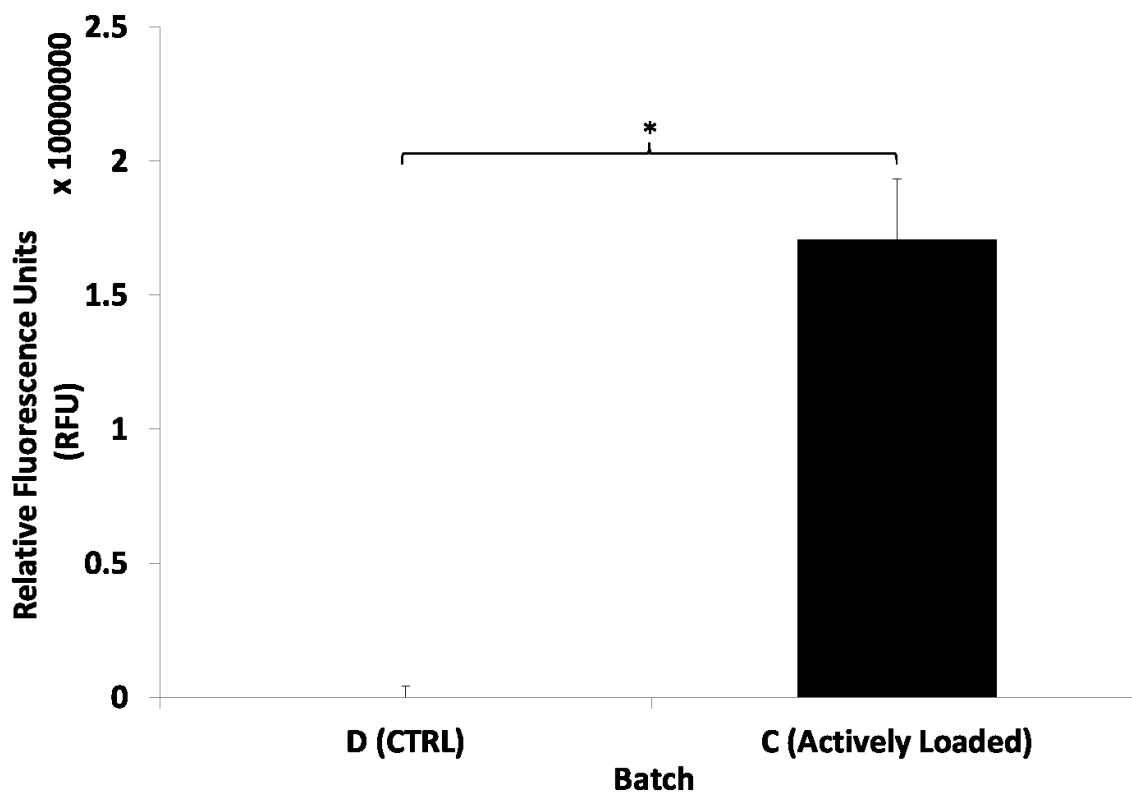


Fig. 7.3.2: Emission Spectra of Conventionally Synthesized Batches

(Excitation wavelength: 324 nm)

Batches A, B and E represent the fluorescence emission of the particles synthesized via HFF. They are the control, passively loaded and actively loaded liposomes respectively. Using the RFU measurement of the control as the baseline value, lots B and E fluoresced at a significantly larger amount (Fig. 7.3.1). Similarly, comparing the unloaded and loaded, conventionally-synthesized vesicles, groups D and C respectively (Fig. 7.3.2), samples containing the DHE demonstrated significantly higher RFU values than the baseline.

7.4 – Discussion

Using HFF, the particles produced by microfluidics resulted in particles which were significantly smaller than those synthesized via a conventional method. The reasoning behind this, as previously described, was the formation of a thin central sheath resulting in a larger surface area to volume ratio. This therefore allowed for greater solvent diffusion out of the compressed stream and ultimately, the formation of smaller nanoliposomes. The vesicles produced in this case were also smaller than those produced at a similar FRR in the characterization experiments (see section 6.2). This could possibly be due to either a modified operational setup (i.e. utilizing inlets 1,2 & 3, as opposed to just the last two) or a by-product of this modified setup, a longer area in which the diffusion could occur (i.e. the first set of curvature, following inlet 2).

Regarding the fluorescence results, initial analysis of Figs. 7.2.2 & 7.2.3 indicated that the fluorescence overlaps with the particles present in the optical microscopy images. This implies that the DHE was in fact encapsulated within the liposomal shells, either in the bilayer, or the aqueous core. However, it is more likely that the compound, due to its hydrophobicity, would be located within the lipid bilayer. In comparison with the images obtained for un-encapsulated DHE (Fig. 7.2.1), there was a clear difference in structural appearance between the two. Plain DHE appears to form very regular spherical shells, whereas in the images obtained in Figs. 7.2.2 & 7.2.3, they were more

irregular. The vesicles also did not all fluoresce, therefore, suggesting that not all of the liposomes contained DHE.

Chapter 8 – Conclusions & Future Work

8.1 – Summary

Herein, we demonstrated a relatively simple-to-manufacture microfluidic device capable of a single-step synthesis and encapsulation method for hydrophobic compounds within DSPC liposomes. Using an innovative, straightforward and optimized channel geometry, we reduced the processing time from more than 24 hours to a matter of hours, depending on the FRR. Additionally, the presence of a dual flow-focusing configuration could potentially allow for multiple loading schemes.

The device went through several iterations, building up from the basic cross-junction for HFF, to the inclusion of 30° inlet angles for optimal flow focusing⁹⁷, and finally, the doubling of the focusing feature. The geometry was created in CAD software and COMSOL fluid dynamics simulations were performed to visualize the effect of various FRRs on the fluid regime. The device was then fabricated according to standard microfabrication techniques, and the simulation results were visually validated with fluid flow in the physical device.

Regarding the synthesis of liposomes on-chip, the particles produced by the device were evaluated for two protocol variables, the initial dissolved phospholipid concentration and FRRs. For the former, at FRRs of both 20 and 150, the particle diameters demonstrated a peculiar trend for an increasing concentration between 1 and 15 mg/mL. Of notable interest was the sudden spike in size around a 6 mg/mL for both

FRRs. Unfortunately, seeing as the formation mechanics of liposomes in injection methods is still not fully understood, no further conclusion could be obtained. We equally demonstrated that for a constant phospholipid concentration, an increase in FRR would result in smaller particles, up to a certain plateau (which was not evaluated in this instance).

By modifying the operational setup, i.e. MilliQ water at the outermost inlet, DSPC:EtOH at the second, and DHE:MeOH at the third, we achieved encapsulation of a fluorescent hydrophobic drug analog, DHE. The fluorescence was used as a binary indicator so as to determine the presence of DHE within the synthesized liposomes. Fluorescence was visually present in optical microscopy images, as well as in fluorescence spectrophotometric sweeps. The vesicles produced by this microfluidic method, versus a conventional ethanol injection process, were approximately 30% smaller in diameter. We also observed that the loading mechanism, be it passive or active, did not significantly affect the hydrodynamic diameters of the particles. However, the actual amount of DHE encapsulated, i.e. the loading efficiency, was not quantified and is listed as a future perspective of this thesis.

8.2 – Future Work

In this investigation, we set about to devise, from the ground up, a novel continuous-flow device for the synthesis of nano-scale lipid vesicles. The device went through several iterations, and initial tests, to become a satisfyingly adequate initial prototype. As with all proof-of-concepts, several physical iterations and optimization steps are required before a suitable platform is created. In view of this, we outline below several improvements to incorporate in any future experiments.

At higher flow rates, the liposome solutions were fairly dilute. Although these FRRs gave the lowest polydispersity values, the dilution of the samples rendered analysis difficult, as seen in Figs. 7.2.2 & 7.2.3 in chapter 7. This also proved futile any attempt to image the liposomes with electron microscopy methods. As such, one suggestion to address this issue would be to replicate the channel geometry with smaller channel widths and heights. Observing Fig. 5.5.2, flow-focusing visualization using dye at the junction, there appears to be much unused space, and thus, our reasoning is that a narrower channel would in turn require lower FRRs to achieve comparable lipid-solvent sheath compression. However, one aspect which must remain in consideration is the increasing channel resistance with finer channels. An additional feature could be the use of an expansion channel after the focusing junction, so as to attempt to harvest and obtain a fairly concentrated liposome solution. Upon resolution of this dilution issue, we further recommend performing electron microscopy to

characterize the lipid-bilayer, or even atomic force microscopy to validate size measurements with our DLS results.

As previously mentioned, the formation mechanism of other phosphatidylcholine-based liposomes when using injection methods is not well understood, and we propose testing this platform with other phospholipids used in microfluidic hydrodynamic focusing syntheses. This step would hopefully result in similar trends observed by others in the field.^{29,98-100} Furthermore, we also recommend testing the current device, v4.0, with a range of phospholipid concentrations between 3 and 6 mg/mL, and possibly developing a mathematical model for the observed pattern with regards to DSPC. On a similar note, we also suggest utilizing COMSOL to model the diffusion occurring at the fluid interface within the channels. The latter, in conjunction with the potential mathematical formation model for DSPC liposomes, could in turn better predict the location of liposome formation. This could furthermore result in improved channel designs and more innovative platforms.

Additionally, this preliminary study only qualitatively investigated the encapsulation of hydrophobic compounds. A subsequent study should include the quantification of the encapsulated agents, via HPLC or tangential flow filtration (TFF), and in turn, the determination of the encapsulation efficiency of this synthesis technique. Regarding the compound type, we further recommend the assessment of the encapsulation of hydrophilic and amphiphilic bioactive agents. One possible operational

setup for the former would simply be the injection of the dissolved molecule into inlet 3 of the device, all other parameters remaining the same. We would therefore expect these compounds to be contained within the aqueous core of the liposome. Likewise, a comparable investigation would be to dissolve both the phospholipid and encapsulable compound in the same mixture and attempting on-chip synthesis without further preprocessing, as what is currently performed by Jahn *et al.*¹⁰¹ With regards to an amphiphilic compound, we speculate that injection via inlet 3 would result in superior encapsulation of the bioactive agent.

Finally, in addition to the potential for use as a rapid test-bed or prototyping platform for novel liposomal formulations, one final proposition would be to adapt the platform, due to its versatility, to the synthesis to a myriad of other nano-/microparticulate systems, such as polymeric composites, hydrogels, or any other compounds necessitating injection processes. Nevertheless, further investigation is required on this aspect. We also postulate that, in conjunction with suitable multi-channel syringes, or readily available open-source options¹⁰³, and multiple devices in a multiplexed array, the optimization time of novel liposomal blends could be drastically reduced from days to mere minutes with such a multiplexed and streamlined setup.

References

- 1 Bangham, A. D., Standish, M. M. & Watkins, J. C. Diffusion of univalent ions across the lamellae of swollen phospholipids. *Journal of molecular biology* **13**, 238-252 (1965).
- 2 Al-Jamal, W. T. & Kostarelos, K. Liposomes: from a clinically established drug delivery system to a nanoparticle platform for theranostic nanomedicine. *Acc Chem Res* **44**, 1094-1104, doi:10.1021/ar200105p (2011).
- 3 Allen, T. M. & Cullis, P. R. Liposomal drug delivery systems: from concept to clinical applications. *Advanced drug delivery reviews* **65**, 36-48, doi:10.1016/j.addr.2012.09.037 (2013).
- 4 Rahimpour, Y. & Hamishehkar, H. Liposomes in cosmeceutics. *Expert Opin Drug Deliv* **9**, 443-455, doi:10.1517/17425247.2012.666968 (2012).
- 5 Reza Mozafari, M., Johnson, C., Hatziantoniou, S. & Demetzos, C. Nanoliposomes and their applications in food nanotechnology. *Journal of liposome research* **18**, 309-327 (2008).
- 6 Bowey, K., Tanguay, J. F. & Tabrizian, M. Liposome technology for cardiovascular disease treatment and diagnosis. *Expert Opin Drug Deliv* **9**, 249-265, doi:10.1517/17425247.2012.647908 (2012).
- 7 Papahadjopoulos, D. & Miller, N. Phospholipid model membranes. I. Structural characteristics of hydrated liquid crystals. *Biochimica et biophysica acta* **135**, 624-638 (1967).
- 8 Mashaghi, S., Jadidi, T., Koenderink, G. & Mashaghi, A. Lipid nanotechnology. *International journal of molecular sciences* **14**, 4242-4282, doi:10.3390/ijms14024242 (2013).
- 9 Jesorka, A. & Orwar, O. Liposomes: technologies and analytical applications. *Annu Rev Anal Chem (Palo Alto Calif)* **1**, 801-832, doi:10.1146/annurev.anchem.1.031207.112747 (2008).
- 10 Gabizon, A. *et al.* Prolonged circulation time and enhanced accumulation in malignant exudates of doxorubicin encapsulated in polyethylene-glycol coated liposomes. *Cancer Res* **54**, 987-992 (1994).
- 11 Taherkhani, S., Mohammadi, M., Daoud, J., Martel, S. & Tabrizian, M. Covalent binding of nanoliposomes to the surface of magnetotactic bacteria for the synthesis of self-propelled therapeutic agents. *ACS Nano* **8**, 5049-5060, doi:10.1021/nn5011304 (2014).
- 12 Lee, W. C. & Tsai, T. H. Preparation and characterization of liposomal coenzyme Q10 for in vivo topical application. *International journal of pharmaceutics* **395**, 78-83, doi:10.1016/j.ijpharm.2010.05.006 (2010).
- 13 Larivière, B. *et al.* Microfluidized liposomes for the acceleration of cheese ripening. *International Dairy Journal* **1**, 111-124, doi:10.1016/0958-6946(91)90003-q (1991).
- 14 Taylor, T. M., Davidson, P. M., Bruce, B. D. & Weiss, J. Liposomal nanocapsules in food science and agriculture. *Crit Rev Food Sci Nutr* **45**, 587-605, doi:10.1080/10408390591001135 (2005).
- 15 Lasic, D. D. The mechanism of vesicle formation. *Biochem J* **256**, 1-11 (1988).
- 16 Barrow, D. A. & Lentz, B. R. Large vesicle contamination in small, unilamellar vesicles. *Biochimica et biophysica acta* **597**, 92-99 (1980).
- 17 Maherani, B., Arab-Tehrany, E., Mozafari, M. R., Gaiani, C. & Linder, M. Liposomes: A Review of Manufacturing Techniques and Targeting Strategies. *Current Nanoscience* **7**, 436-452, doi:10.2174/157341311795542453 (2011).
- 18 Brunner, J., Skrabal, P. & Hauser, H. Single bilayer vesicles prepared without sonication. Physico-chemical properties. *Biochimica et biophysica acta* **455**, 322-331 (1976).
- 19 Meure, L. A., Foster, N. R. & Dehghani, F. Conventional and dense gas techniques for the production of liposomes: a review. *AAPS PharmSciTech* **9**, 798-809, doi:10.1208/s12249-008-9097-x (2008).

- 20 Batzri, S. & Korn, E. D. Single Bilayer Liposomes Prepared without Sonication. *Biochimica et biophysica acta* **298**, 1015-1019, doi:Doi 10.1016/0005-2736(73)90408-2 (1973).
- 21 Deamer, D. & Bangham, A. D. Large volume liposomes by an ether vaporization method. *Biochimica et biophysica acta* **443**, 629-634, doi:[http://dx.doi.org/10.1016/0005-2736\(76\)90483-1](http://dx.doi.org/10.1016/0005-2736(76)90483-1) (1976).
- 22 Deamer, D. W. PREPARATION AND PROPERTIES OF ETHER-INJECTION LIPOSOMES *. *Annals of the New York Academy of Sciences* **308**, 250-258, doi:10.1111/j.1749-6632.1978.tb22027.x (1978).
- 23 Gentine, P., Bourel-Bonnet, L. & Frisch, B. Modified and derived ethanol injection toward liposomes: development of the process. *Journal of liposome research* **23**, 11-19, doi:10.3109/08982104.2012.717298 (2013).
- 24 Szoka, F., Jr. & Papahadjopoulos, D. Procedure for preparation of liposomes with large internal aqueous space and high capture by reverse-phase evaporation. *Proceedings of the National Academy of Sciences of the United States of America* **75**, 4194-4198 (1978).
- 25 Angelova, M. I. & Dimitrov, D. S. Liposome Electroformation. *Faraday Discuss* **81**, 303-+, doi:Doi 10.1039/Dc9868100303 (1986).
- 26 Mozafari, M., Reed, C. & Rostron, C. Development of non-toxic liposomal formulations for gene and drug delivery to the lung. *Technology and Health Care* **10**, 342-344 (2002).
- 27 Mozafari, M. R., Reed, C. J., Rostron, C., Kocum, C. & Piskin, E. Construction of stable anionic liposome-plasmid particles using the heating method: a preliminary investigation. *Cellular & molecular biology letters* **7**, 923-927 (2002).
- 28 Mozafari, M. R. Liposomes: an overview of manufacturing techniques. *Cellular & molecular biology letters* **10**, 711-719 (2005).
- 29 Zook, J. M. & Vreeland, W. N. Effects of temperature, acyl chain length, and flow-rate ratio on liposome formation and size in a microfluidic hydrodynamic focusing device. *Soft Matter* **6**, 1352-1360, doi:Doi 10.1039/B923299k (2010).
- 30 Schaschke, C. 87 (Oxford University Press).
- 31 Otake, K., Imura, T., Sakai, H. & Abe, M. Development of a new preparation method of liposomes using supercritical carbon dioxide. *Langmuir : the ACS journal of surfaces and colloids* **17**, 3898-3901, doi:Doi 10.1021/La010122k (2001).
- 32 Eikani, M. H., Goodarznia, I. & Mirza, M. Supercritical carbon dioxide extraction of cummin seeds (*Cuminum cyminum* L.). *Flavour and Fragrance Journal* **14**, 29-31, doi:Doi 10.1002/(Sici)1099-1026(199901/02)14:1<29::Aid-Ffj765>3.0.Co;2-G (1999).
- 33 Hu, Q. H. Supercritical carbon dioxide extraction of *Spirulina platensis* component and removing the stench. *Journal of Agricultural and Food Chemistry* **47**, 2705-2706, doi:10.1021/jf9812432 (1999).
- 34 McHugh, M. A. & Krukonis, V. J. Supercritical fluid extraction. Principles and practice. (1986).
- 35 Yaws, C. L. (Knovel).
- 36 Anton, K., Frederiksen, L. & Van Hoogevest, P. (Google Patents, 1997).
- 37 Castor, T. P. & Chu, L. (Google Patents, 1998).
- 38 Bustami, R. T., Chan, H.-K., Dehghani, F. & Foster, N. R. Recent applications of supercritical fluid technology to pharmaceutical powder systems. *KONA Powder and Particle Journal* **19**, 57-70 (2001).
- 39 Frederiksen, L., Anton, K., van Hoogevest, P., Keller, H. R. & Leuenberger, H. Preparation of liposomes encapsulating water-soluble compounds using supercritical carbon dioxide. *J Pharm Sci* **86**, 921-928, doi:10.1021/js960403q (1997).

- 40 Otake, K. *et al.* Preparation of liposomes using an improved supercritical reverse phase evaporation method. *Langmuir : the ACS journal of surfaces and colloids* **22**, 2543-2550, doi:10.1021/la051654u (2006).
- 41 Barnadas-Rodríguez, R. & Sabés, M. Factors involved in the production of liposomes with a high-pressure homogenizer. *International journal of pharmaceuticals* **213**, 175-186 (2001).
- 42 Olson, D. W., White, C. H. & Richter, R. L. Effect of pressure and fat content on particle sizes in microfluidized milk. *J Dairy Sci* **87**, 3217-3223, doi:10.3168/jds.S0022-0302(04)73457-8 (2004).
- 43 Sorgi, F. L. & Huang, L. Large scale production of DC-Chol cationic liposomes by microfluidization. *International journal of pharmaceuticals* **144**, 131-139, doi:Doi 10.1016/S0378-5173(96)04733-3 (1996).
- 44 Massing, U., Cicko, S. & Ziroli, V. Dual asymmetric centrifugation (DAC)--a new technique for liposome preparation. *Journal of controlled release : official journal of the Controlled Release Society* **125**, 16-24, doi:10.1016/j.jconrel.2007.09.010 (2008).
- 45 Adrian, J. E., Wolf, A., Steinbach, A., Rossler, J. & Suss, R. Targeted delivery to neuroblastoma of novel siRNA-anti-GD2-liposomes prepared by dual asymmetric centrifugation and sterol-based post-insertion method. *Pharmaceutical research* **28**, 2261-2272, doi:10.1007/s11095-011-0457-y (2011).
- 46 Li, C. & Deng, Y. A novel method for the preparation of liposomes: freeze drying of monophasic solutions. *J Pharm Sci* **93**, 1403-1414, doi:10.1002/jps.20055 (2004).
- 47 Cui, J., Li, C., Deng, Y., Wang, Y. & Wang, W. Freeze-drying of liposomes using tertiary butyl alcohol/water cosolvent systems. *International journal of pharmaceuticals* **312**, 131-136, doi:10.1016/j.ijpharm.2006.01.004 (2006).
- 48 Wang, T. *et al.* Preparation of submicron unilamellar liposomes by freeze-drying double emulsions. *Biochimica et biophysica acta* **1758**, 222-231, doi:10.1016/j.bbamem.2006.01.023 (2006).
- 49 Pick, U. Liposomes with a large trapping capacity prepared by freezing and thawing of sonicated phospholipid mixtures. *Arch Biochem Biophys* **212**, 186-194, doi:[http://dx.doi.org/10.1016/0003-9861\(81\)90358-1](http://dx.doi.org/10.1016/0003-9861(81)90358-1) (1981).
- 50 Traikia, M., Warschawski, D. E., Recouvreur, M., Cartaud, J. & Devaux, P. F. Formation of unilamellar vesicles by repetitive freeze-thaw cycles: characterization by electron microscopy and ³¹P-nuclear magnetic resonance. *Eur Biophys J* **29**, 184-195, doi:10.1007/s002490000077 (2000).
- 51 Macdonald, R. C., Jones, F. D. & Qiu, R. Z. Fragmentation into Small Vesicles of Dioleoylphosphatidylcholine Bilayers during Freezing and Thawing. *Bba-Biomembranes* **1191**, 362-370, doi:Doi 10.1016/0005-2736(94)90187-2 (1994).
- 52 Hwang, S. Y. *et al.* Effects of operating parameters on the efficiency of liposomal encapsulation of enzymes. *Colloids and surfaces. B, Biointerfaces* **94**, 296-303, doi:10.1016/j.colsurfb.2012.02.008 (2012).
- 53 Costa, A. P., Xu, X. & Burgess, D. J. Freeze-anneal-thaw cycling of unilamellar liposomes: effect on encapsulation efficiency. *Pharmaceutical research* **31**, 97-103, doi:10.1007/s11095-013-1135-z (2014).
- 54 Wagner, A., Vorauer-Uhl, K. & Katinger, H. Liposomes produced in a pilot scale: production, purification and efficiency aspects. *European journal of pharmaceuticals and biopharmaceutics : official journal of Arbeitsgemeinschaft fur Pharmazeutische Verfahrenstechnik e.V* **54**, 213-219, doi:[http://dx.doi.org/10.1016/S0939-6411\(02\)00062-0](http://dx.doi.org/10.1016/S0939-6411(02)00062-0) (2002).

- 55 Wagner, A., Vorauer-Uhl, K., Kreismayr, G. & Katinger, H. The crossflow injection technique: an improvement of the ethanol injection method. *Journal of liposome research* **12**, 259-270, doi:10.1081/LPR-120014761 (2002).
- 56 Wagner Andreas, A., Vorauer-Uhl, K., Kreismayr, G. & Katinger, H. Enhanced protein loading into liposomes by the multiple crossflow injection technique. *Journal of liposome research* **12**, 271-283 (2002).
- 57 Zhong, J. *et al.* Large scale preparation of midkine antisense oligonucleotides nanoliposomes by a cross-flow injection technique combined with ultrafiltration and high-pressure extrusion procedures. *International journal of pharmaceutics* **441**, 712-720, doi:10.1016/j.ijpharm.2012.10.023 (2013).
- 58 Foudeh, A. M., Fatanat Didar, T., Veres, T. & Tabrizian, M. Microfluidic designs and techniques using lab-on-a-chip devices for pathogen detection for point-of-care diagnostics. *Lab on a chip* **12**, 3249-3266, doi:10.1039/c2lc40630f (2012).
- 59 Nguyen, N. T., Shaegh, S. A., Kashaninejad, N. & Phan, D. T. Design, fabrication and characterization of drug delivery systems based on lab-on-a-chip technology. *Advanced drug delivery reviews* **65**, 1403-1419, doi:10.1016/j.addr.2013.05.008 (2013).
- 60 Jahn, A., Vreeland, W. N., Gaitan, M. & Locascio, L. E. Controlled vesicle self-assembly in microfluidic channels with hydrodynamic focusing. *Journal of the American Chemical Society* **126**, 2674-2675, doi:10.1021/ja0318030 (2004).
- 61 Hood, R. R., DeVoe, D. L., Atencia, J., Vreeland, W. N. & Omiatek, D. M. A facile route to the synthesis of monodisperse nanoscale liposomes using 3D microfluidic hydrodynamic focusing in a concentric capillary array. *Lab on a chip* **14**, 2403-2409, doi:10.1039/c4lc00334a (2014).
- 62 Jaafar-Maalej, C., Charcosset, C. & Fessi, H. A new method for liposome preparation using a membrane contactor. *Journal of liposome research* **21**, 213-220, doi:10.3109/08982104.2010.517537 (2011).
- 63 Charcosset, C. Membrane processes in biotechnology: an overview. *Biotechnol Adv* **24**, 482-492, doi:10.1016/j.biotechadv.2006.03.002 (2006).
- 64 Laouini, A., Jaafar-Maalej, C., Sfar, S., Charcosset, C. & Fessi, H. Liposome preparation using a hollow fiber membrane contactor--application to spironolactone encapsulation. *International journal of pharmaceutics* **415**, 53-61, doi:10.1016/j.ijpharm.2011.05.034 (2011).
- 65 Cullis, P., Mayer, L., Bally, M., Madden, T. & Hope, M. Generating and loading of liposomal systems for drug-delivery applications. *Advanced drug delivery reviews* **3**, 267-282 (1989).
- 66 Deamer, D. W., Prince, R. C. & Crofts, A. R. The response of fluorescent amines to pH gradients across liposome membranes. *Biochimica et biophysica acta* **274**, 323-335, doi:[http://dx.doi.org/10.1016/0005-2736\(72\)90180-0](http://dx.doi.org/10.1016/0005-2736(72)90180-0) (1972).
- 67 Nichols, J. W. & Deamer, D. W. Catecholamine Uptake and Concentration by Liposomes Maintaining Ph-Gradients. *Biochimica et biophysica acta* **455**, 269-271, doi:Doi 10.1016/0005-2736(76)90169-3 (1976).
- 68 Haran, G., Cohen, R., Bar, L. K. & Barenholz, Y. Transmembrane ammonium sulfate gradients in liposomes produce efficient and stable entrapment of amphipathic weak bases. *Biochimica et biophysica acta* **1151**, 201-215 (1993).
- 69 Fritze, A., Hens, F., Kimpfler, A., Schubert, R. & Peschka-Suss, R. Remote loading of doxorubicin into liposomes driven by a transmembrane phosphate gradient. *Biochimica et biophysica acta* **1758**, 1633-1640, doi:10.1016/j.bbamem.2006.05.028 (2006).
- 70 Gubernator, J. *et al.* The encapsulation of idarubicin within liposomes using the novel EDTA ion gradient method ensures improved drug retention in vitro and in vivo. *Journal of controlled*

- release : official journal of the Controlled Release Society **146**, 68-75, doi:10.1016/j.jconrel.2010.05.021 (2010).
- 71 Fox, R. W., Pritchard, P. J. & McDonald, A. T. *Fox and McDonald's introduction to fluid mechanics*. (John Wiley & Sons, Inc., 2011).
- 72 Hessel, V., Löwe, H. & Schönfeld, F. Micromixers—a review on passive and active mixing principles. *Chemical Engineering Science* **60**, 2479-2501, doi:10.1016/j.ces.2004.11.033 (2005).
- 73 Kuribayashi, K., Tresset, G., Coquet, P., Fujita, H. & Takeuchi, S. Electroformation of giant liposomes in microfluidic channels. *Meas Sci Technol* **17**, 3121-3126, doi:Doi 10.1088/0957-0233/17/12/S01 (2006).
- 74 Olson, F., Hunt, C. A., Szoka, F. C., Vail, W. J. & Papahadjopoulos, D. Preparation of Liposomes of Defined Size Distribution by Extrusion through Polycarbonate Membranes. *Biochimica et biophysica acta* **557**, 9-23, doi:Doi 10.1016/0005-2736(79)90085-3 (1979).
- 75 Dittrich, P. S., Heule, M., Renaud, P. & Manz, A. On-chip extrusion of lipid vesicles and tubes through microsized apertures. *Lab on a chip* **6**, 488-493, doi:10.1039/b517670k (2006).
- 76 Pradhan, P. *et al.* A facile microfluidic method for production of liposomes. *Anticancer Res* **28**, 943-947 (2008).
- 77 Funakoshi, K., Suzuki, H. & Takeuchi, S. Formation of giant lipid vesiclelike compartments from a planar lipid membrane by a pulsed jet flow. *Journal of the American Chemical Society* **129**, 12608-12609, doi:10.1021/ja074029f (2007).
- 78 Utada, A. S. *et al.* Monodisperse double emulsions generated from a microcapillary device. *Science* **308**, 537-541, doi:10.1126/science.1109164 (2005).
- 79 Shum, H. C., Lee, D., Yoon, I., Kodger, T. & Weitz, D. A. Double emulsion templated monodisperse phospholipid vesicles. *Langmuir : the ACS journal of surfaces and colloids* **24**, 7651-7653, doi:10.1021/la801833a (2008).
- 80 Tan, Y. C., Hettiarachchi, K., Siu, M., Pan, Y. R. & Lee, A. P. Controlled microfluidic encapsulation of cells, proteins, and microbeads in lipid vesicles. *Journal of the American Chemical Society* **128**, 5656-5658, doi:10.1021/ja056641h (2006).
- 81 Sugiura, S. *et al.* Novel method for obtaining homogeneous giant vesicles from a monodisperse water-in-oil emulsion prepared with a microfluidic device. *Langmuir : the ACS journal of surfaces and colloids* **24**, 4581-4588, doi:10.1021/la703509r (2008).
- 82 Ota, S., Yoshizawa, S. & Takeuchi, S. Microfluidic formation of monodisperse, cell-sized, and unilamellar vesicles. *Angew Chem Int Ed Engl* **48**, 6533-6537, doi:10.1002/anie.200902182 (2009).
- 83 Kurakazu, T. & Takeuchi, S. in *Micro Electro Mechanical Systems (MEMS), 2010 IEEE 23rd International Conference on*. 1115-1118 (IEEE).
- 84 Matosevic, S. & Paegel, B. M. Stepwise synthesis of giant unilamellar vesicles on a microfluidic assembly line. *Journal of the American Chemical Society* **133**, 2798-2800, doi:10.1021/ja109137s (2011).
- 85 Jung, S. Y., Retterer, S. T. & Collier, C. P. On-demand generation of monodisperse femtolitre droplets by shape-induced shear. *Lab on a chip* **10**, 2688-2694, doi:10.1039/c0lc00120a (2010).
- 86 van Swaay, D. & deMello, A. Microfluidic methods for forming liposomes. *Lab on a chip* **13**, 752-767, doi:10.1039/c2lc41121k (2013).
- 87 Takagi, J., Yamada, M., Yasuda, M. & Seki, M. Continuous particle separation in a microchannel having asymmetrically arranged multiple branches. *Lab on a chip* **5**, 778-784, doi:10.1039/b501885d (2005).

- 88 Yamada, M., Nakashima, M. & Seki, M. Pinched flow fractionation: continuous size separation of particles utilizing a laminar flow profile in a pinched microchannel. *Anal Chem* **76**, 5465-5471, doi:10.1021/ac049863r (2004).
- 89 Lu, L., Irwin, R. M., Coloma, M. A., Schertzer, J. W. & Chiarot, P. R. Removal of excess interfacial material from surface-modified emulsions using a microfluidic device with triangular post geometry. *Microfluidics and Nanofluidics*, 1-14 (2014).
- 90 Allen, T. M. & Cullis, P. R. Drug delivery systems: entering the mainstream. *Science* **303**, 1818-1822, doi:10.1126/science.1095833 (2004).
- 91 *COMSOL Multiphysics: Version 3.5a. MEMS Module : user's guide.* (Comsol, 2008).
- 92 Wustner, D. *et al.* Quantitative assessment of sterol traffic in living cells by dual labeling with dehydroergosterol and BODIPY-cholesterol. *Chemistry and physics of lipids* **164**, 221-235, doi:10.1016/j.chemphyslip.2011.01.004 (2011).
- 93 Robalo, J. R., do Canto, A. M., Carvalho, A. J., Ramalho, J. P. & Loura, L. M. Behavior of fluorescent cholesterol analogues dehydroergosterol and cholestatrienol in lipid bilayers: a molecular dynamics study. *The journal of physical chemistry. B* **117**, 5806-5819, doi:10.1021/jp312026u (2013).
- 94 Elimelech, M., Gregory, J., Jia, X. & Williams, R. A. 277-279 (Elsevier).
- 95 Hood, R. R., Vreeland, W. N. & DeVoe, D. L. Microfluidic remote loading for rapid single-step liposomal drug preparation. *Lab on a chip* **14**, 3359-3367, doi:10.1039/c4lc00390j (2014).
- 96 Di Carlo, D. Inertial microfluidics. *Lab on a chip* **9**, 3038-3046, doi:10.1039/b912547g (2009).
- 97 Liu, K. *et al.* in *Bioinformatics and Biomedical Engineering, 2007. ICBBE 2007. The 1st International Conference on.* 1121-1124 (IEEE).
- 98 Kennedy, M. J., Ladouceur, H. D., Moeller, T., Kirui, D. & Batt, C. A. Analysis of a laminar-flow diffusional mixer for directed self-assembly of liposomes. *Biomicrofluidics* **6**, 44119, doi:10.1063/1.4772602 (2012).
- 99 Mijajlovic, M., Wright, D., Zivkovic, V., Bi, J. X. & Biggs, M. J. Microfluidic hydrodynamic focusing based synthesis of POPC liposomes for model biological systems. *Colloids and surfaces. B, Biointerfaces* **104**, 276-281, doi:10.1016/j.colsurfb.2012.12.020 (2013).
- 100 Balbino, T. A. *et al.* Continuous flow production of cationic liposomes at high lipid concentration in microfluidic devices for gene delivery applications. *Chemical Engineering Journal* **226**, 423-433, doi:DOI 10.1016/j.cej.2013.04.053 (2013).
- 101 Jahn, A. *et al.* Microfluidic mixing and the formation of nanoscale lipid vesicles. *ACS Nano* **4**, 2077-2087, doi:10.1021/nn901676x (2010).
- 102 Jahn, A., Vreeland, W. N., DeVoe, D. L., Locascio, L. E. & Gaitan, M. Microfluidic directed formation of liposomes of controlled size. *Langmuir : the ACS journal of surfaces and colloids* **23**, 6289-6293, doi:10.1021/la070051a (2007).
- 103 Wijnen, B., Hunt, E. J., Anzalone, G. C. & Pearce, J. M. Open-source syringe pump library. *PLoS One* **9**, e107216, doi:10.1371/journal.pone.0107216 (2014).

Appendix

A1 – Microfabrication Steps

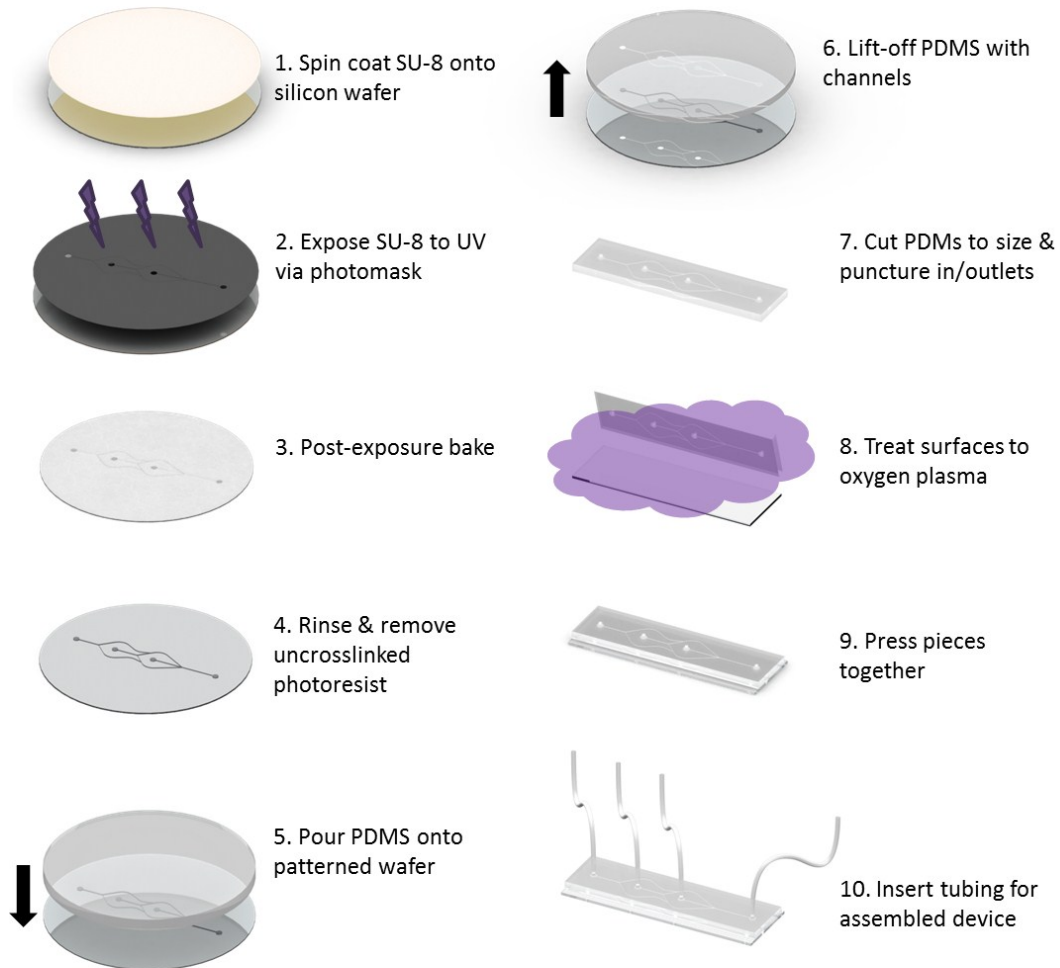


Fig. A1: Soft lithography protocol

Additional details: 1) Spin at 1700 rpm for 100 μm thickness. Soft bake to evaporate solvent. 2) Exposure energy requires: 317 mJ/cm^2 . 3) Bake at 65°C for ≈ 4 min., then 95°C for ≈ 9 min. 4) Develop for 8 min., rinse with fresh solution for 10 sec., rinse with IPA for 10 sec. 5) Mould silanized prior to this step. Cured for 1 hour at 70°C. 6) Gently lift-off so as to not damage channels. 7) Protect channel side with tape to avoid contamination. 8) Plasma treatment for 1 minute at $\approx 50\text{W}$. 9) Gently press together, eliminating all air bubbles between surfaces. 10) Insert tubing approximately $\frac{3}{4}$ down into PDMS.

A2 – Flow Visualization Image Capture Setup



Fig. A2: Camera setup for flow visualization using food dyes within microfluidic device.

A3 – CFD Simulations Results

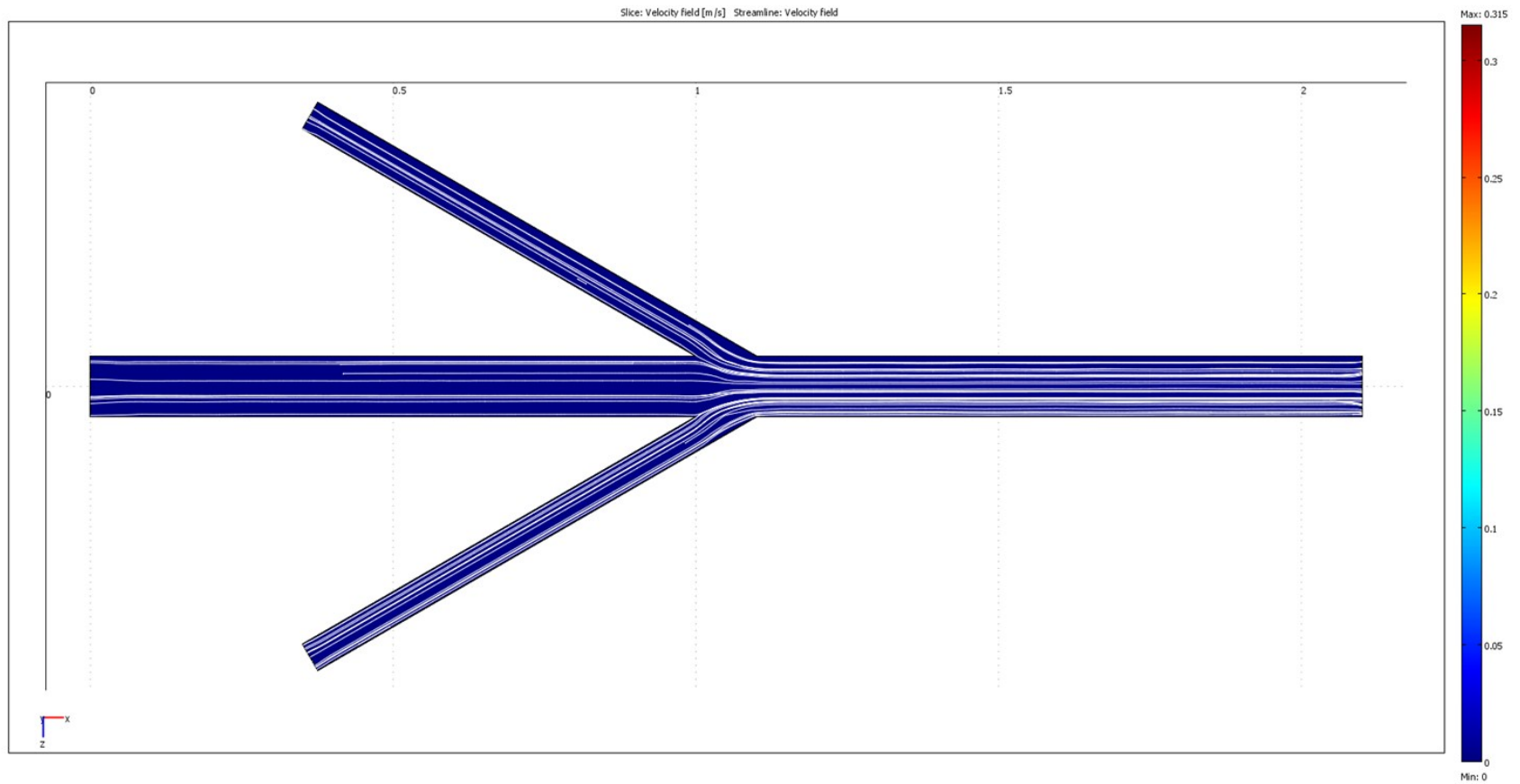


Fig. A3-1: v4.0 Junction CFD Simulation for FRR 2

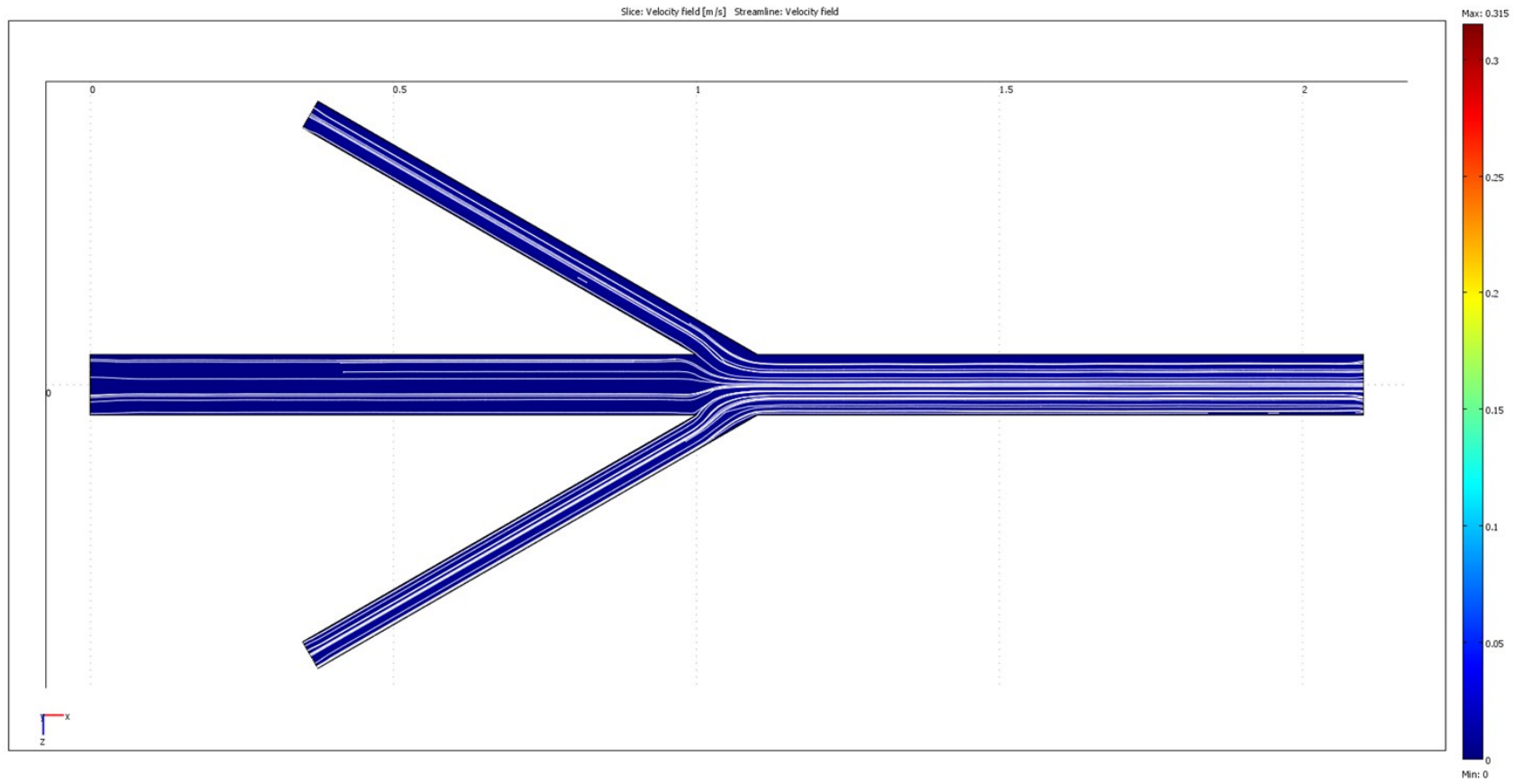


Fig. A3-2: v4.0 Junction CFD Simulation for FRR 5

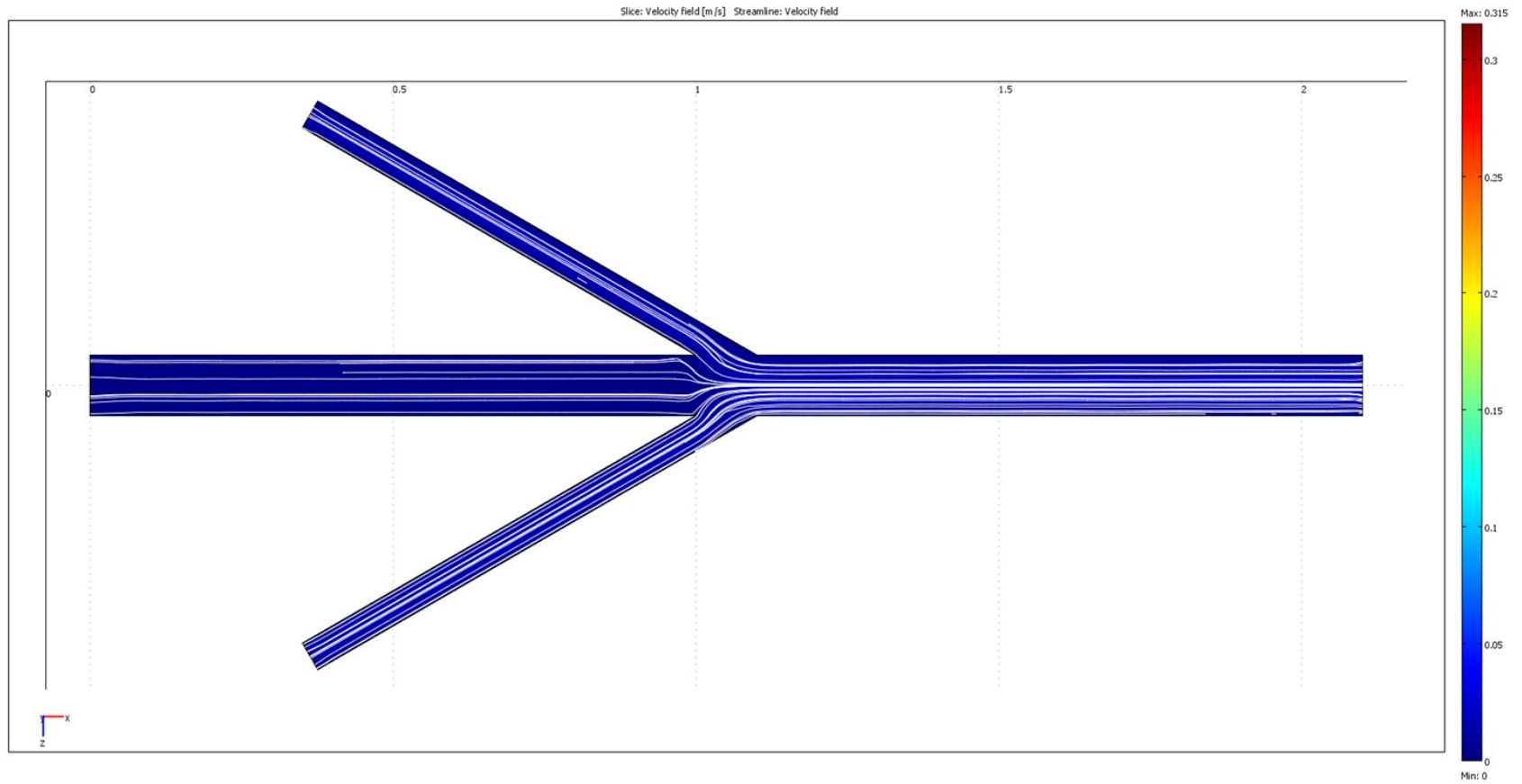


Fig. A3-3: v4.0 Junction CFD Simulation for FRR 10

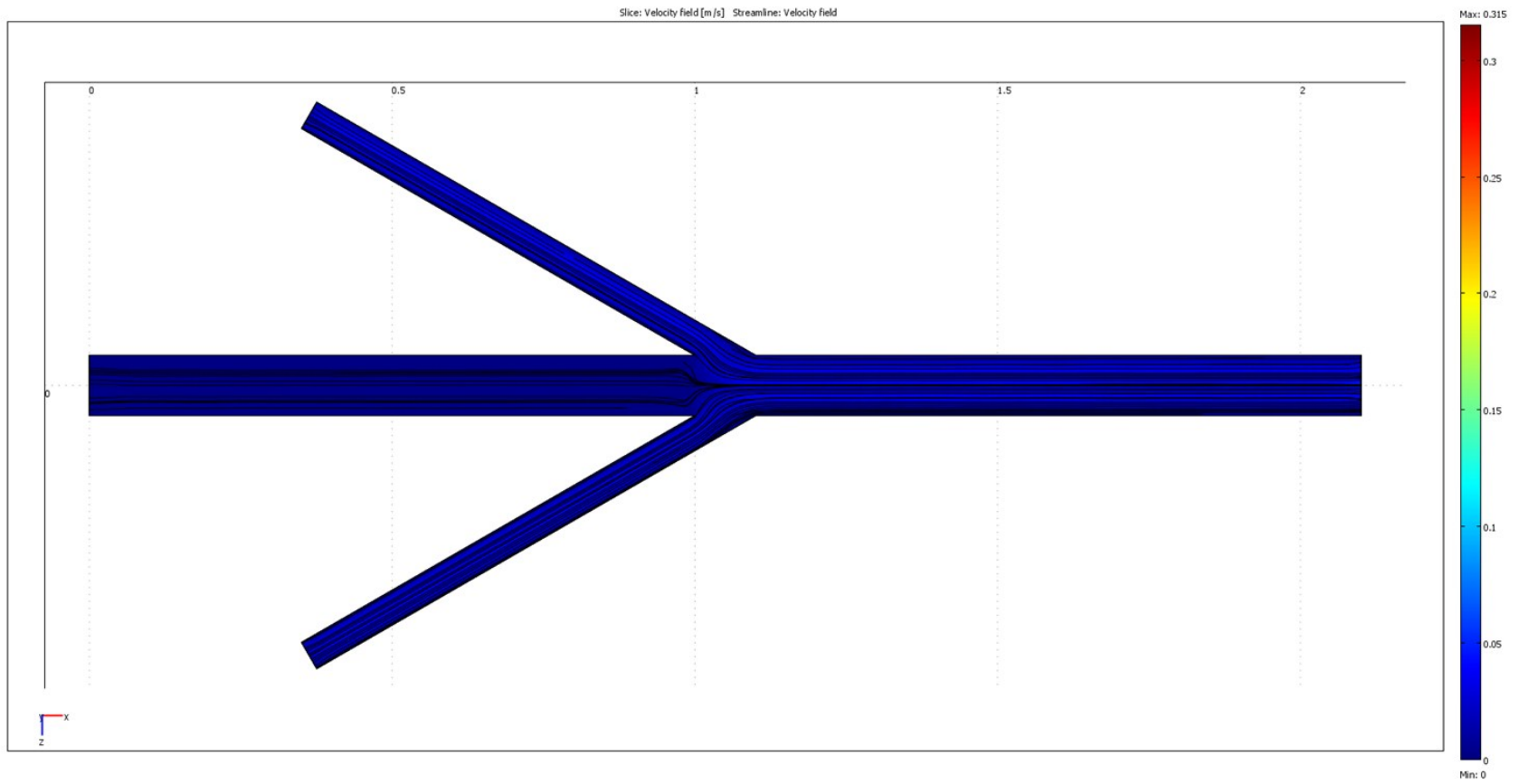


Fig. A3-4: v4.0 Junction CFD Simulation for FRR 20

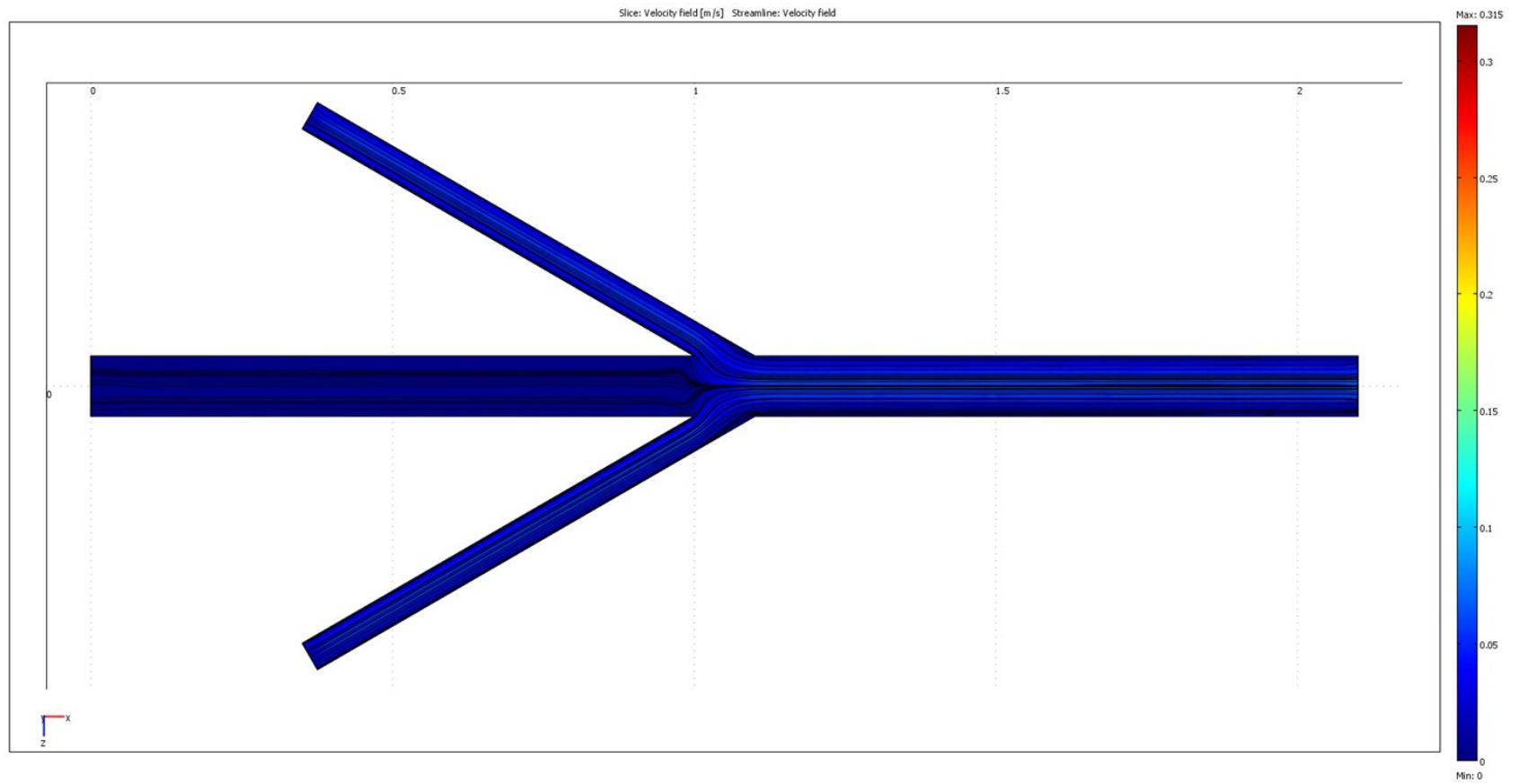


Fig. A3-5: v4.0 Junction CFD Simulation for FRR 30

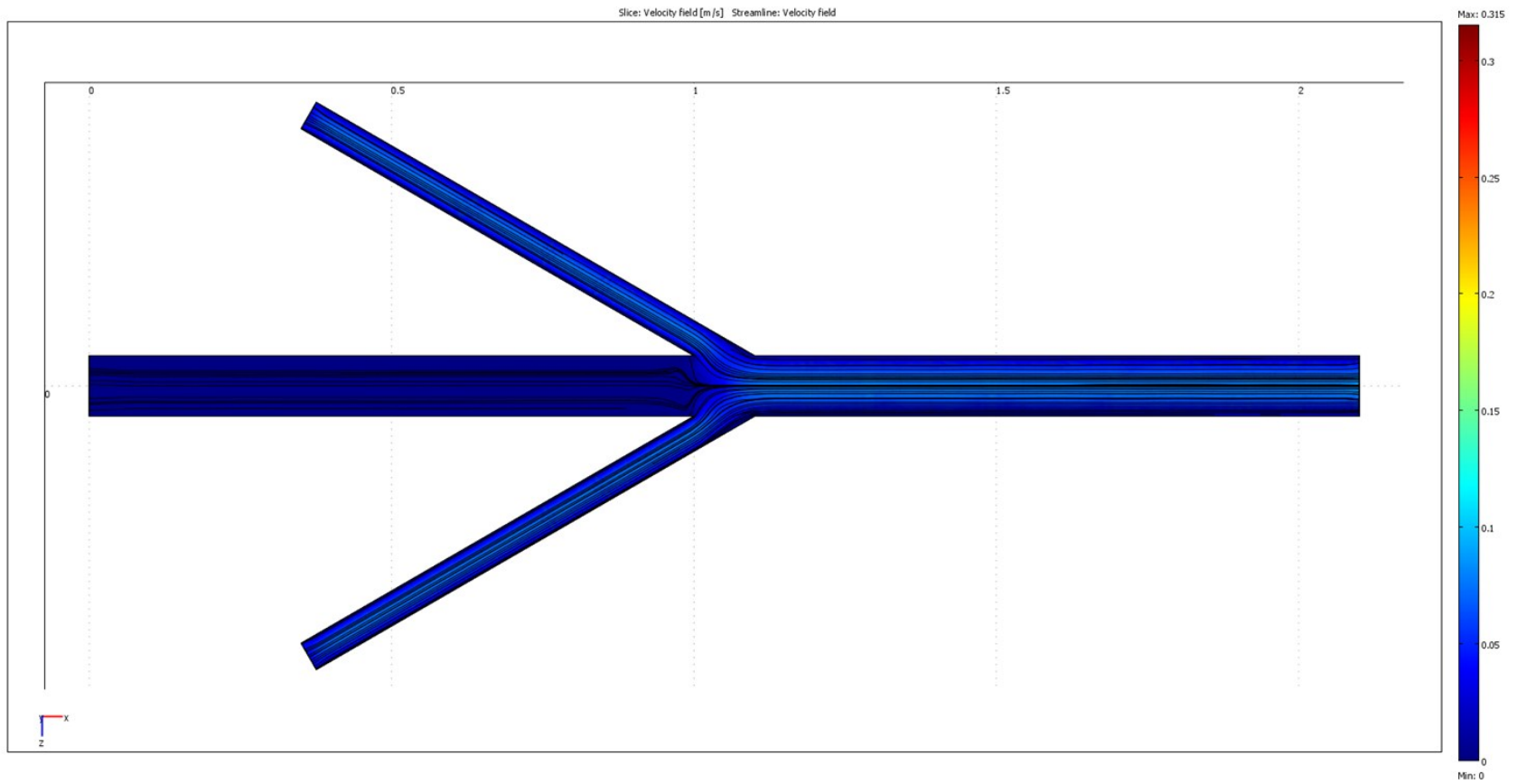


Fig. A3-6: v4.0 Junction CFD Simulation for FRR 40

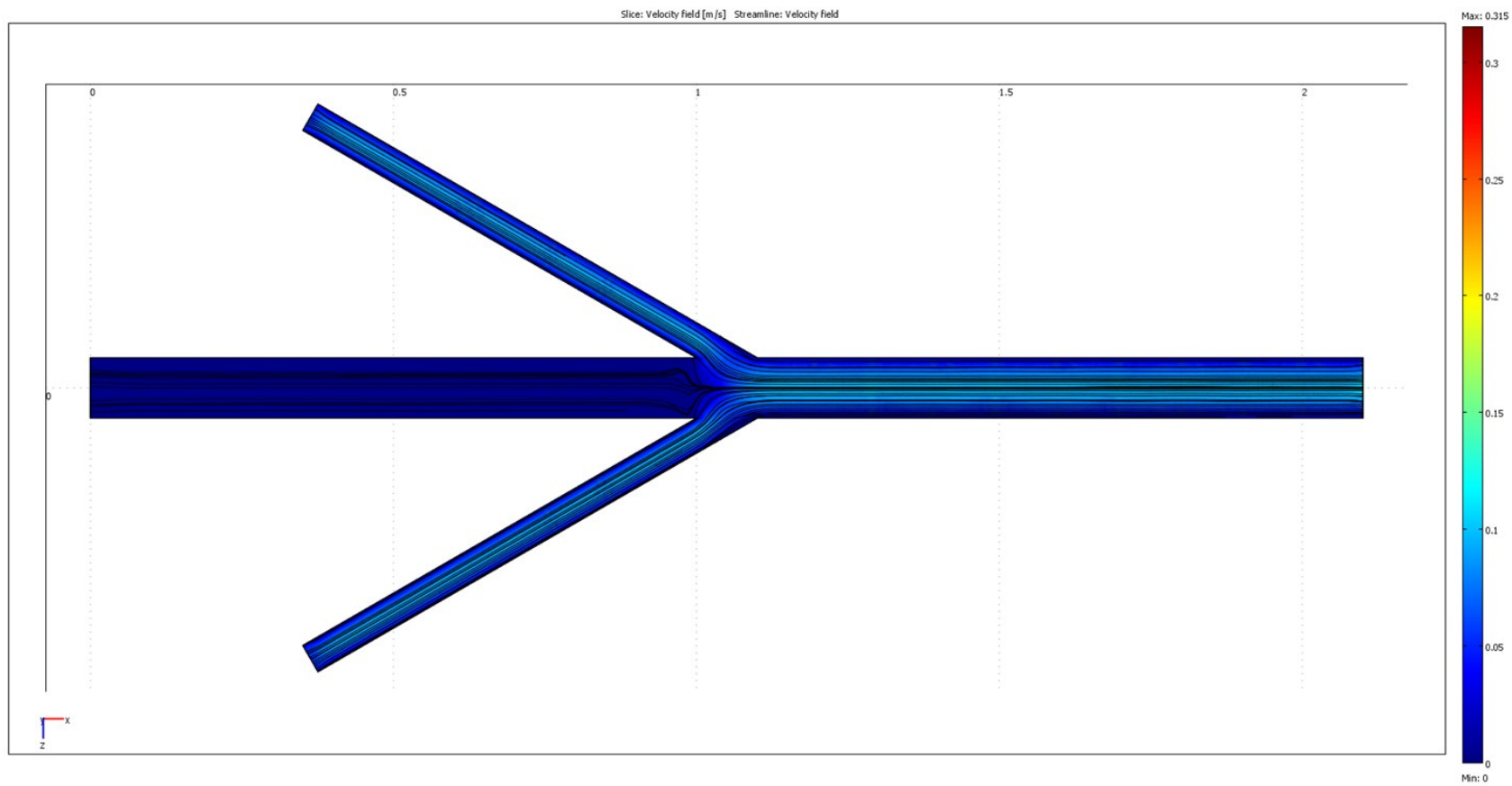


Fig. A3-7: v4.0 Junction CFD Simulation for FRR 50

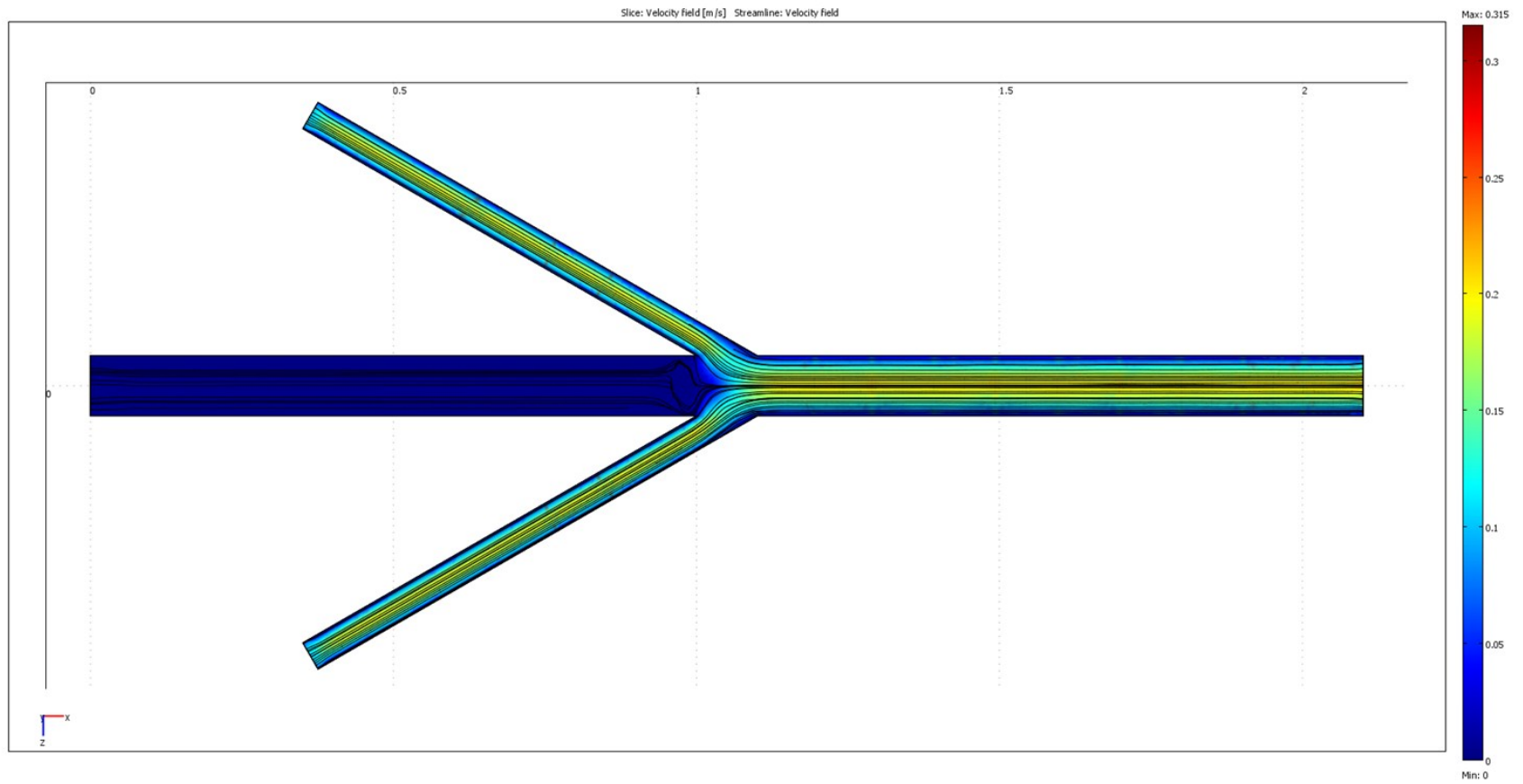


Fig. A3-8: v4.0 Junction CFD Simulation for FRR 100

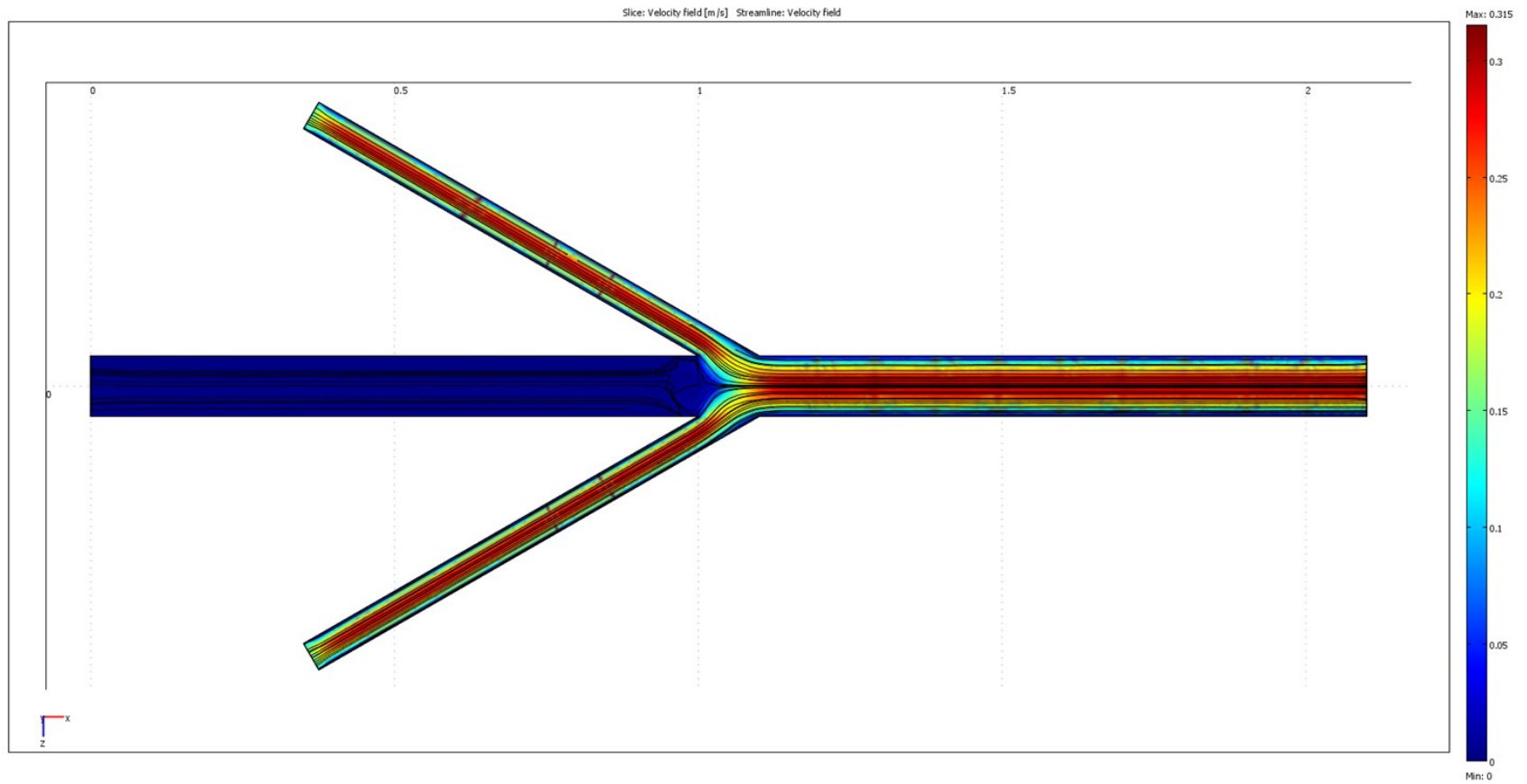


Fig. A3-9: v4.0 Junction CFD Simulation for FRR 15